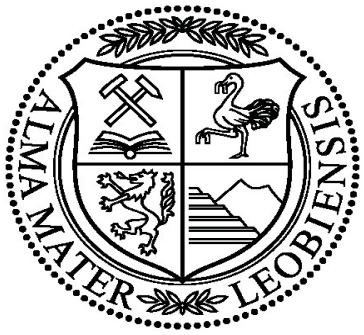

Gas Condensate Banking – Application of Pressure Transient Analysis to Determine Production Impairment and Compositional Effects.

By **Enrique Alejandro Perdomo Echenique**
Chair of Reservoir Engineering
Montanuniversität Leoben
February 2016

University Advisor:
Heinemann, Zoltan. Univ.-Prof .PhD.

Industrial Advisor:
Torsten, Clemens. PhD.

Declaration of authenticity

I declare in lieu of oath, that I wrote this thesis and performed the associated research myself, using only the literature cited in this thesis.

Enrique Alejandro Perdomo Echenique

February 2016

Abstract

A rich gas condensate field is being studied. After discovering the field, a number of production tests have been performed and the fluids were sampled. The results of pressure transient analysis show strong condensate banking even for the short production period. Also, the analysis indicated near wellbore velocity stripping effects. In this master thesis, the effect of liquid drop out near the wellbore will be investigated using compositional simulation. The simulations will include velocity stripping effects and will investigate the sampling of rich gas condensates for gas production below the dew point pressure. The results will then be applied for prediction of condensate banking and to look at the development of condensate/gas ratio.

Moreover, forecasting hydrocarbon production from gas condensate fields is challenging owing to the compositional effects in the reservoir and near-wellbore. In the near-wellbore, condensate blockage is reducing the productivity of the wells. Condensate drop-out in the reservoir leads to decreasing condensate/gas ratios. To forecast hydrocarbon production, the original fluid composition and condensate blockage has to be determined.

For the example field investigated here, numerical simulation of pressure transient behavior was also used to validate the initial condensate/gas ratio and relative permeabilities. The results indicate that the composition of the sample used for PVT analysis had to be modified to match the pressure derivative of the well test. Forecasting hydrocarbon production without these modifications leads to over-prediction of gas production, under-prediction of condensate production and a nine times longer gas production plateau than including the modified data.

Kurzfassung

Ein Gas Kondensat Feld wurde untersucht. Nach der Entdeckung des Feldes wurden einige Produktionstests durchgeführt und Flüssigkeitsproben genommen. Die Ergebnisse von instationären Druckverlaufsanalysen zeigen starke Kondensatbildung bereits bei kurzer Produktionszeit. Die Analyse hat außerdem auf Strömungsgeschwindigkeitsverluste in der Nähe des Bohrloches hingewiesen. In dieser Masterarbeit wird der Effekt von Flüssigkeitsausfall in der Nähe des Bohrloches mit Hilfe von kompositioneller Simulation untersucht. Die Simulationen werden die Strömungsgeschwindigkeitsverluste umfassen und werden das Probenehmen von Gaskondensaten bei Gasproduktion unter dem Drucktaupunkt untersuchen. Die Ergebnisse werden dann für die Vorhersage der bohrlochnahen Kondensatbildung und des Kondensat / Gas Verhältnisses angewandt.

Ferner ist das Vorhersagen der Kohlenwasserstoffproduktion von Gaskondensatfeldern schwierig aufgrund der kompositionellen Effekte in der Lagerstätte und der näheren Bohrlochumgebung. In der Nähe des Bohrloches reduzieren Kondensate die Produktivität der Sonde. Kondensatbildung in der Lagerstätte führt zu einem geringeren Kondensat / Gas Verhältnis. Um die Kohlenwasserstoffproduktion vorherzusagen müssen die ursprüngliche Fluidzusammensetzung und die Blockierung durch Kondensate bestimmt werden.

Für das Lagerstättenbeispiel wurde auch numerische Simulation des instationären Druckverhaltens angewandt um das initiale Kondensat / Gas Verhältnis und die relativen Permeabilitäten zu validieren. Die Ergebnisse zeigen, dass die Zusammensetzung der für die PVT Analyse verwendeten Probe modifiziert werden muss, um die Druckderivative der Drucktests reproduzieren zu können. Ohne diese Veränderungen führt die Vorhersage der Kohlenwasserstoffproduktion zu einer zu hohen Prognose für die Gasproduktion, einer zu niedrigen Prognose für die Kondensatproduktion und zu einem neunmal längeren Gasproduktionsplateau im Vergleich zu den Ergebnisse unter Verwendung der modifizierten Daten.

Acknowledgments

I would like to thank my advisor Dr. Torsten Clemens (OMV) for guiding me through the research that made this thesis possible.

I would also like to say thank you to my second advisor Univ. Prof. PhD. Zoltan Heinemann and Dr. Gregor Mittermeir for all the support provided by the Chair of Reservoir Engineering at the Institute of Petroleum Engineering, University of Leoben.

Other people I would like to thank are Dr. Curtis Witson and Dr. Singh Kameshwar (PERA Group) for the discussion and help in my questions.

To my parents, and my love.

Table of contents

List of Figures

List of Tables

Notation

B_o, oil formation volume factor

R_s, solution gas ratio

B_w, water formation volume factor

S_i, saturation of the phase i (w, wetting, n, nonwetting)

T_i, transmissibility of the phase i

ϕ, porosity

N, shape function

W, weight function

p_{ci}, capillary pressure of the phase i

f_w, fractional flow of water

q_i, flow velocity of the phase i

ρ_i, density of the phase i

Z, depth

g, gravitational acceleration

λ_i, fluid mobility of the phase i

F, flux

k, permeability

k_{ri}, relative permeability of the phase i

t, time

Superscripts:

n = old time level

n+1= new time level

x = old or new time level

Subscripts:

k = submatrix block index between 1 to J

m = matrix

o = oil

w = water

Chapter 1

Introduction

Gas condensate reservoirs are characterized by complex fluid behavior, which is different from conventional gas reservoirs. As the reservoir is depleted, the pressure fall below the dewpoint pressure, leading to condensation which in consequence will cause a two phase flow in the reservoir impacting the gas productivity and the overall gas recovery. The processes and consequences which undergo in the two phase flow have been extensively studied, however, they are still not fully understood.

One of the most important processes in gas condensate reservoir is the formation of "concentric" saturation zones, these were described by (Economides et al. 1987), they describe the existence of three saturation zones, a first region far from the well where the reservoir pressure is above the dewpoint pressure thus only a gas phase exists, a second region where the pressure is below the dewpoint pressure and liquid starts to condensate but it is not mobile, and a third region which is the near wellbore region where both gas and condensate will flow towards the well, generating a reduction in the gas mobility. This last region continued to be of special interest for many researchers, in Danesh et al. (1994) described the influence of high production rates in relative permeability, they proposed that in the very near wellbore area capillary number effects will positively influence the gas relative permeability. In order to describe the capillary number effects, different mathematical models have been proposed, the most well-known models was presented by Henderson et al. (2001) and Whitson et al. (2003), both models relate immiscible relative permeability curves with the capillary number through a function were a new relative permeability curve is calculated. With the same objective of a better understanding of gas condensate reservoirs, Bozorgzadeh et al. (2004) continued with the application of well test analysis data and pressure transient analysis, such as the Buourdet derivative curve in order to validate the size of condensate bank radius. Here they include the previously described saturation zones and the capillary number effects.

In this thesis, a well located in a gas condensate reservoir is studied. The well "M1" has been identified to be producing below the dewpoint pressure. Thus gas and condensate is produced. Moreover, a well test pressure analysis was performed, in which drawdown and buildup periods were conducted. Consequently, a pressure transient analysis of the buildup periods was executed. The conclusion of this analysis indicates the existence of a condensate bank and in the near wellbore region capillary number effects are seen. Moreover, the PVT fluid analysis which was performed has said to represent the initial composition of the reservoir fluid. Accounting with the well test and PVT data, in this thesis I perform a numerical simulation of the M1 well in order to match the well test data and the pressure transient analysis results. Accomplishing this match will result in the validity of the PVT data and propose a rock-fluid model which will include with the capillary number effects. The final matched model can be applied as base for a full field study, and thus for predictions of the condensate bank and well productivity.

First, the investigation starts with a basic introduction of the most relevant theoretical background, such as the definition of gas condensate reservoir, the concept of capillary number effects and well test analysis in gas condensate reservoirs. Next, the radial simulation model and its input data are

presented. The research continues with a sensitivity analysis, which is performed with the intention of understanding the influence of the most uncertain variables in the simulation model. Afterwards, the results and analysis of the history matching processes is given. Then, a forecast study is performed in order to understand the impact of the results in possible predictions. Finally, an overall conclusion of the thesis is presented.

Chapter 2

Theoretical Background

2.1 Literature Review

2.2 Gas Condensate Reservoirs.

One of the most important issue in reservoir engineering is the correct classification and understanding of the reservoir fluid properties and thermodynamic behavior. This must be determined at early time of the field life, and its correct determination will be critical in the field development such as the determination of the plan of depletion, methods of fluid sampling, design of surface equipment, correct estimation of volumes in place and recoverable quantities, etc. Therefore, several definitions in the classification of reservoirs have been proposed, for instance one of the classical definitions based on the fluid phase behavior is the following:

- Dry Gas
- Gas Condensate
- Volatile Oil
- Black Oil
- Heavy Oil
- Oil Sands
- Asphalts-Bitumen

In order to select in which of the above categories a given fluid belongs to, is mainly dependent on the reservoir conditions, such as temperature and pressure, equally important is the fluid composition. As shown Figure 2.1, the phase envelope of a given fluid composition will differ its classification depending on the pressure at a given reservoir temperature condition. A major difference can be noticed between a gas condensate reservoir and a gas reservoir, in a gas condensate reservoir, the system experiences two hydrocarbon phases at reservoir conditions, thus condensate liquid and gas will exist.

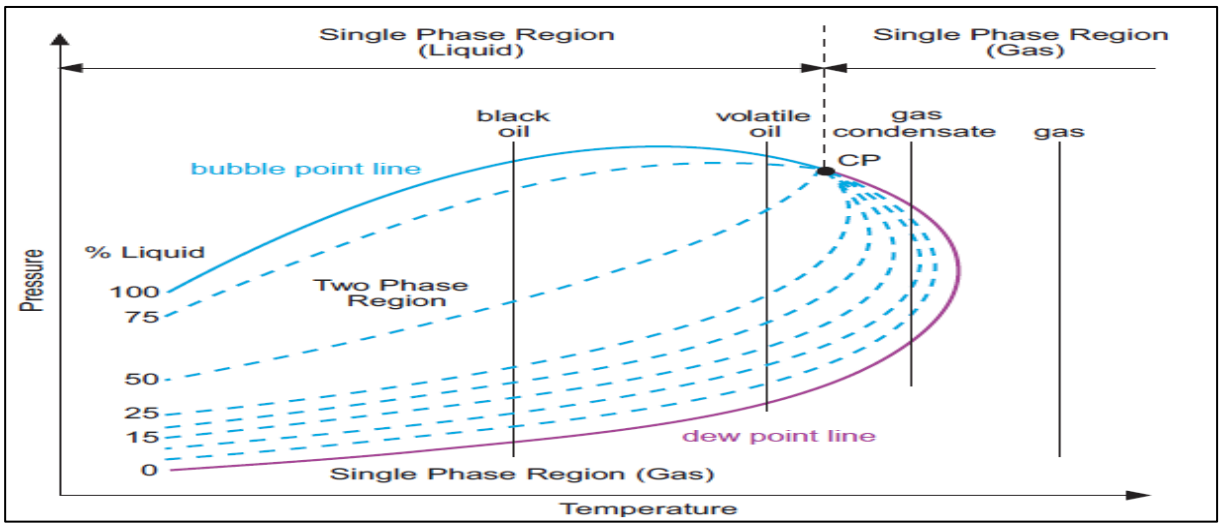

Figure 2.1 Phase Behavior of Reservoir Fluids. (Heimo A. 2015)

Moreover, as for the classification of a gas condensate reservoir, several characteristics can be distinguished from the other categories. Such as, in the phase diagram the critical point is below and to the left of the envelope, resulting that in gas condensates the content of heavy hydrocarbons is much lower than for other liquid hydrocarbon classification. Also, it is noticed that the cricondentherm point (T_{cr}) is bigger than the reservoir temperature ((T_r).

2.2.1 Gas Condensate Flow Behavior

The description of the behavior of a gas condensate fluid can be described by the interpretation of Figure 2.2, which represents a typical gas condensate phase envelope. Assuming that the initial conditions are at 6000 psia and constant temperature of 200 °F (Point A) only a gas phase, as the pressure decreases reaching the critical pressure of 4890 psia, retrograde condensation will occur. As the reservoir is being more depleted, the pressure will drop below the dew point pressure and condensate will form and start to accumulate in bigger quantities. The condensate liquid which starts to form is richer in heavier components, since they are the first components which start to condensate. Further on, as the pressure continues to decrease, more condensate drops out until it reaches a maximum liquid dropout.

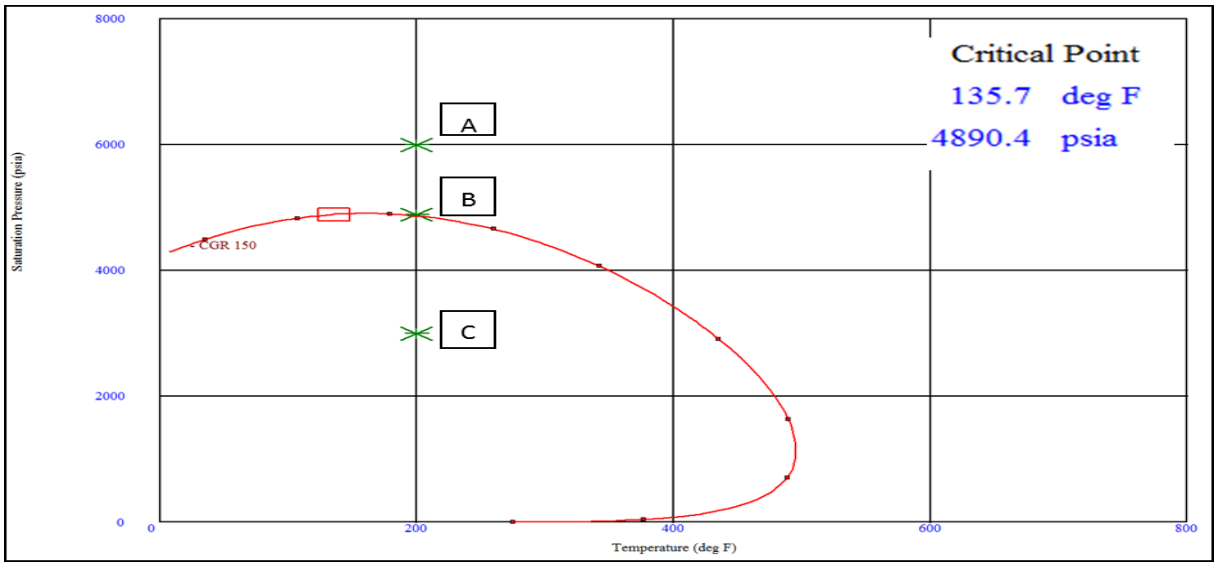

Figure 2.2 Typical gas condensate phase envelope

2.2.2.1 Flow Regimes and Gas Condensate Composition Behavior

Drawdown

Several authors (Ali et al. 1997, Economides et al. 1987, Whitson et al. 1995), have described the flow behavior of gas condensate reservoir during depletion when the Bottomhole pressure (BHP) falls below the dewpoint pressure, based on theoretical, field and laboratory investigations. Moreover, the identification of the development of different flow regions was identified, the regions are three and can be visualized in Figure 2.3, and the description of the regions is the following:

Region 1: Two phase reservoir, mobile condensate and mobile gas. (Presv<Pdew & Soc<So).

As the BHP continues to decrease during depletion, the gas condensate saturation continues to accumulate, this will increase and overcome the Soc, hence, the condensate starts to mobilize together with the gas and then it is produced. Region 1 is the main source of well impairment, due to the reduction of the gas relative permeability caused by condensate blockage.

Region 2: Two phase reservoir, immobile condensate and mobile gas. (Presv<Pdew & Soc>So)

As the reservoir pressure declines towards the well, the Presv will become lower than the Pdew. Therefore ,condensate starts to drop, and the condensate bank starts to develop. However, only gas is mobile since the condensate saturation is lower than the critical condensate saturation (Soc).

In this region, the overall gas condensate and gas composition changes with production time. The heavy components increase in the liquid phase generating changes in the phase envelope of both phases. As for the gas, this becomes leaner and the gas condensate becomes heavier in components.

Region 3: Single phase gas reservoir.

This region consists of only one phase where the reservoir pressure (Presv) is higher than the dew point pressure (Pdew). Thus, only gas is flowing and no compositional change is seen. The original gas composition is present in this region and it is constant through its limits when the condition of Presv>Pdew.

Region 4: Immediate well vicinity.

This region has the same conditions as region 1, with the difference that gas relative permeability is maintained high. Several authors have described this phenomenon (Fussel et al. 1973, Novosad 1996), one of the most accepted theories describes a velocity dependent relative permeability, where high production rates and low interfacial tension cause an increase of the relative permeability to the gas. This is called stripping effects, capillary number effects or positive coupling and it will be further discussed in this study.

The presence of these three regions may or may not exist; it is mostly dependent on which stage of the reservoir depletion the system is. For instance, if the reservoir pressure is above the dew point pressure, only region 3 will exist, or if the reservoir pressure is below the dew point pressure and the condensate saturation is below the critical condensate saturation then only region 2 and 3 will exist.

Buildup

As the well is shut in, the pressure increase towards the initial conditions. Thus, it could be expected that all the gas condensate will revaporize, due to the original PVT properties of the gas. This thought is valid when the gas condensate composition is constant with time, however, as mentioned previously, during depletion the composition of both phases (condensate & gas) changes with time, the condensate become richer in heavy components and the gas becomes leaner, while the light components are produced. These changes can be such that the in the near wellbore region the fluid modifies from having a gas condensate behavior to a critical gas condensate and finally becoming a volatile oil (Fussel et al. 1973).

Moreover, as presented in detail by Economides et al (1987) and Fussell et al. (1973), low oil revaporization is also influenced by hysteresis effect caused by the impediment of reverse fluid migration due to condensate mass accumulation and reservoir pressure gradient.

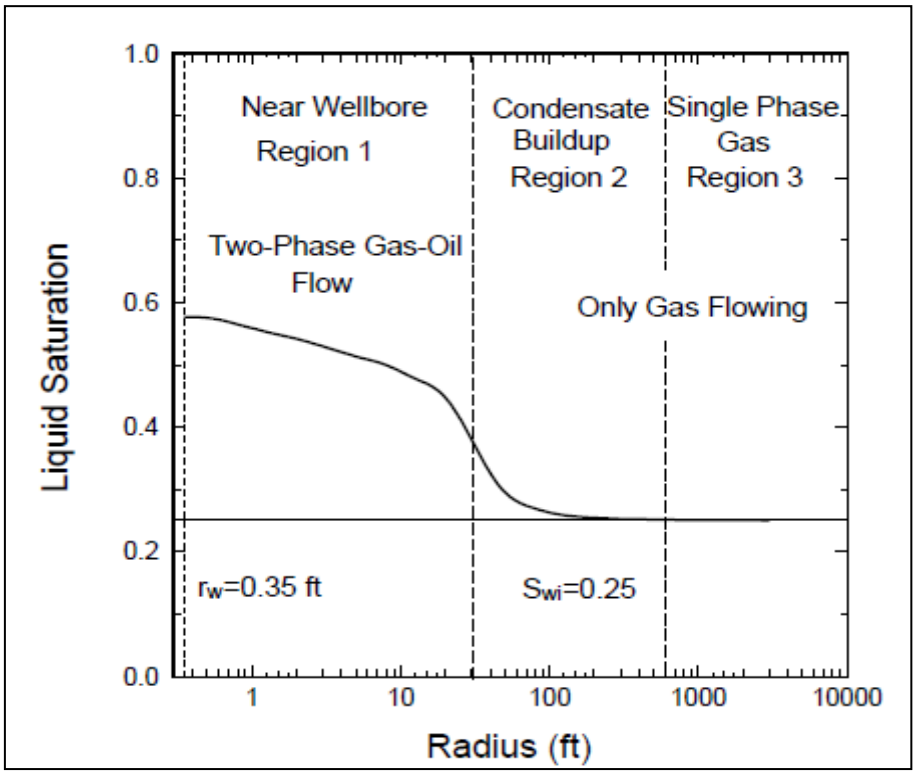

Figure 2.3 Flow Regimes in Gas Condensate Reservoirs (Whitson et al. 2000)

2.2.2 Gas Condensate Relative Permeability

As previously mentioned region 1 is of main importance in the performance of gas productivity in gas condensate reservoir, mainly due to the reduction in gas relative permeability due the flow of the gas condensate fluid within this region. Moreover, it was also mentioned that a 4th region may exist, where due to an increase in the gas velocity the relative permeability to gas is affected maintaining high values. Therefore, the chosen relative permeability model which represents all the above regions is crucial in the correct modeling of the fluid flow in gas condensate reservoirs.

2.2.2.1 Immiscible Relative Permeability Model

As one of the characteristics of fluid flow in gas condensate reservoir is an immiscible behavior with low capillary number, the relative permeability used in this study is based on the Corey model (Brooks and Corey 1966) the immiscible equations for Gas-Oil and Oil-Water system are the following:

$$Krg = Krg_{(Sorg)} * \left(\frac{Sg - Sgc}{1 - Sgc - Sorg}\right)^{ng} \quad \text{Eq. 1}$$

$$Kro = Krog_{(Sgc)} * \left(1 - \frac{Sg - Sgc}{1 - Sgc - Sorg}\right)^{no} \quad \text{Eq. 2}$$

$$Krw = Krw_{(Sorw)} * \left(\frac{Sw - Swc}{1 - Swc - Sorw}\right)^{nw} \quad \text{Eq. 3}$$

Where:

$Krw = Relative\ Permeability\ to\ the\ water.$

$Krw_{(Sorw)} = Relative\ permeability\ to\ the\ water\ at\ Residual\ oil\ Saturation.$

$Sw = Water\ Saturation.$

$Swc = Connate\ Water\ Saturation.$

$Sorw = Residual\ Oil\ Saturation\ to\ the\ water.$

$Nw = Corey\ Exponent\ of\ water.$

$Krg = Relative\ Permeability\ to\ the\ gas.$

$Krg_{(Sorg)} = Relative\ permeability\ to\ the\ gas\ at\ Residual\ oil\ Saturation.$

$Sg = Gas\ Saturation.$

$Sgc = Connate\ Gas\ Saturation.$

$Sorg = Residual\ Oil\ Saturation\ to\ the\ gas.$

$Ng = Corey\ Exponent\ of\ water.$

$Kro = Relative\ Permeability\ to\ the\ Oil.$

$Krog_{(Sgc)} = Relative\ permeability\ to\ the\ oil\ at\ Critical\ gas\ Saturation.$

$No = Corey\ Exponent\ of\ oil.$

2.2.2.2 Velocity Dependent Relative Permeability

Several authors (Botorgzadeh et al. 2007, Danesh et al. 1994 and Henderson et al. 2007) have mentioned the increment of gas mobility in the vicinity of the wellbore where two phases flow exist. This increment has been seen at high production rates and it is due to capillary number effects (positive coupling or velocity stripping). In order to explain the theory behind these effects one must first define the concept of capillary number, which is represented by the following equation:

$$Nc = \frac{v * \mu}{\sigma} \qquad \text{Eq. 4}$$

Where:

$Nc = Capillary\ Number$

$v = Gas\ Velocity$

$\mu = Gas\ Viscosity$

$\sigma = Gas - Oil\ Surface\ Tension$

As seen in equation 4, the capillary number is a function of three variables, interfacial tension, fluid viscosity and the fluid velocity (function of flow rate). Moreover, a typical flow through a porous media has a capillary number of approximately 10^{-6} (Eclipse Technical Description 2014).

Due to the importance of acknowledging the effects of capillary number in gas condensate flow behavior, different models surged in order to describe these effects. The two most known models

are the Heriot-Watt (Henderson et al. 2007) and the Fevang-Whitson (Whitson et al. 1999a), both models are now presented.

Heriot-Watt Model

This model was developed based on experimental studies; it was based on the variation of the interfacial tension. Results of this study showed that relative permeability a dependency on high fluid velocities, and as it is well known in both gas and condensate saturations. Therefore, there objective was to create a correlation which relates the effects of a high velocity-rate with relative permeability. In order to do so, they relate the capillary number (which is dependent in velocity, viscosity and interfacial tension) through a function (Eq.5, Eq. 6 and Eq. 7) in which a new relative permeability curve is calculated, this function is the velocity dependent relative permeability curve and its main impact is on the "straightening" of the relative permeability curve, which hence will mean a more miscible relative permeability curve.

$$Y = \frac{Ncb}{Nc} \quad \text{Eq. 5}$$

$$Xg = 1 - e^{m\frac{Ncb}{Nc}} \quad \text{Eq. 6}$$

$$Kr = (Y * Krb) + (1 - Y) * Krm \quad \text{Eq. 7}$$

Where:

$Nc = Capillary\ Number$

$Ncb = Base\ Capillary\ Number$

$m = Parameter\ whcih\ controls\ the\ variability\ of\ the\ critical\ fluid\ saturation$

$Krb = Base\ Input\ relative\ permeability\ curves.$

$Krm = Miscible\ Relative\ Permeability\ Curves\ (Straight\ line).$

$Kr = New\ Relative\ Permeability\ Curve.$

Fevang -Whitson Model

Similarly to the previous Heriot-Watt Model, this model proposes a generalized relative permeability model, where the immiscible relative permeability curves are linked with the miscible curves through a function which is dependent on the capillary number. However, the difference between the models is that the Fevang-Whitson model is based on a fractional flow approach. In their study they demonstrate that the main relationship that defines the steady-state flow in gas condensate wells is based on the relative permeability to the gas (Krg) as a function of the Krg/Kro, thus Krg=f(krg/kro).

The transition function is based on the following function:

$$f_I = \frac{1}{(\alpha * Nc)^n + 1} \quad \text{Eq. 8}$$

Where α is a constant which depended on the rock properties, such as in equation 9.

$$\alpha = \frac{2 * 10^4}{\sqrt{K\emptyset}} \qquad \text{Eq. 9}$$

Where K will be the rock absolute permeability and ∅ the rock porosity. Furthermore, the capillary number function is included in the relative permeability of gas by equation 10.

$$Krg = \left(f_I * K_{rgI}\right) + (1 - f_I) * K_{rgM} \qquad \text{Eq. 9}$$

Where:

$K_{rgI} = Immiscible\ gas\ relative\ permeability.$

$K_{rgM} = Miscible\ gas\ relative\ permeability.$

The limit of this model is that it can only be used for the steady-state region where both gas and oil are flowing. Nevertheless, the advantage is that only one set of parameters are required to define the model, such as α and the exponent n.

2.3 PVT Measurements in Gas Condensate Reservoirs

Conventionally, three standard laboratory experiments of pressure, volume and temperature (PVT) on reservoir fluids exist. These methods are the differential liberation experiment (DLE), constant composition expansion (CCE) and constant volume depletion (CVD). The objective of these experiments is to characterize and understand the behavior of the reservoir fluid; therefore it is necessary to acquire fluid samples which accurately reflect the composition of the reservoir fluid.

PVT in gas condensate reservoirs is different from oil PVT analysis. First the experiments required are only the CVD and CCE, secondly, however, only two experiments are carried out the PVT analysis in gas condensate reservoirs are performed in more detail. For example, the fluid heavy fraction is analyzed to identify mayor components and also it is necessary to characterize it by extended carbon groups, since phase behavior models are very sensitive to the heavy components of gas condensate systems (Danesh 1998).

2.3.1 Constant Composition Expansion (CCE).

This experiment is used to measure the dewpoint pressure, single phase gas Z-factors and oil relative volume which is the liquid dropout curve at pressure below the dewpoint pressure.

The procedure of this experiment is illustrated in Figure 2.4, and it consists of a cell which is filled with a known quantity of reservoir fluid at a constant temperature through the entire test (Isothermal process). The test starts at a pressure which is above the dewpoint pressure (In Fig. 2.4 at 6000psia), in order to secure that the fluid is at a single phase, afterwards the pressure is lowered in several steps in order to measure the expansion of the fluid, above and below the dewpoint pressure.

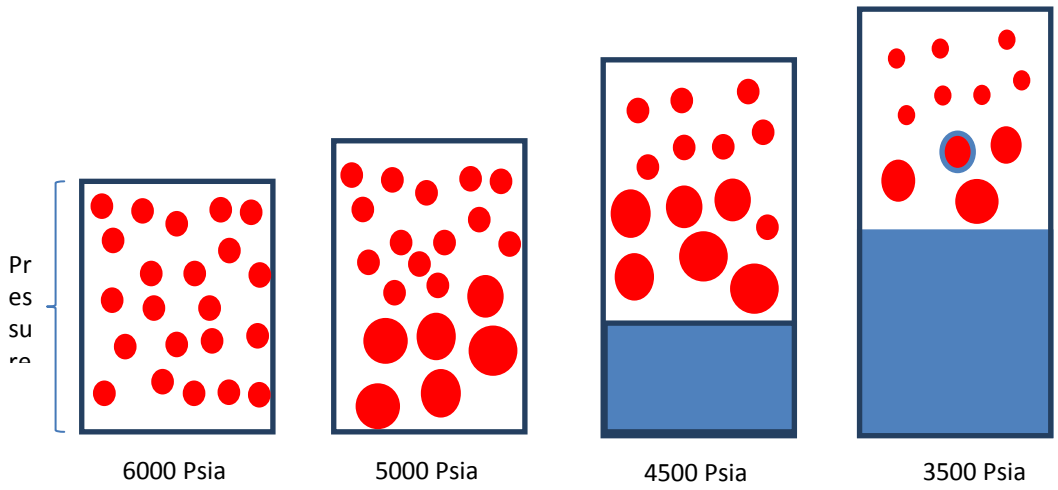

Figure 2.4 Constant Composition Expansion Experiment.

2.3.2 Constant Volume Depletion (CVD).

An important test for gas condensate fluids is the CVD, it provides a survey of the phase and volumetric changes of the sample (isothermal process). This experiment provides data that can be used directly by the reservoir engineer, such as produced –well stream composition and surface products vs reservoir pressure, liquid dropout and revaporization that occurs during pressure depletion, among others.

The process of the CVD experiment is presented in figure 2.5, the process consists of stepwise pressure depletion by increasing the cell volume. Part of the gas is expelled from the cell until the volume of the cell equals the volume at the dewpoint pressure. This process is repeated several times at different pressure steps. A more detailed explanation of the CVD and CCE experiments can be found in Danesh (1998).

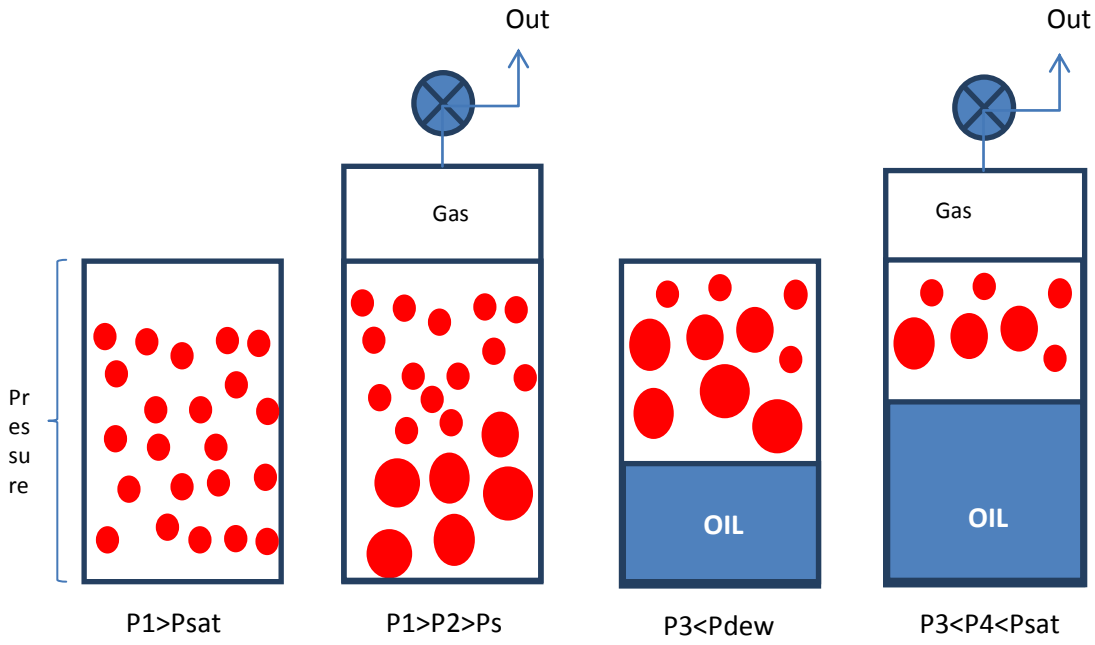

Figure 2.5 Constant Volume Depletion Experiment.

2.3.3 Equation of State (EOS).

The EOS are equations which relate pressure, volume and temperature in order to accurately describe the volumetric and phase behavior of a fluid, which could be a pure compound or a mixture. The minimum input data required to make an EOS is the specific gravity of the heaviest components, molar compositions and molecular weight. The EOS can be used to calculate the properties of all the involved phases, thus guaranteeing the consistence in reservoir processes that approach critical conditions (Whitson et al. 1999b).

The most simple EOS known is the ideal gas equation (Eq. 10), where p represents the pressure, V is the volume, R is a constant value for each gas, T the temperature and n is the number of moles.

$$pV = nRT \qquad \text{Eq. 10}$$

The equation 10 is as its own name says used only for ideal gases; however the reservoir fluids do not behave as an ideal gas, thus equation 10 is not valid. Nevertheless, Eq. 10 is the base equation for the Cubic EOS's which are commonly applied in reservoir engineering. The most famous Cubic EOS in reservoir engineering is the Peng Robinson EOS (PR EOS), which was developed in 1976 at the University of Alberta. The PR EOS is given by

$$p = \frac{RT}{v-b} - \frac{a}{v(v+b)+b(v-b)} \qquad \text{Eq. 11}$$

and:

$$a = \Omega_a^o \frac{R^2 T^2}{Pc} a_o \qquad \text{Eq. 12}$$

$$b = \Omega_b^o \frac{RT}{Pc} \qquad \text{Eq. 13}$$

$$a_o = \left[a + m(1 - \sqrt{T_r}\right]^2 \qquad \text{Eq. 14}$$

$$m = 0.3796 + 1.485\omega - 0.1644\omega^2 + 0.01667\omega^3 \qquad \text{Eq. 15}$$

Where:

$\omega = Acentric\ Factor$

$Tr = Reduced\ Temperature$

$Pc = Critical\ Pressure$

$a = "Attraction"\ parameter$

$b = "Repulsion"\ parameter$

$\Omega_a^o = 0.45724$

$\Omega_b^o = 0.07780$

An important requirement in gas condensate reservoir is stated in Patacchini et al. (2014), which is that for the EOS development is necessary to have a set of components that descries all the reservoir

samples of the given field. Due to the possibility of having heterogeneities in the reservoir, which might lead to different reservoir fluids in different parts of the reservoir.

2.4 Well Test Analysis in Gas Condensate Reservoirs.

2.4.1 Introduction

The basic equation in which all the pressure transient analysis (PTA) is performed is the diffusion equation, which in its radial form is given by

$$\frac{\partial P}{\partial t} = \frac{k}{\phi \mu C_t} \frac{1}{r} \left[\frac{\partial}{\partial r} \left(r \frac{\partial p}{\partial r} \right) \right] \qquad \text{Eq. 16}$$

This equation is derived when combining the simplest form of the Darcy equation, the material balance relation (slightly compressible fluid assumption) and the law of conservation of mass. Thus it describes the flow of a single phase slightly compressible fluid in a homogeneous reservoir.

However, the assumptions made for the above equation are rarely met. Especially for dry gas reservoirs and gas condensate reservoirs, were the fluid properties (compressibility and viscosity) are strongly dependent on pressure. Moreover, in the case of gas condensate reservoir the assumption single phase is not valid since multiphase flow may occur.

As seen previously equation 16 cannot be applied for the case of having a compressible fluid, for instance the case of a gas. In order to extend the diffusivity equation for gases Al-Hussainy and Ramey (1966) introduced the called pseudopressure function is introduced, which is the following:

$$m(p) = 2 \int_0^P \frac{P}{\mu Z} dP \qquad \text{Eq. 17}$$

This pseudopressure equation introduces nonlinearities to the diffusivity equation (Eq. 16), which will now acquire the form of:

$$\frac{\partial m(P)}{\partial t} = 0.0002637 \frac{k}{\phi \mu C_t} \frac{1}{r} [\nabla^2 m(p)] \qquad \text{Eq. 18}$$

Equation 18 can be considered as a linear equation only when the terms outside of the derivate (diffusion term) are constant through all time. However, this requirement is not always met, especially when a pressure gradient occurs and the viscosity and compressibility will have different values in different parts of the reservoir. In analytical solutions of equation 18 this issue is solved by the use of psuedotime function and by a material balance correction. However, for numerical solution (Numerical Reservoir Simulation) this issue is not perceived, mainly because the gas diffusivity equation is entered in each cell, thus accounting for the pressure changes in “local” and “global” scale. The difference of solving the gas diffusivity equation and the “liquid” diffusivity equation by the use of a numerical simulator is that for the case of gases a nonlinear solver must applied. It must be mentioned that by using a numerical model the solution of the equation 18 is much more rigorous and in many cases much more precise than analytical models.

2.4.2 Pressure Transient Analysis (PTA).

The pressure transient analysis is a developed methodology which helps to interpret the data, which was acquired during well test such as:

- Flow tests
- Drill-Stem test
- Buildup Test
- Production Test
- Drawdown Test
- RFT
- Interface Test.

As for the interest of this study the data acquired was from a Buildup and Drawdown Test. However, the PTA was only performed to the Buildup data, specifically studying only the Bourdet Derivative, thus only this theory of the PTA for Buildup data is presented in this theoretical section.

2.4.2.1 Buildup PTA.

A Buildup test is performed usually after a Drawdown period which is when a well is produced at a constant rate during a specified period of time (t_D). After the drawdown period the well is shut in and the pressure is again recorded for a period of time (t_B). Commonly, for gas condensate reservoir the most valuable data is obtained from the Buildup test and its interpretation is done by means of the Bourdet Derivative.

The derivative analysis is used in order to estimate the values of the parameters such as permeability and skin, also crucially for gas condensate reservoirs it is used to identify the flow regimes present in the reservoir. The derivate is defined as the slope of the data when plotted in a semilog scale; this plot leads to the Bourdet Derivative plot which is defined as the slope of the semilog plot displayed in a loglog plot, such as (Bourdet D. 1983):

$$\Delta p' = \frac{d(\Delta p)}{dln(\Delta t)} = \Delta t \frac{d(\Delta p)}{d(\Delta t)} \qquad \text{Eq. 19}$$

Where the Bourdet derivative is calculates using a simple three-point approximation formula, as

$$Bourdet\_\Delta p' = \frac{\left(\frac{\Delta P_{i-1}}{\Delta T_{i-1}}\right)\Delta \ln(T_{i+1}) + \left(\frac{\Delta P_{i+1}}{\Delta T_{i+1}}\right)\Delta \ln(T_{i-1})}{\Delta \ln(T_{i-1}) - \Delta \ln(T_{i+1})} \qquad \text{Eq. 20}$$

The derivative plot can be visualized in figure 2.4. Here the importance and practicality of the derivative is highlighted, one can see that depending on the shape of the curve the different fluid mobilities and flow regions (Bilinear, linear, and radial flow) can be identified, moreover it shows that one can identify which part of the curve represents the regions of the reservoir from the well, such as the near wellbore region, the reservoir region and the boundaries.

The Bourdet derivative plot is particularly (as it will be presented in this thesis) important for gas condensate reservoirs. As it has been demonstrated in previous studies (Botorgzadeh et al. 2006), it is possible to identify from the derivative curve (Fig. 2.5) the different saturation regions which were presented in the section 2.2. This information is crucial in further economical estimations such as well productivity and production impairment.

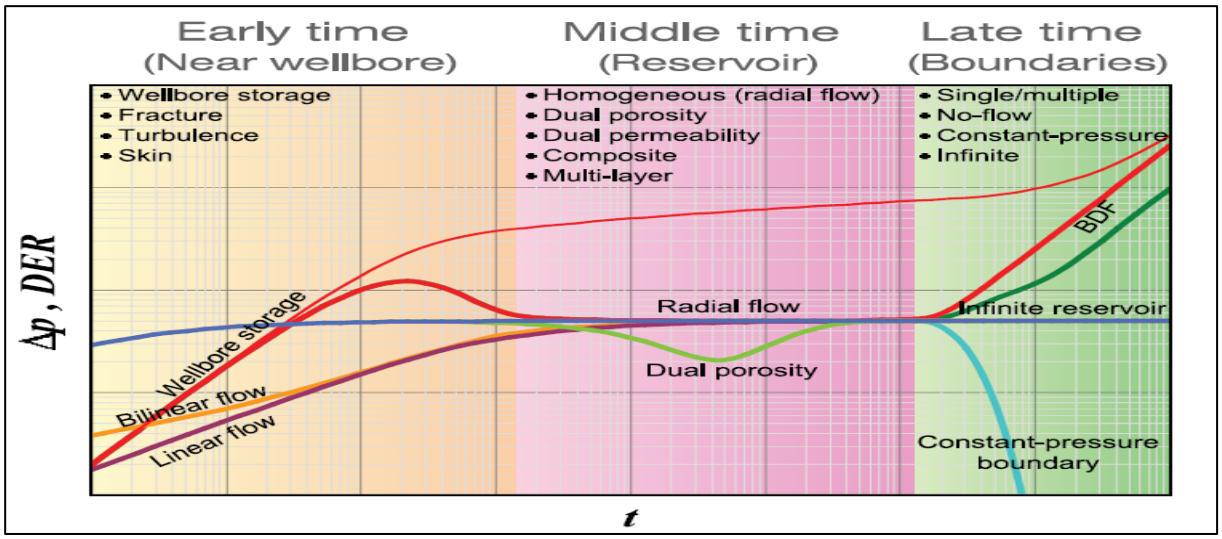

Figure 2.4 Bourdet Derivative, lol-log plot. (Feteke Association 2012)

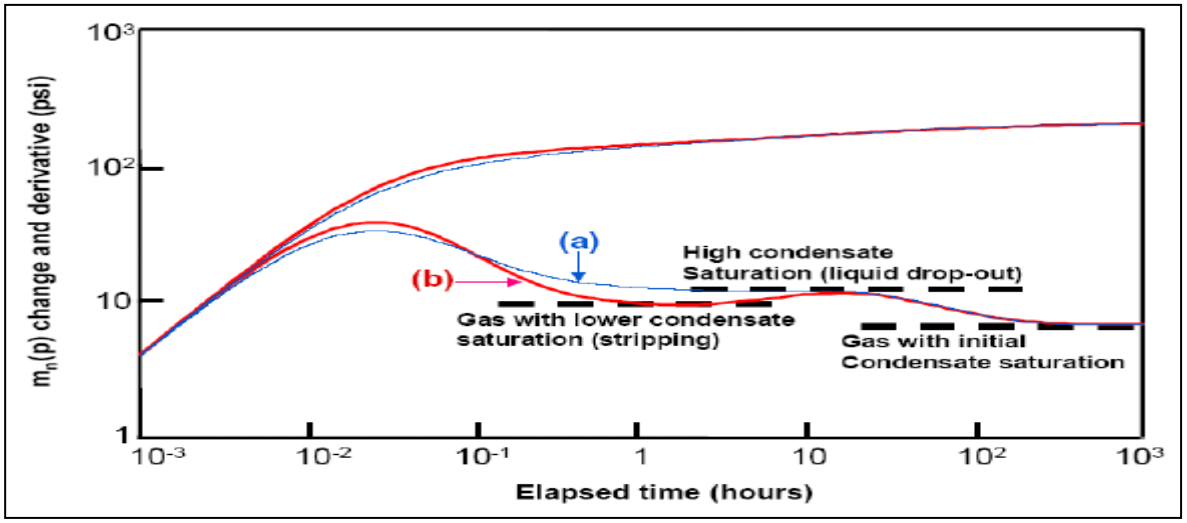

Figure 2.5 Bourdet Derivative-Gas Condensate Reservoir, lol-log plot. (Botorgzadeh et al. 2006)

Chapter 3

Gas Condensate Reservoir Simulation Model Description

3.1 Introduction.

The principal objective of this study is to model and understand the performance of the well test analysis performed in the well M1, which is located in a gas condensate reservoir. Thus, with the help of numerical simulation software and well test analysis software, a 3-Dimensional, radial grid model was developed and evaluated. Due to the features of a gas condensate reservoir and in pursue of accurate results, a fine grid radial model was developed using the compositional simulator E300 by Schlumberger.

Therefore, this section presents a description of the simulation grid, the input parameters such as the petrophysical data and PVT model.

3.2 Simulation Grid.

3.2.1 Implemented Grid Model.

A fine grid-radial model consisting of 953 cells in radial direction was defined. The grid dimensions in the radial direction are presented in Table 3.1. The grid cells are spaced with an increment of$\Delta = 0.01$, so that:

$$D_r = \Delta + D_{r-1} \qquad \text{Eq. 4}$$

Where:
D_r = Grid size dimension (feet).
Δ= Constant increment (feet).
D_{r-1} = Grid size dimension of the previous cell (feet).

Moreover, the grid consists of 1 layer in Z-direction; the size of this cell represents the thickness of the production layer, which is equal to 164 ft (petrophysical interpretation). A single producer well lies at the center of the reservoir and is assumed to be perforated across the height of the production layer. The radius of the first cell is equal to the increment, thus 0.01 ft. The external radius of the reservoir (5010.45 feet) was defined in order to consider an infinite effect, as it is desired that the pressure never reaches the boundary.

The grid can be visualized in figures 3.1 and 3.2.

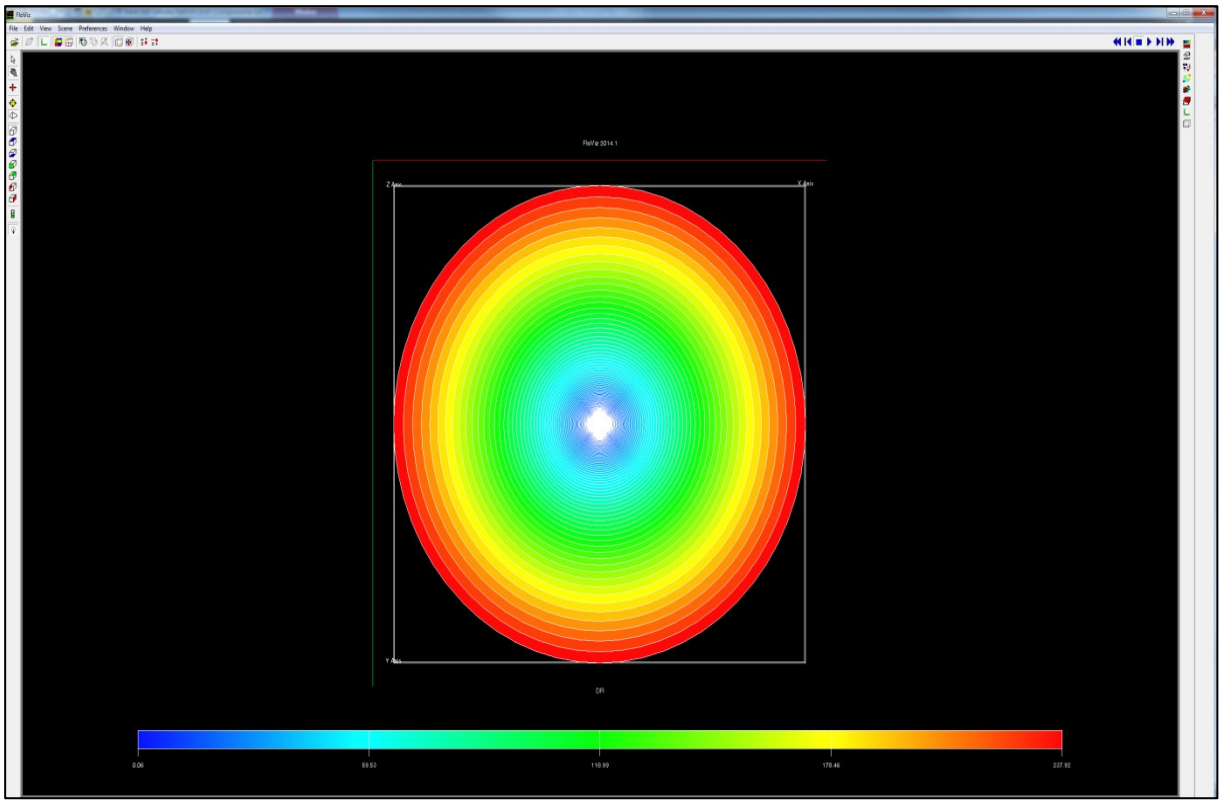

Figure 3.1. Radial Grid Model Dimensions

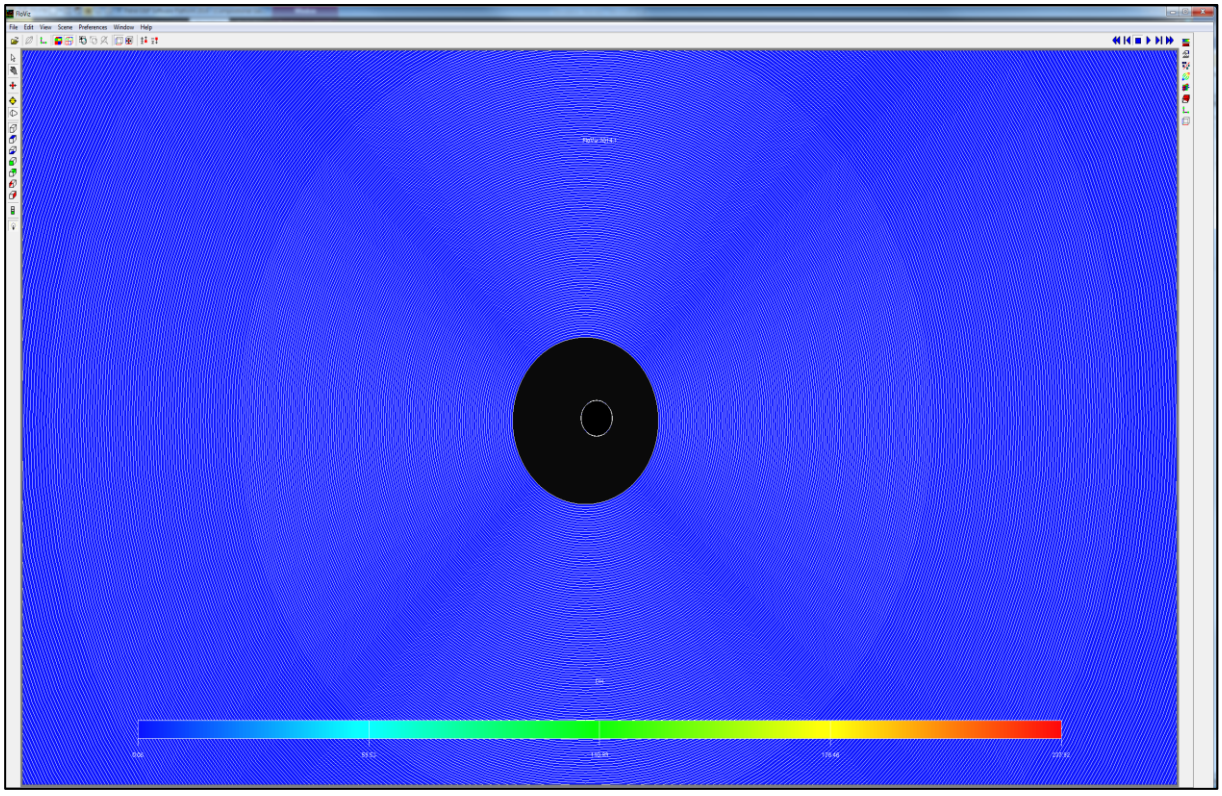

Figure 3.2. Radial Grid Model Dimensions, Zoom in the near wellbore region

Cell Number	Radius (ft)	Cell Number	Radius (ft)	Cell Number	Radius (ft)	Cell Number	Radius (ft)	Cell Number	Radius (ft)
125*	0,06	842	5,7	878	24,24	914	55,74	950	100,2
75*	0,07	843	6,04	879	24,94	915	56,8	951	101,62
150*	0,08	844	6,39	880	25,65	916	57,87	952	103,05
25*	0,09	845	6,75	881	26,37	917	58,95	953	104,49
435*	0,1	846	7,12	882	27,1	918	60,04		
811	0,12	847	7,5	883	27,84	919	61,14		
812	0,15	848	7,89	884	28,59	920	62,25		
813	0,19	849	8,29	885	29,35	921	63,37		
814	0,24	850	8,7	886	30,12	922	64,5		
815	0,3	851	9,12	887	30,9	923	65,64		
816	0,37	852	9,55	888	31,69	924	66,79		
817	0,45	853	9,99	889	32,49	925	67,95		
818	0,54	854	10,44	890	33,3	926	69,12		
819	0,64	855	10,9	891	34,12	927	70,3		
820	0,75	856	11,37	892	34,95	928	71,49		
821	0,87	857	11,85	893	35,79	929	72,69		
822	1	858	12,34	894	36,64	930	73,9		
823	1,14	859	12,84	895	37,5	931	75,12		
824	1,29	860	13,35	896	38,37	932	76,35		
825	1,45	861	13,87	897	39,25	933	77,59		
826	1,62	862	14,4	898	40,14	934	78,84		
827	1,8	863	14,94	899	41,04	935	80,1		
828	1,99	864	15,49	900	41,95	936	81,37		
829	2,19	865	16,05	901	42,87	937	82,65		
830	2,4	866	16,62	902	43,8	938	83,94		
831	2,62	867	17,2	903	44,74	939	85,24		
832	2,85	868	17,79	904	45,69	940	86,55		
833	3,09	869	18,39	905	46,65	941	87,87		
834	3,34	870	19	906	47,62	942	89,2		
835	3,6	871	19,62	907	48,6	943	90,54		
836	3,87	872	20,25	908	49,59	944	91,89		
837	4,15	873	20,89	909	50,59	945	93,25		
838	4,44	874	21,54	910	51,6	946	94,62		
839	4,74	875	22,2	911	52,62	947	96		
840	5,05	876	22,87	912	53,65	948	97,39		
841	5,37	877	23,55	913	54,69	949	98,79		

Table 3.1 Grid Cell Dimensions

3.3 Input Data.

3.3.1 PVT Data.

A surface separator fluid sample and its PVT analysis were available for the well M1. The details of the fluid sample are presented in table 3.2. Furthermore, the PVT study consisted of experiments such as constant composition expansion (CCE), constant volume depletion (CVD) and single stage flash. The results of these experiments indicate that the reservoir fluid can be classified as a rich gas condensate fluid.

It must be mentioned that between the years 2003 (After the well test analysis date) and 2011 (PVT study), the well was closed, thus as no hydrocarbon production was performed it is assumed that the PVT sample represents the initial conditions of the reservoir.

Moreover, after the PVT study was completed, the modeling of an Equation of State (EOS) was elaborated by the group PERA (Petroleum Engineering Reservoir Analyst). The objective of this study was the development a fluid characterization model based on the measured PVT data. Therefore, a

41-component EOS fluid characterization based on Peng-Robinson (1979) EOS model with volume shift was developed, for the viscosity calculations the Lorentz-Bray-Clark correlation was used. Afterwards the EOS model was compared with the PVT sample results in order to validate its accuracy, the results are presented in Figures 3.2 to 3.4.

As one of the objectives obtained from this study is to implement the EOS model into a radial grid simulation model which can be afterwards incorporated in a full field simulation model, it is impractical for various reasons (memory, CPU), to used such a detailed 41 EOS component model. Consequently, a pseudoization procedure was applied until developing a final EOS model of 8 components. The final composition of the 8-component EOS model is presented in table 3.3.

Well	**M1**
Test (12-2011)	CIT
Sample Type	Separator
Reservoir Pressure	5360 psia
Reservoir Temperature	220 °F
Separator Conditions	
Pressure	5360 psia
Temperature	77 °F
API	54 °
Recombination CGR	
Sep-bbl/MMscf	193
STB/MMscf	156
Reservoir Fluid (Zero Flash)	
CGR	115 STB/MMscf
C1	72.8 mole %
API	48.8°
Pdew	4635 psia
C7+	8.2 mole %
Temp	220 °F

Table 3.2. Summary of the reservoir fluid samples

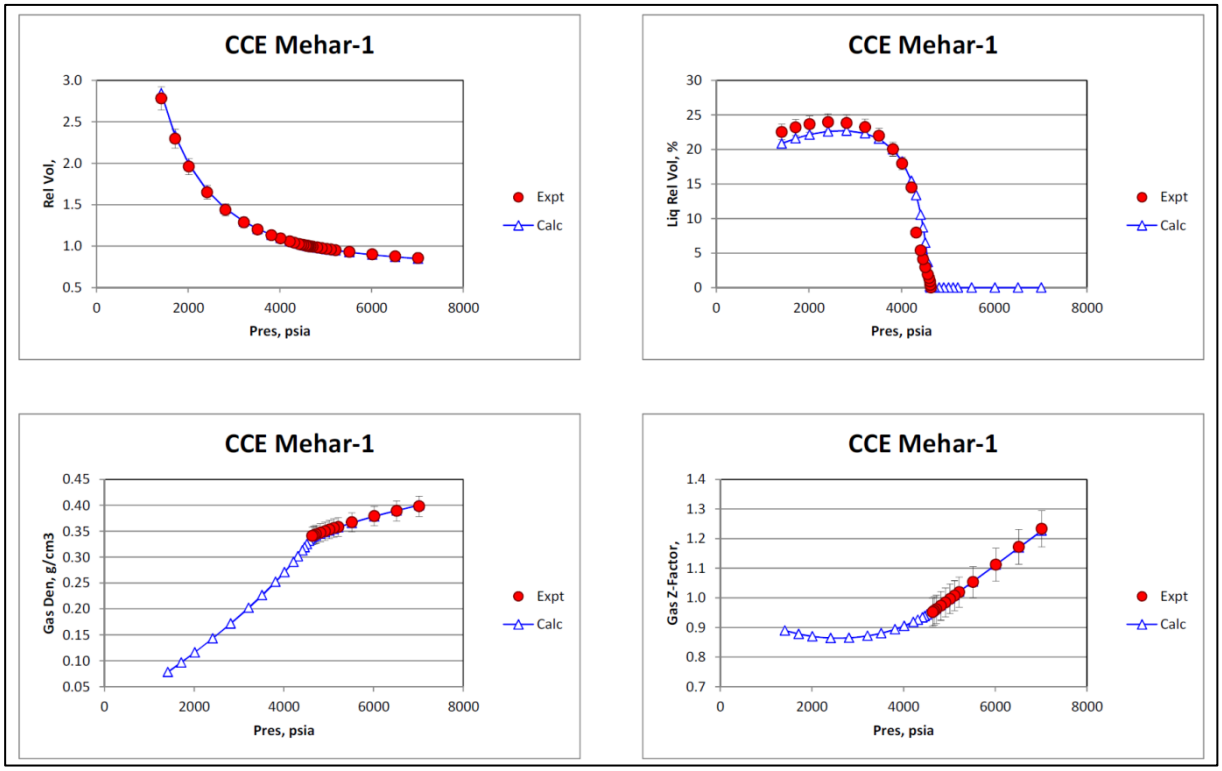

Figure 3.3. Measured and EOS-41comp predicted PVT properties from CCE.

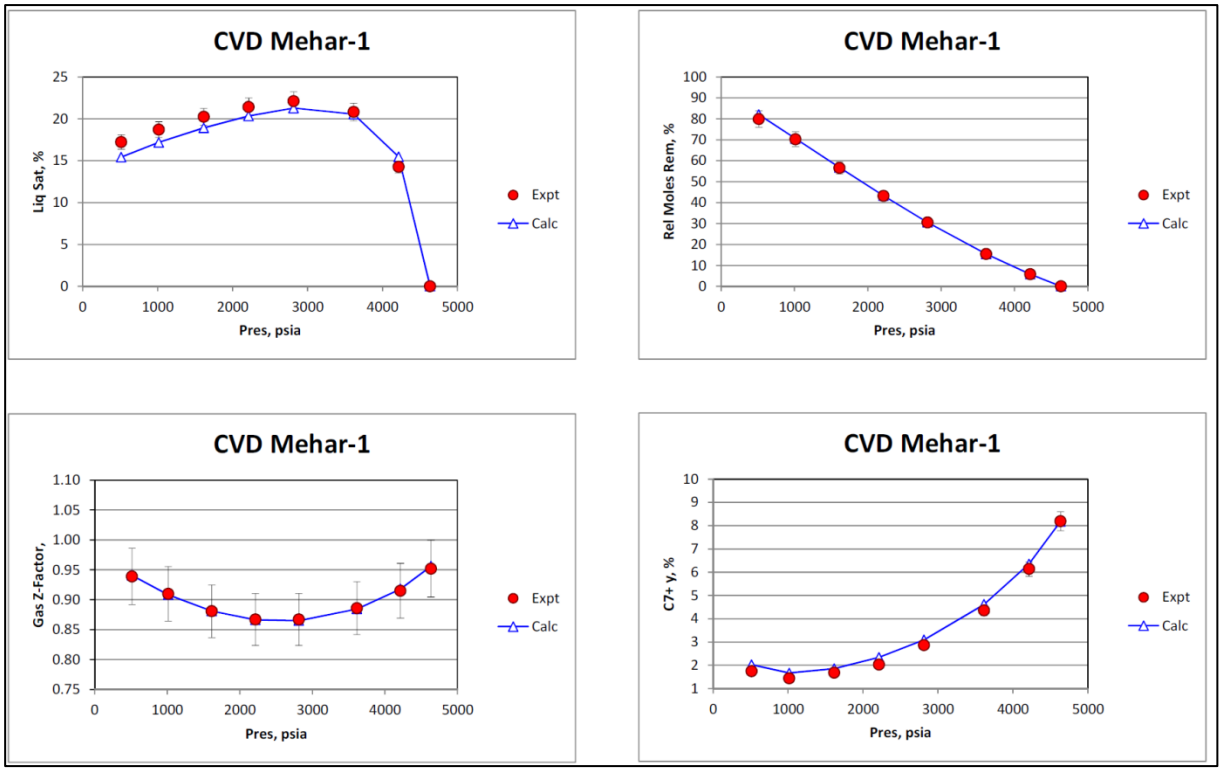

Figure 3.4. Measured and EOS-41comp predicted PVT properties from CVD

Well	M1
EOS	Peng Robinson (1979)
Viscosity	LBC correlation
8 Components Model	
Components:	Mole %
C1N2	76.0647
C2C3CO2	9.9271
C4C6	5.8310
C7C8	3.2792
C9C10	2.0281
C11C14	1.7409
C15C35	1.1260
C36+	0.0031

Table 3.3 8-Component EOS Model (PERA Company Results)

3.3.2 Relative Permeability Model.

Relative permeability curves have a substantial impact in the reservoir well performance for gas condensate reservoirs, even more when the pressure is below the dew point pressure and multiphase flow occurs. Thus, an accurate laboratory measurement of this property would the ideal case. However, this is rarely possible.

Regarding this study, no data of Special Core Analysis (SCAL) was available. Thus, it was necessary to use relative permeability correlations in order to generate the data. Therefore, Corey immiscible relative permeabilities correlations were used, the equations for Corey correlations were presented in Chapter 2. It can be mentioned that several researches such as Botorgzadeh et al (2007), have applied Corey correlations in the study of gas condensate reservoirs.

Due to the uncertainty of parameters required for the calculation of the relative permeabilities curves (Corey correlation); a sensitivity analysis was performed in order to guarantee the consistency of the results with the well test analysis and the history matching. Hence, the curves are presented in sections 4 and 5.

Chapter 4

Sensitivity Analysis

A sensitivity analysis is performed as an advantage in understanding the impact of the selected parameters in the undergoing study. Therefore, the following chapter presents a sensitivity study which attempts to increase the confidence of the simulation results by understanding the impact of the most uncertain variables.

The selected parameters for the sensitivity study are presented in table 4.1. Regarding the relative permeability curves, velocity dependent relative permeability model and absolute permeability, they were selected mainly due to the non-availability of the data. On the other hand, the well radius value was known, however, as a result of inconsistency between the simulation results and the observed data this parameter was considered in the sensitivity study.

Parameter
Relative Permeability Curves
Wellbore Radius
Velocity Dependent Relative Permeability Curves

Table 4.1 Sensitivity Parameters

As indicated previously, the objective of this research is focused on the modeling of the well test analysis performed in well M1. Therefore, the Sensitivity analysis will be done while simulating the well test data which is presented in the following subsection 4.1.

4.1 Well Test Data.

A Drill Stem Test (DST) was performed in the well M1 in the year 2003. The objective of this test was to evaluate the hydrocarbon potential in the M-Sand from the interval 3581-3620 meters. The test involved four drawdown periods and three buildup periods. Table 4.2 presents a summary of the DST data.

Test	DST
Perforation interval	3581-3620 m
Mid-perforations	3600.5
Choke Size	40/64”
Gauge Depth	3319.26 m

Table 4.2 DST Summary

The data presented in figure 4.1 represents the gas flow rates and bottomhole pressures of the entire test, which consisted of four flow and three buildup period. Although, all the data of the well test is presented, this study is focused mainly on first drawdown and first buildup period (DD1 and BU1).

The calculation of Log-Log plot of pressure and pressure derivative for buildup 1 (Fig. 4.2), was performed using the well test analysis software, KAPPA. It should be noticed that although, KAPPA software allows calculations using analytical models (i.e. Radial Composite) and numerical simulation,

the software was used for the calculation of the derivative only, and the display of the results. Thus, no simulation model was executed with KAPPA.

Hence, as no simulation or analytical model was executed with KAPPA, the only calculation done by the software is to calculate the pseudo-pressure (with input data from E300), the Log-Log plot and derivative of the pseudo-pressure. This workflow can be visualized in figure 4.3.

The input data required for KAPPA to perform the previous calculations are the following:

- Pressure Data. (E300-Results & Well-Test History data)
- Elapsed Time. (E300-Results & Well-Test History data)
- Z-Factor. (PVT Data)
- Gas Viscosity. (PVT Data)

Analyzing the Bourdet pressure derivative curve one can identify the zones which were previously mentioned in the theory section. The first stabilization of the pressure derivative is seen between the times 0.01 and 0.1 (hr), this region is identified as the near wellbore region and as we will see in the following sections, it is influenced by parameters such as the wellbore radius and the called striping effects. The second stabilization is identified between the times 0.1 and approximately 10 (hr), this period is described as the condensate build up region or 2nd region. Finally the 3rd stabilization is defined after 10 hr, which represents the gas with the initial condition.

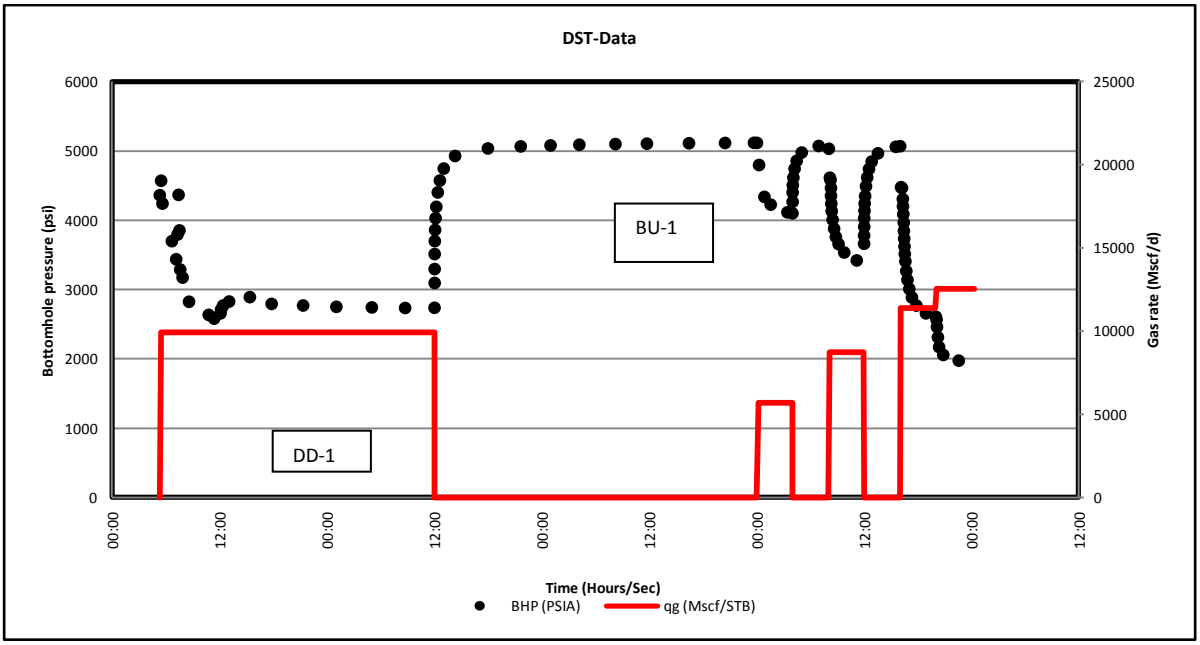

Figure 4.1 M1- DST data for the M1 well. Four drawdown periods and 3 buildup periods.

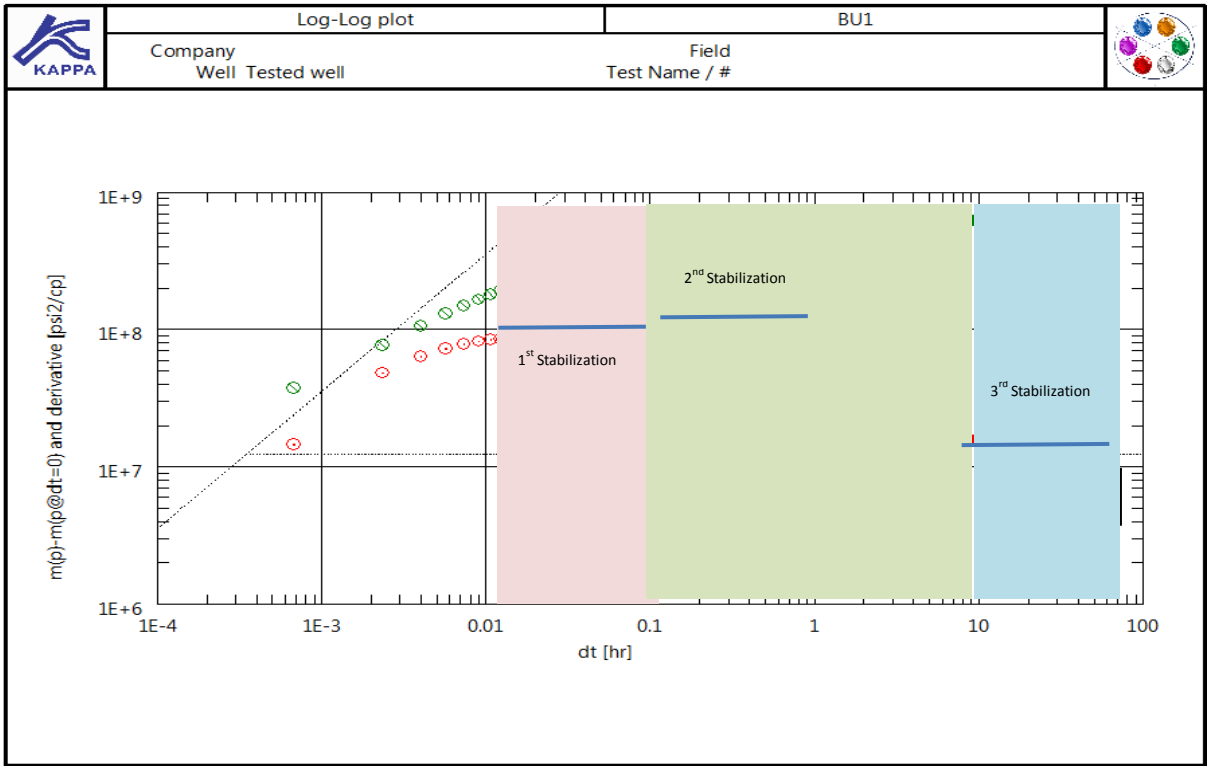

Figure 4.3. M1- Log-Log plot (green curve) and Pressure derivative (red curve) for BU1

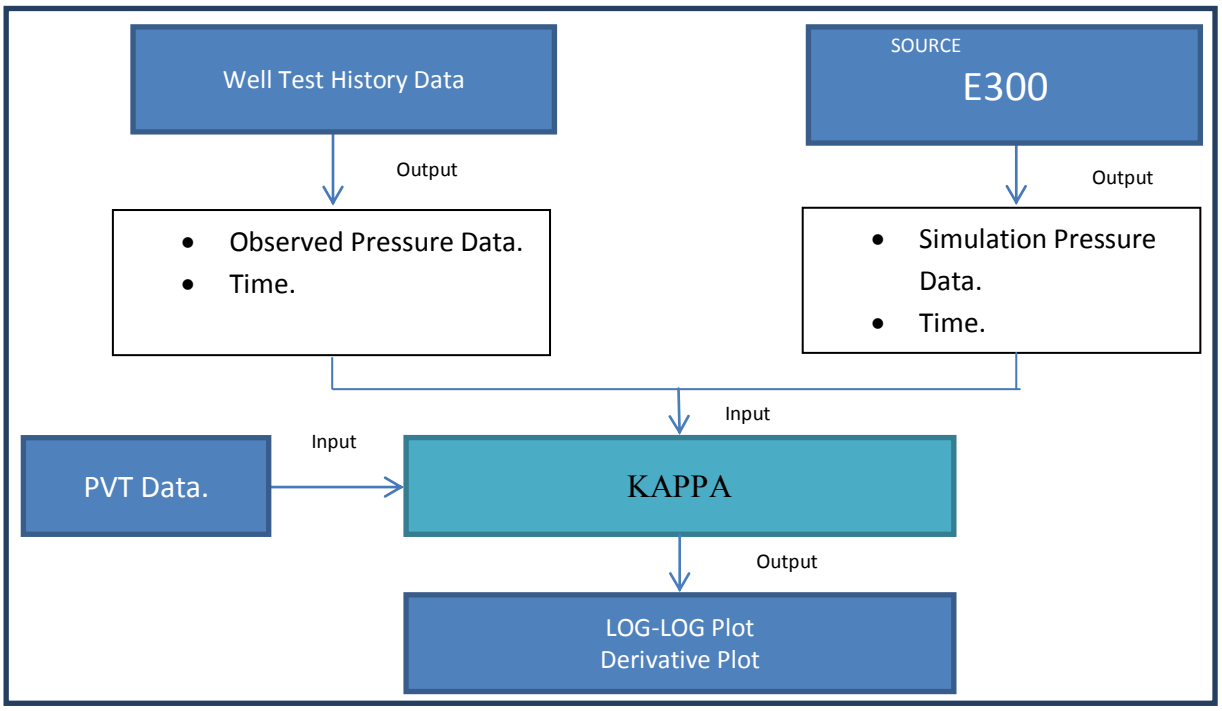

Figure 4.2. Workflow for Pressure Data Analysis

4.2 Effects of Relative Permeability Curves.

The definition of one relative permeability model to represent the fluid flow of a gas condensate reservoir is very complex (Montzeri et al. 2011). The dependence in capillary pressure, flow rate, fluid

compositional change, interfacial tension, and the not always available laboratory measurements, makes the relative permeability curves one of the most uncertain parameters in the characterization of rock-fluid properties.

The relative permeability curves used are based on three phase system (gas, oil, water), using Corey immiscible relative permeability equation (Chapter 2), a total of 11 curve sets (Table 4.2) were evaluated. The parameters studied are the Corey exponents for gas and oil (n_g,n_o), gas relative permeability at irreducible oil saturation ($K_{rg(Sorg)}$), oil relative permeability at connate gas saturation ($K_{ro(Sgc)}$) and residual oil saturation (S_{org}).

Model	S_{gc}	S_{oc}	n_g	n_o	$K_{rg(Sorg)}$	$K_{ro(Sgc)}$
1	0	0.15	3,5	3,5	0.8	0.8
2	0	0.05	3,5	3,5	0.8	0.8
3	0	0.3	3,5	3,5	0.8	0.8
4	0	0.15	2	2	0.8	0.8
5	0	0.15	3,5	2	0.8	0.8
6	0	0.15	2	3,5	0.8	0.8
7	0	0.15	3,5	3,5	1	0.8
8	0	0.15	3,5	3,5	0.4	0.8
9	0	0.15	3,5	3,5	0.8	1
10	0	0.15	3,5	3,5	0.8	0.4

Table 4.2 Relative Permeability models

In order to obtain a better understanding of the individual influence of each parameter in the results, a base model was taken as reference (Model 1), where through the different sensitivities the parameters which were not been studied were kept constant and equal to Model 1. Models 1-3 study the influence of $S_{org,}$ models 4-6 consider the impact of n_g and n_o and finally model 7-11 contemplate changes in $K_{ro(Sgc)}$ and $K_{rg(Sorg)}$.

The oil-water relative permeabilities and the following parameters (Table 4.3.) were constant through all the sensitivities runs:

Parameter	Value
Absolut Permeability (Kabs)	2.63 mD.
Wellbore Radius	1.6 Ft.
Porosity	5%
Rock Compressibility @ Pref	9.8141 E-7 1/psi

Table 4.3 Reservoir parameters

4.2.1 Critical Oil saturation.

Critical oil saturation defines the threshold value at which the oil starts to get mobile. Thus, it can be expected that for different critical values the productivity index and condensate buildup will be influenced.

Model 1, 2 and 3 represent the Sensitivity cases for the critical oil saturation study. Figure 4.2 displays the BHP results for the three models. As expected, model 3 which has the highest value of

critical oil saturation (Soc=0.3), has the highest decline in the BHP, this is due to a bigger impairment of the well productivity generated by a higher accumulation of the condensate buildup (Fig. 4.3), and in consequence a lower gas productivity index (Fig. 4.4) which forces the BHP to decrees in order to meet the required amount of gas constraint.

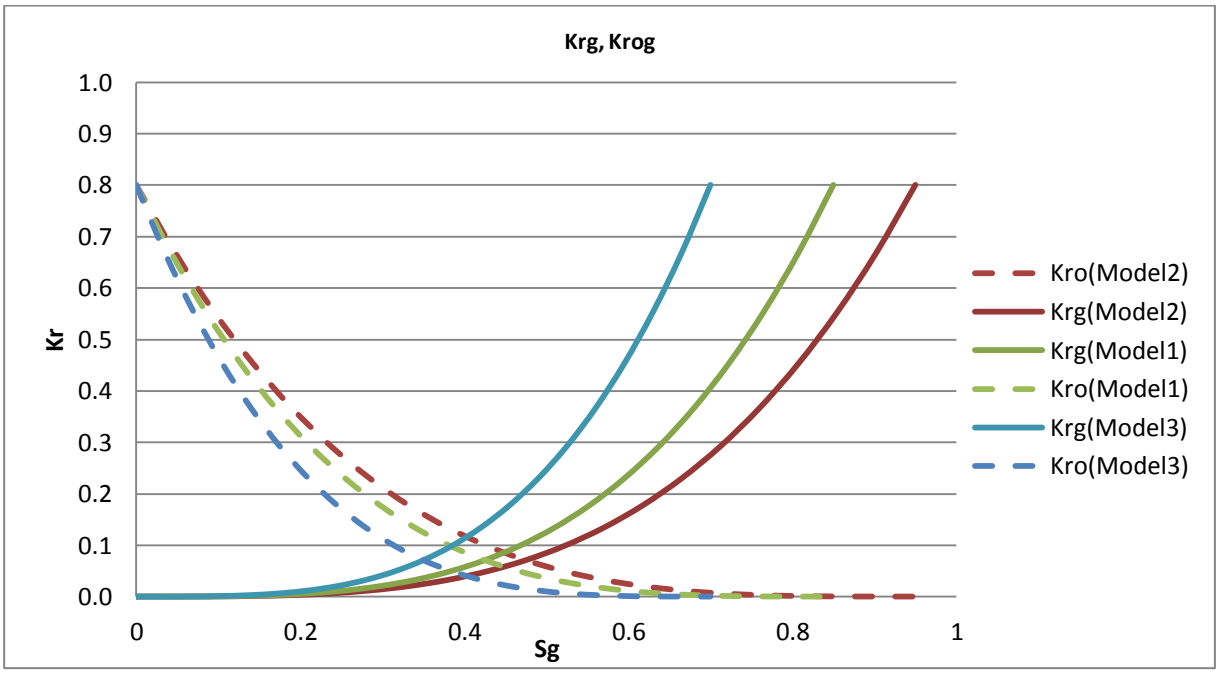

Figure 4.1. Relative Permeability for Critical Oil Saturation Sensitivity

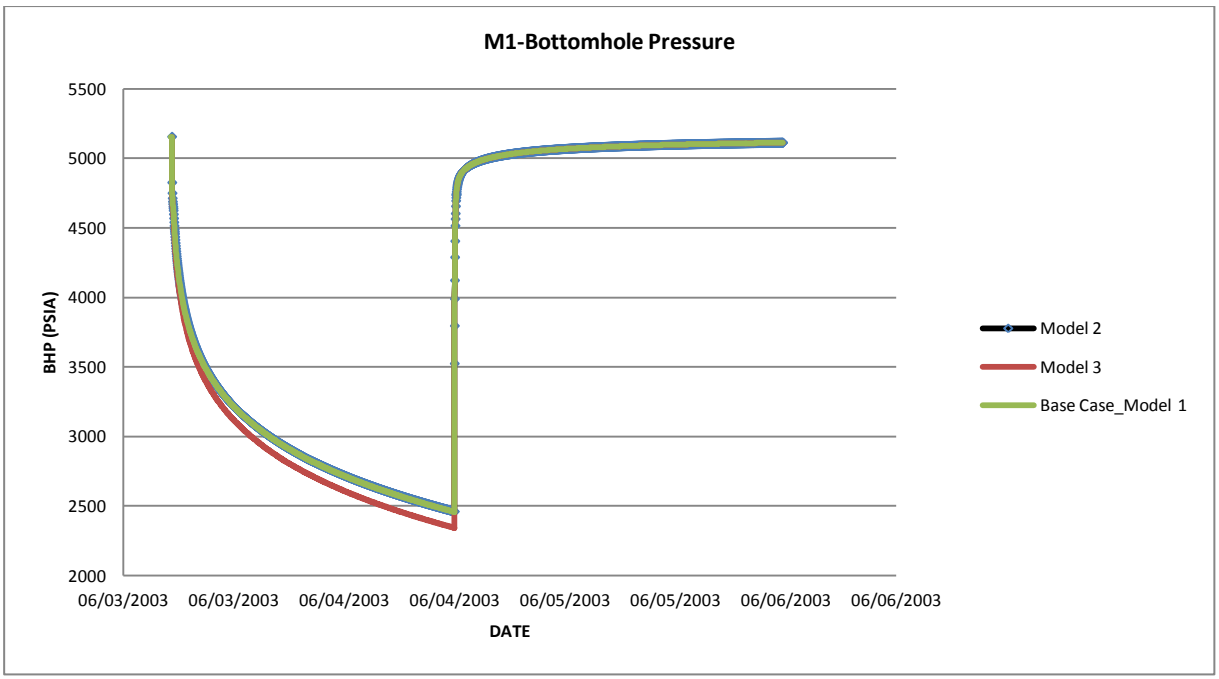

Figure 4.2. Bottomhole Pressure- Soc Analysis

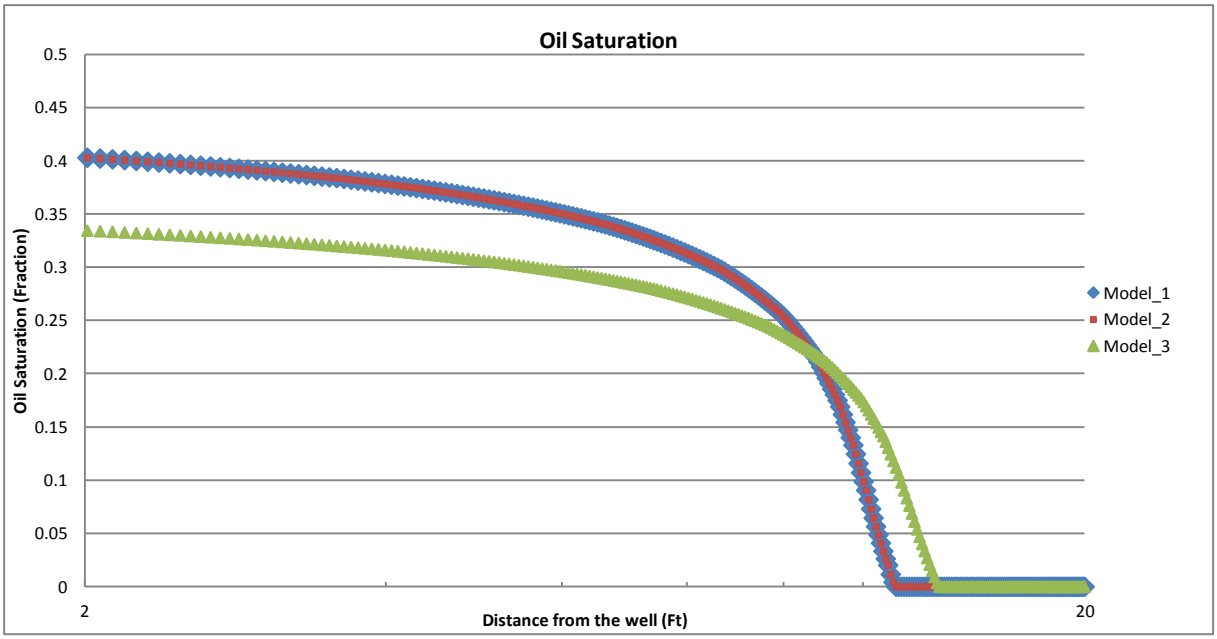

Figure 4.3. Oil Saturation Pressure for Soc Analysis (End of Drawdown)

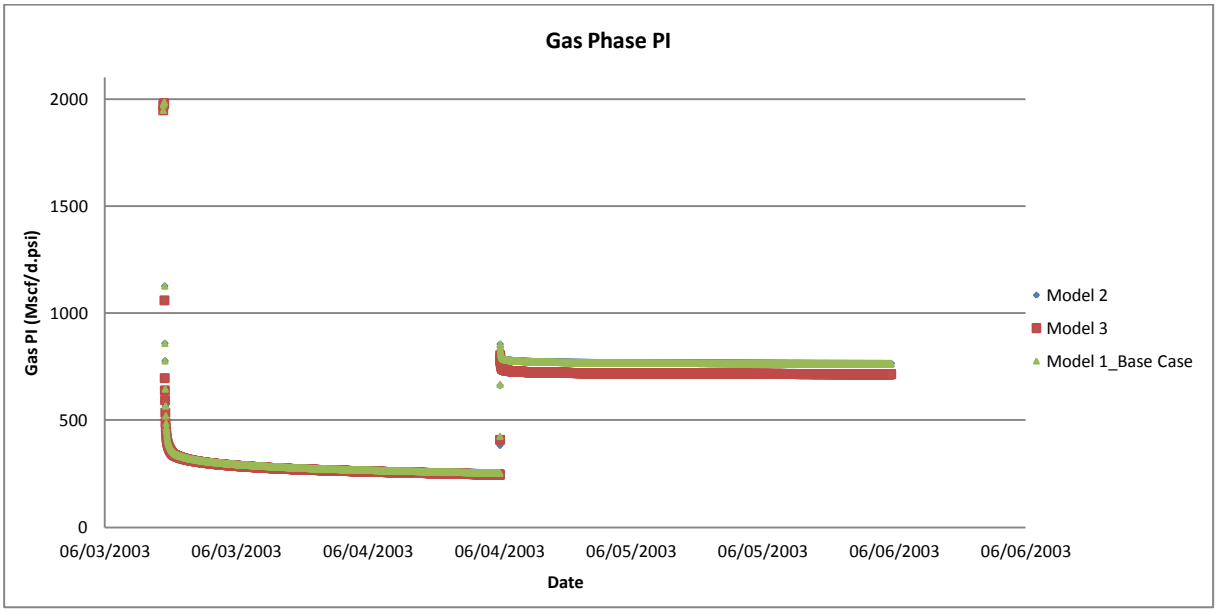

Figure 4.4. Gas Phase Productivity Index- Soc Analysis

4.2.2 Corey Exponents.

Four models are studied in this section (Table 4.4), a variation of different values of the Corey exponents for both, gas and oil equations are used. The relative permeability curves can be seen in figure 4.5.

Model	S_{gc}	S_{oc}	n_g	n_o	$K_{rg(Sorg)}$	$K_{ro(Sgc)}$
1	0	0.15	3,5	3,5	0.8	0.8
4	0	0.15	2	2	0.8	0.8
5	0	0.15	3,5	2	0.8	0.8
6	0	0.15	2	3,5	0.8	0.8

Table 4.4. Relative Permeability models

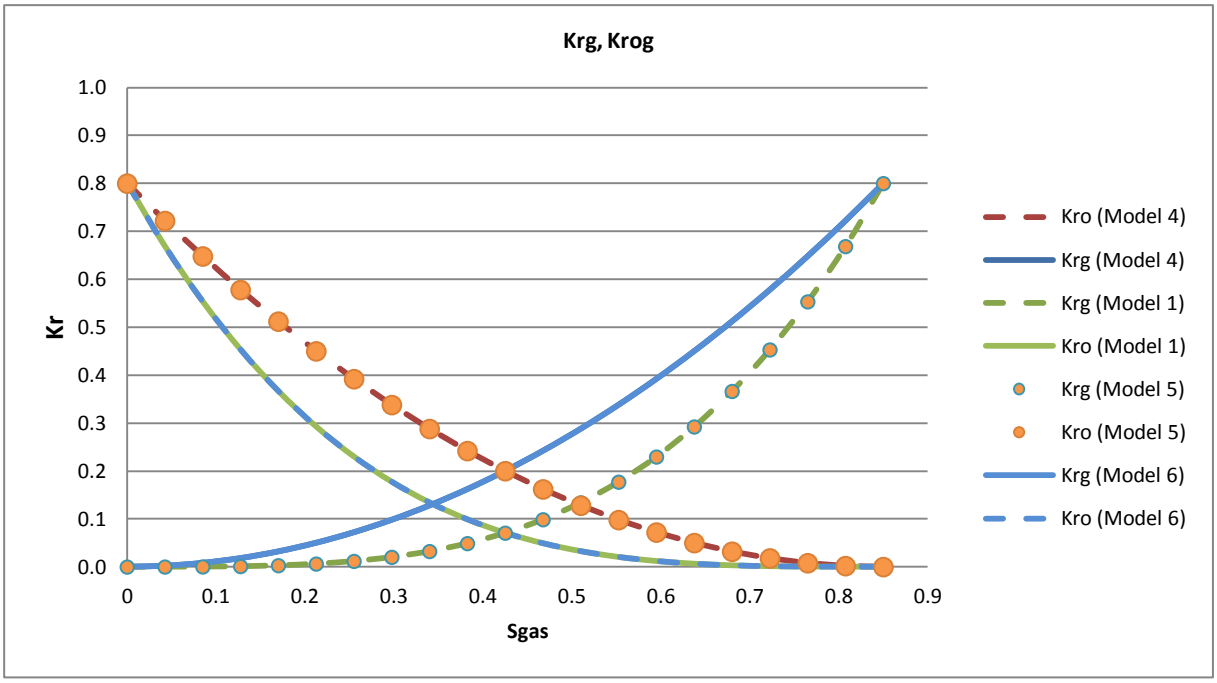

Figure 4.5. Relative Permeability for Corey Exponents Sensitivity

Compering the results for the different sensitivities (Corey Exponents), the following is concluded:

- A clear tendency is seen when comparing figures 4.7 and 4.8, the base case which models the highest values of N_g and N_o shows the lowest productivity index and thus the highest decrease in the BHP. On the other hand, Model 4 which presents the lowest values of the Corey exponents results in the highest gas production index. These results are to be expected, as for lower N_g and N_o it generates relative permeability curves which approach a "X" shape curve, thus as shown in Bardon et al. (1980), the system approaches to miscibility (Lower Interfacial Tension) and thus a higher mobility of the fluids causing a higher productivity index for the draw down period.

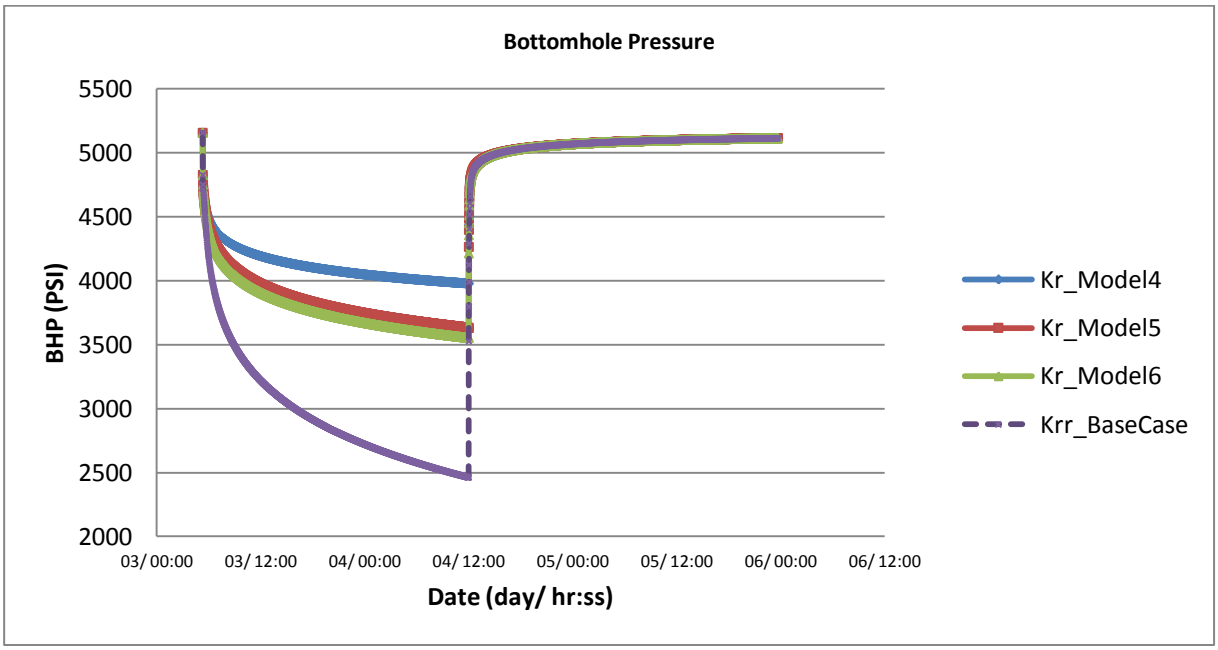

Figure 4.7. Bottomhole Pressure- Corey Exponent Analysis

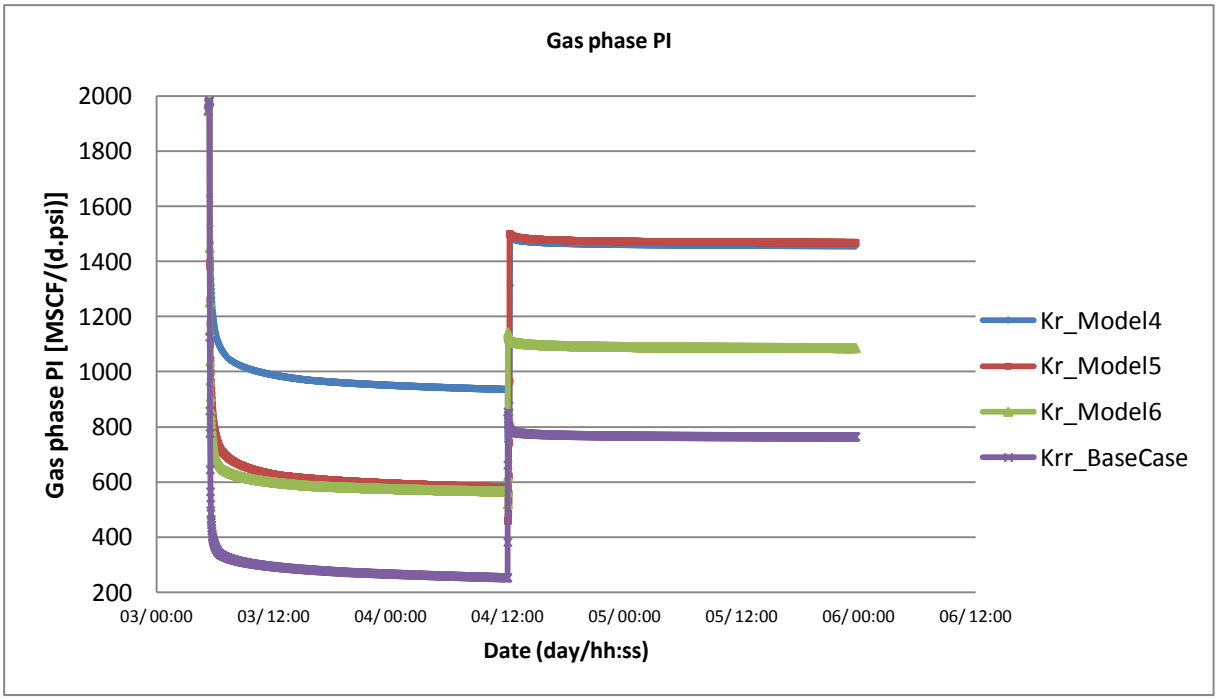

Figure 4.8. Gas Phase Productivity Index - Corey Exponent Analysis (End of DD1)

- The highest values of oil saturation (Fig 4.9.) is present in model 6, these results demonstrate the great impact of N_o over the oil production (Fig. 4.10). Compering models 6 and 1 with the remaining models it is clear that with a high N_o the oil production becomes lower, thus a higher fluid accumulation.

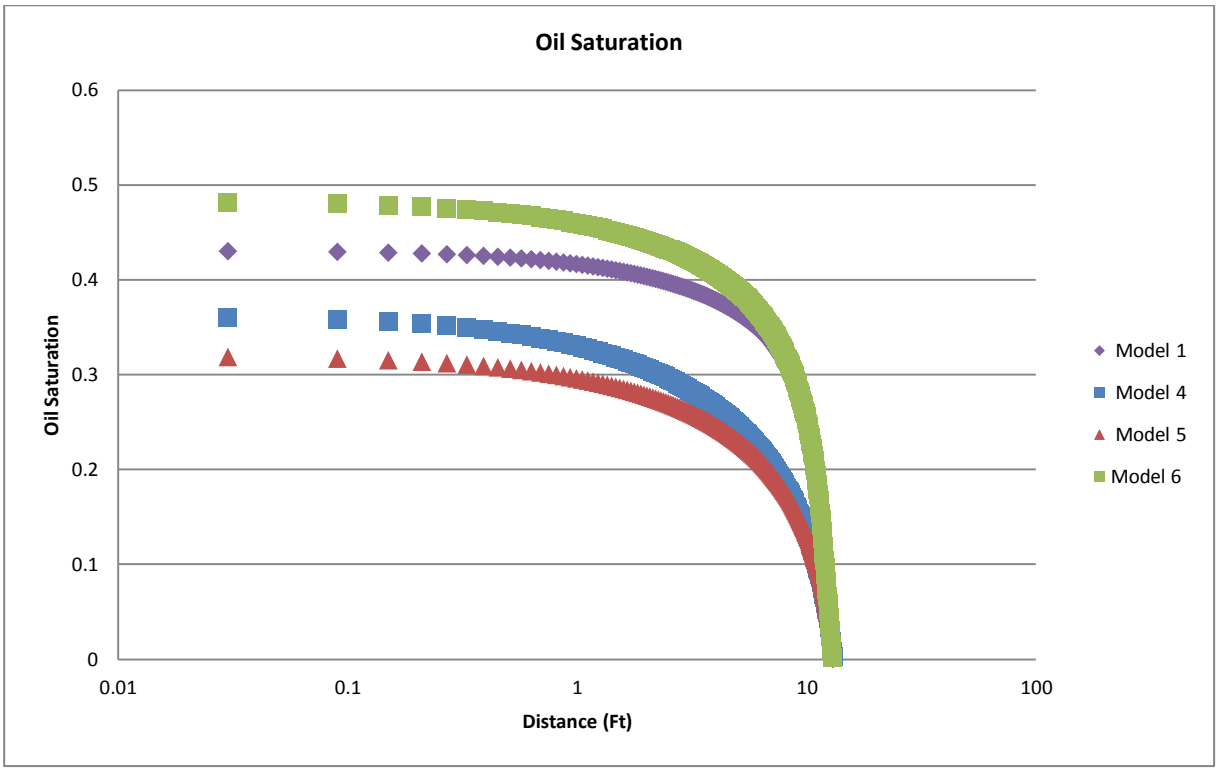

Figure 4.9. Oil Saturation - Corey Exponent Analysis (End of DD1)

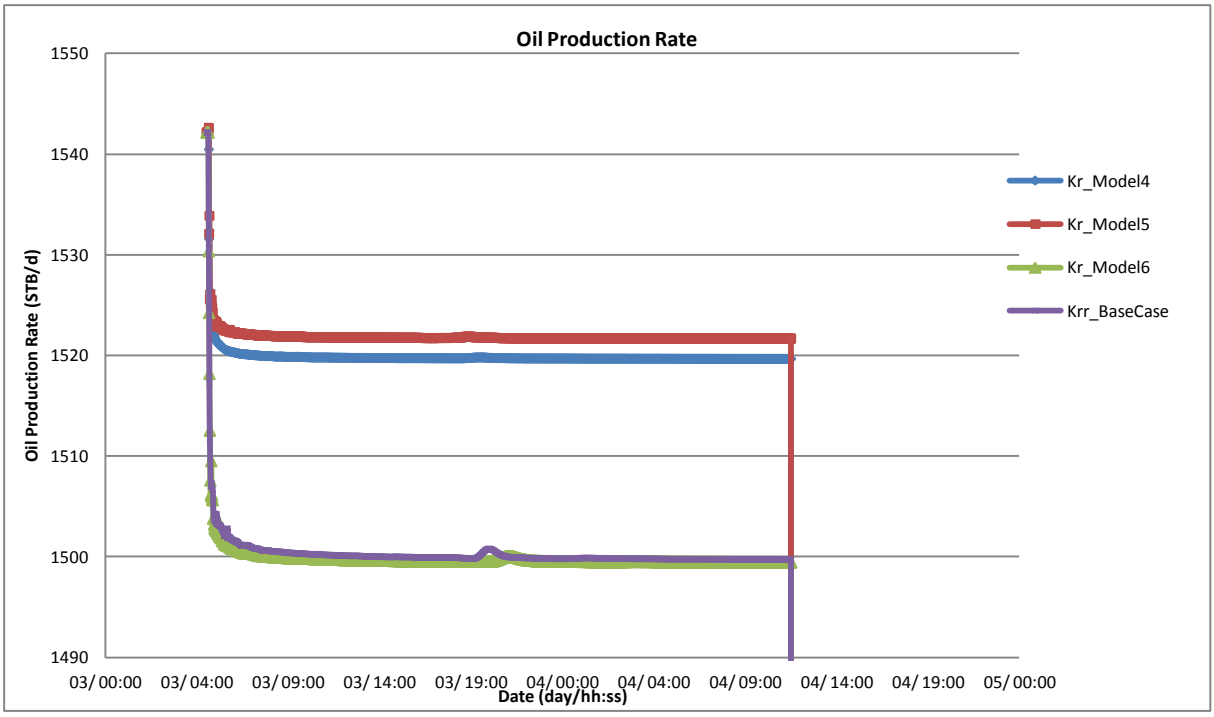

Figure 4.10. Oil Production Rate - Corey Exponent Analysis (End of DD1)

4.2.3. Relative Permeability Endpoints.

Gas Relative permeability at Irreducible Liquid Saturation .

Models 1, 7 and 8 are studied in this section. The results of the simulation show a high influence of $K_{rg(Sorg)}$ in the productivity, as for model 8 which has the lowest value of $K_{rg(Sorg)}$ the lowest production index is obtained, the value of $K_{rg(Sorg)}$ is so small that that the required gas constraint (9929.50 MSCF/day) cannot be constantly achieved (Figure 4.13). Contrary model 7 results in the highest productivity index, indeed due to a higher value of $K_{rg(Sorg)}$.

As for the oil saturation (Figure 4.15), a clear trend is seen, a lower $K_{rg(Sorg)}$ produces a higher oil bank accumulation. This higher oil saturation is generated due to an interconnected set of relations, the lower $K_{rg(Sorg)}$ causes a lower availability of the rock to transmit system fluids (Gas-Oil), meaning that each fluid component will travel with more difficulty and thus accumulating while increasing the fluids viscosity and decreasing the total mobility of the fluid towards the well. This can be explained by analyzing figure 4.16, the viscosity increases substantially for model 8 which will generate lower oil mobility (Fig. 4.16) and thus a higher oil accumulation than for the other models.

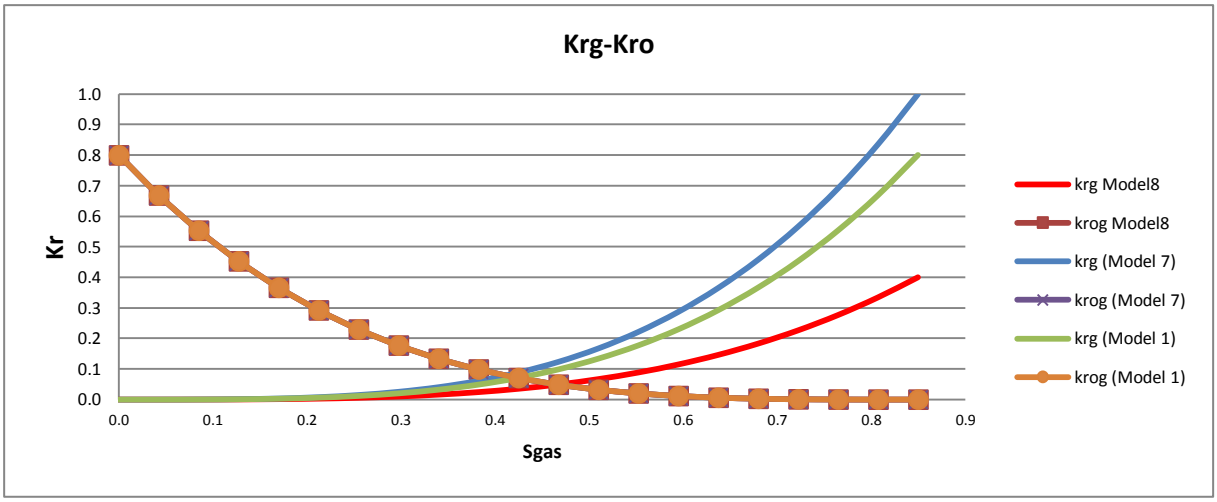

Figure 4.11. Relative Permeability for Corey Exponents Sensitivity

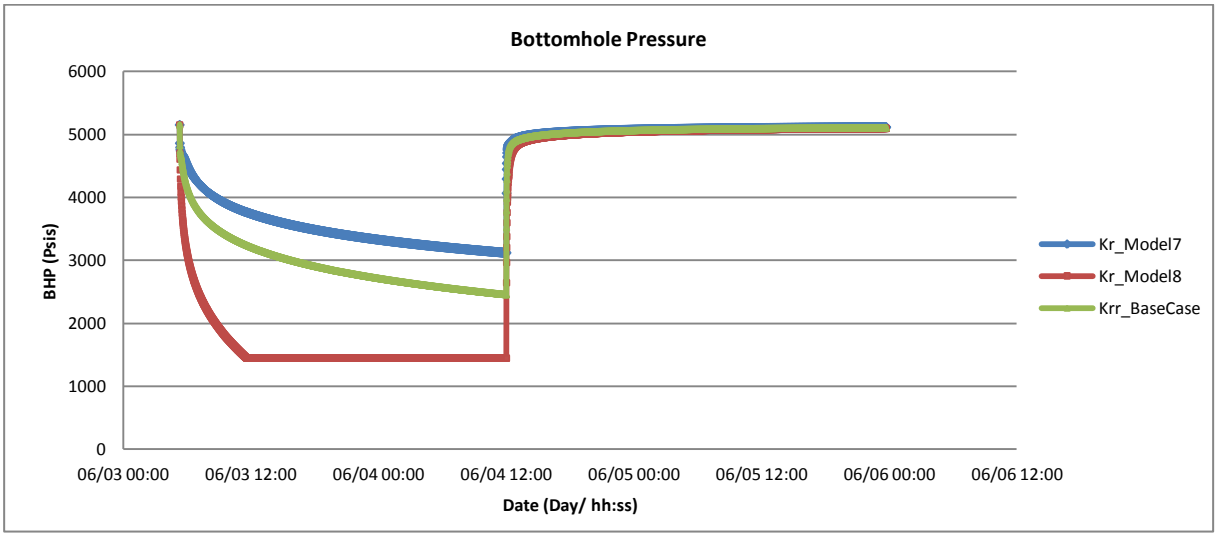

Figure 4.12. Bottomhole Pressure- Gas Relative Permeability Analysis

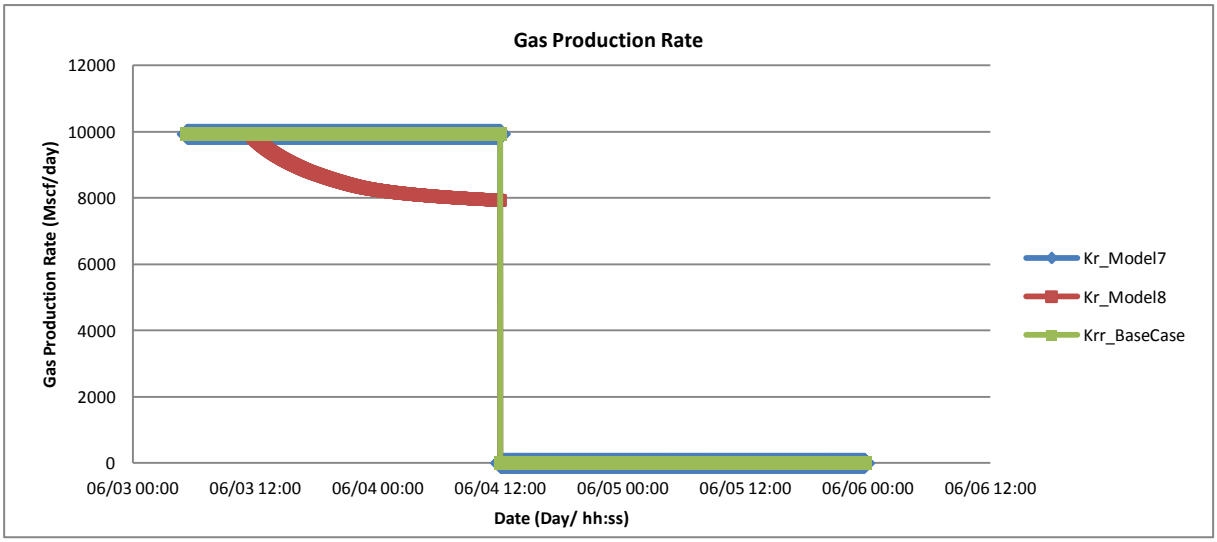

Figure 4.13. Bottomhole Pressure- Gas Relative Permeability Analysis

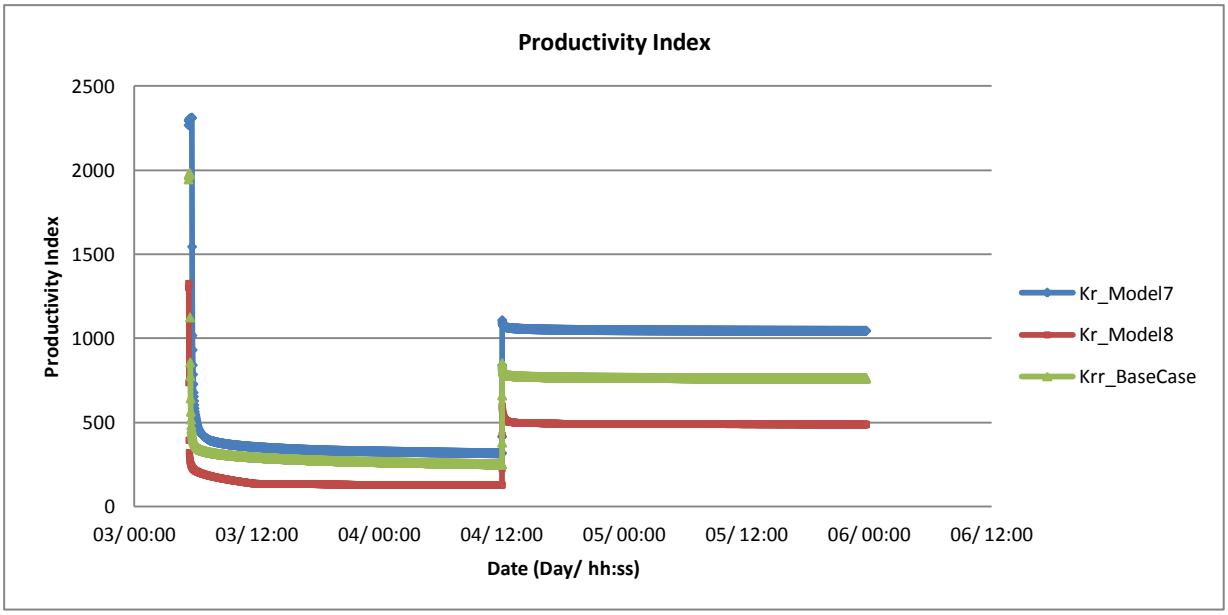

Figure 4.14. Productivity Index- Gas Relative Permeability Analysis

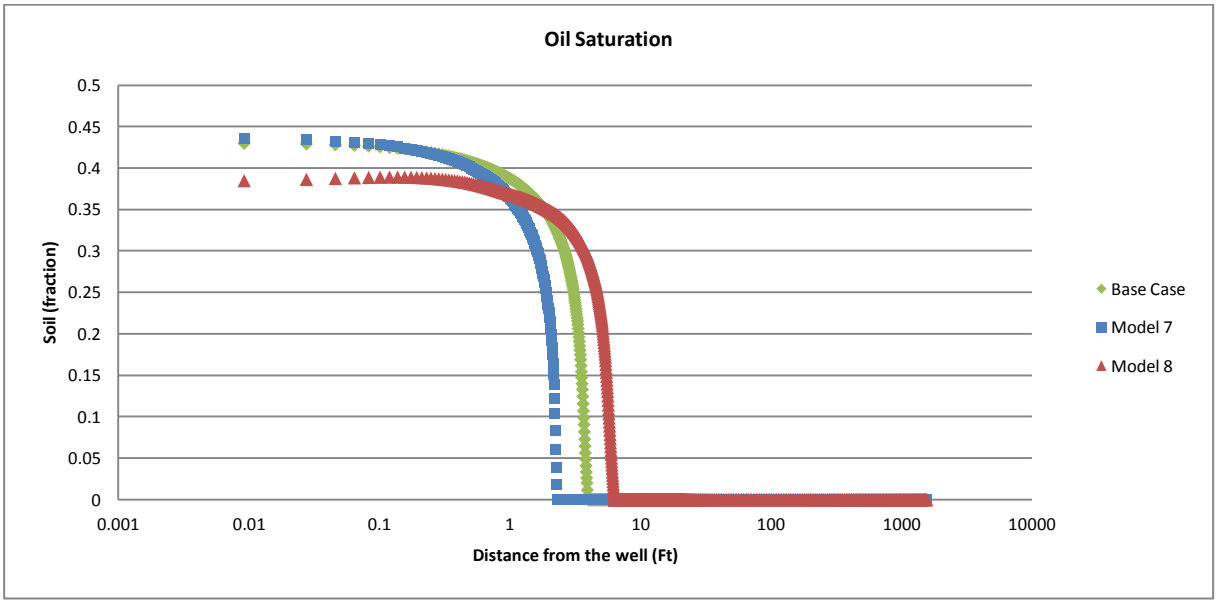

Figure 4.15. Oil Saturation - Gas Relative Permeability Analysis (End of DD1)

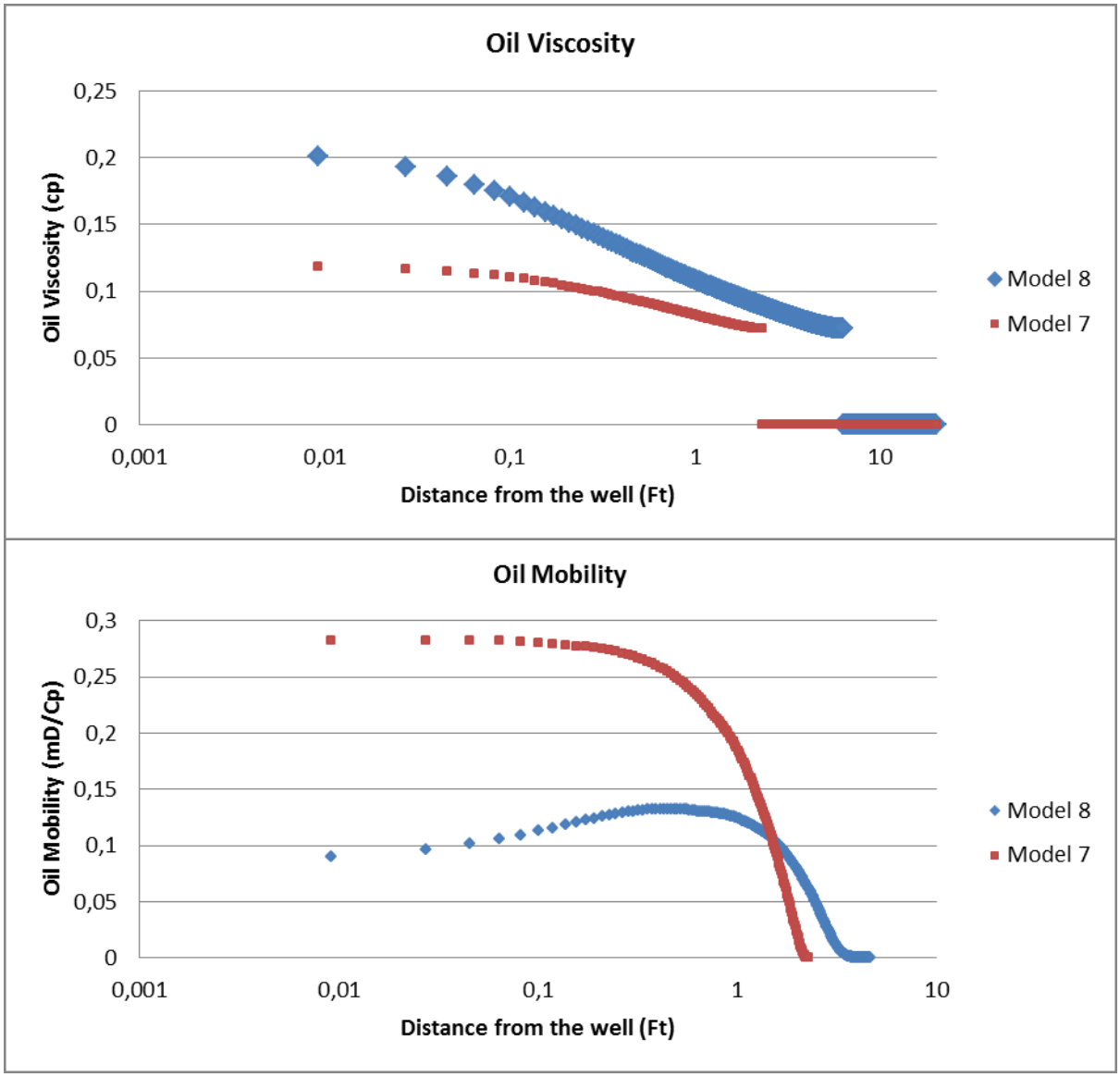

Figure 4.16. Oil Viscosity and Mobility - Gas Relative Permeability Analysis (End of DD1)

Oil Relative permeability at Connate Gas Saturation.

A decrease in $K_{ro(Sgc)}$ will generate a decrease in the mobility of the fluid and thus a lower productivity index. Model 1, 9 and 10 (Fig. 17) are studied in order to confirm this finding. As seen in figures 4.18 and 4.1 the productivity index follows the tendency described above, moreover the same trend as for $K_{rg(Sorg)}$ occurs for the oil saturation and oil mobility (Figures 4.19), however, if one evaluates the significance of the impact of the variables ($K_{rg(Sorg)}$ and $K_{ro(Sgc)}$) in the well productivity and the oil saturation buildup, one can conclude that the $K_{rg(Sorg)}$ has the highest influence.

As an overall conclusion of the relative permeability uncertainty study the following can be stated:

- $K_{rg(Sorg)}$ has a high impact in the wells productivity. Low values will generate low productivity and in consequence it will affect the extension of the oil buildup through its link with the oil mobility.

- Critical oil saturation has small effects in the well productivity. However, it does influence the extension of the condensate as it is the threshold for the condensate to be mobile.
- Higher productivity is seen for Corey exponents that tend to a more miscible system, thus for lower Corey exponents a higher productivity index is obtained. Moreover, oil saturation seems to be influenced mostly by the values of $N_{o,}$ were for higher values the oil saturation becomes greater.

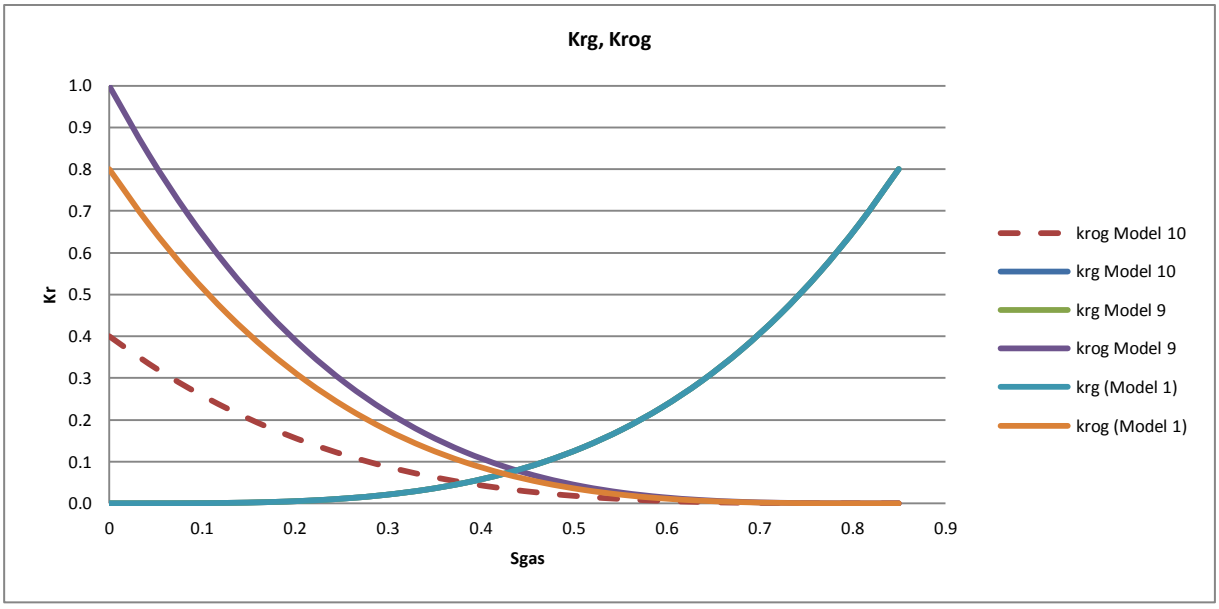

Figure 4.17. Relative Permeability - Oil Relative Permeability Analysis

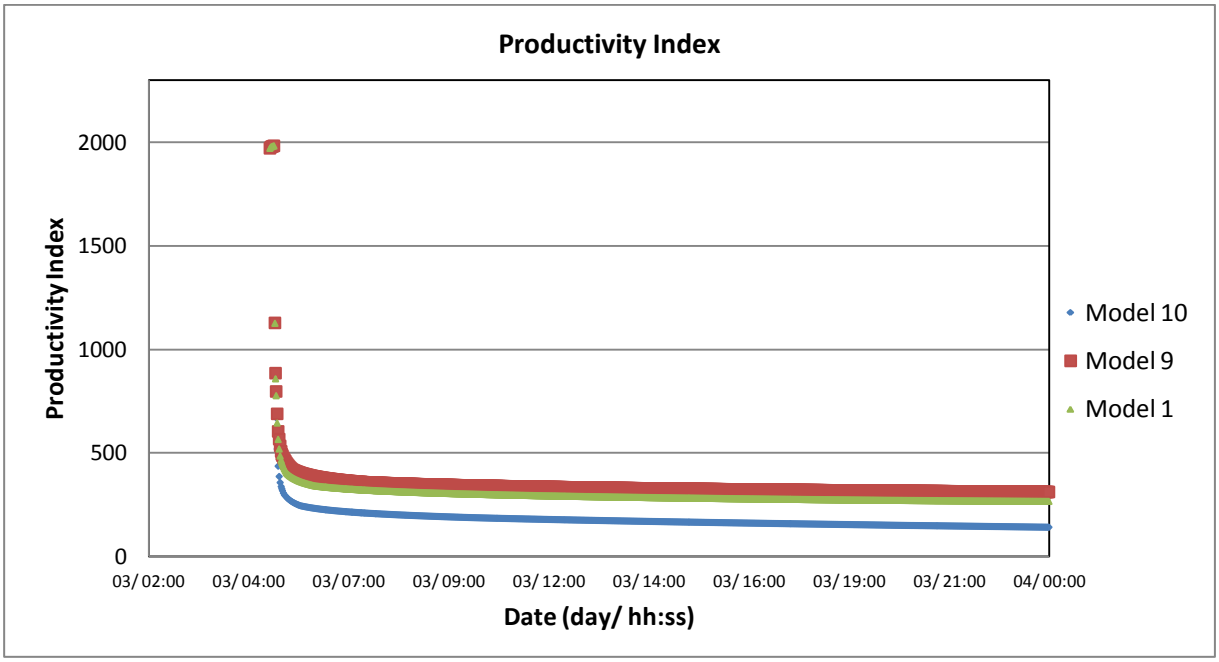

Figure 4.18. Productivity Index- Oil Relative Permeability Analysis

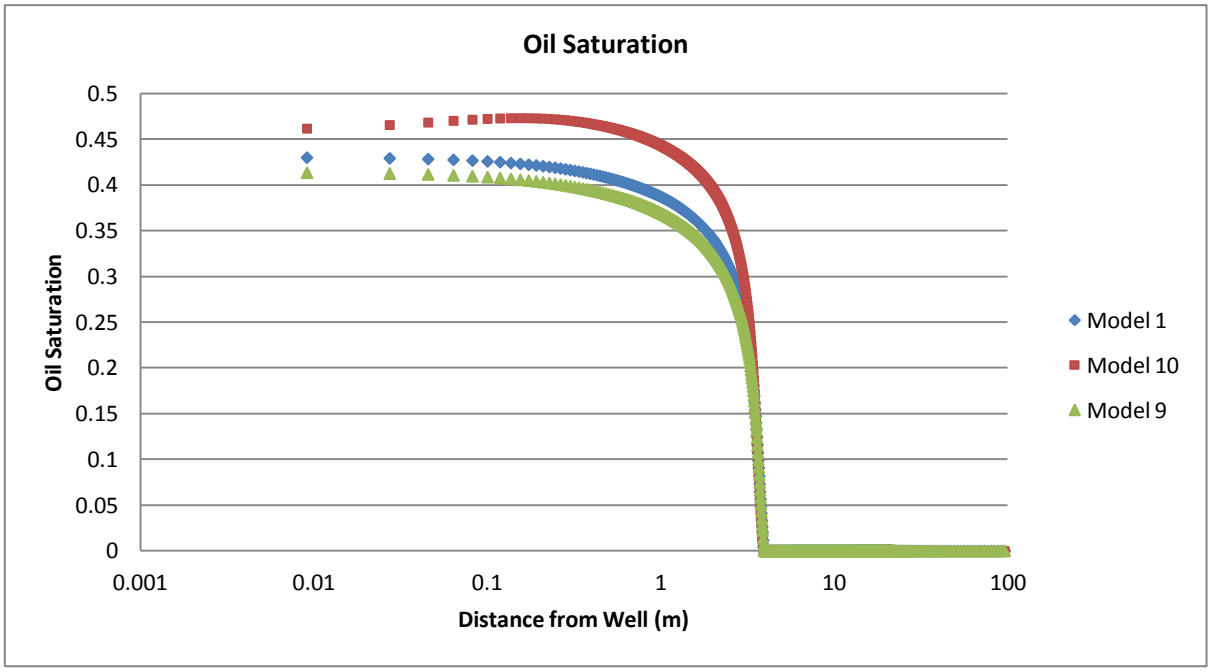

Figure 4.19. Oil Saturation- Oil Relative Permeability Analysis.

4.3. Effects of Wellbore Radius.

Wellbore radius represents the radius through which the reservoir fluids will flow towards the well, usually in many equations (i.e. Pressure transient analysis) this radius is assumed to be cylindrical. However, r_w is hardly cylindrical due to the effect of perforations guns, cement, casing, etc. The r_w commonly is assumed as the radius of the drill bit or the outside radius of casing plus the effect of the perforation guns, nevertheless whichever value is assumed it is still true that it holds great uncertainty.

A set of four cases with different wellbore radiuses (r_w) are evaluated in this section. The oil-water and gas-oil relative permeabilities are equal to the model 1 presented in the previous uncertainty analysis, also the following parameters (Table 4.5.) were constant through all the sensitivities runs:

Parameter	Value
Absolut Permeability (Kabs)	2.63 mD.
Porosity	5%
Rock Compressibility @ Pref	9.8141 E-7 1/psi

Table 4.5. Reservoir parameters

In order to a have a reference point in the analysis of the distribution of the results case 1 is selected as the base case. The following table presents the values for the evaluated cases:

Case	Wellbore Radius (ft)
1 (base case)	0.25
2	0.75
3	1
4	1.75

Table 4.6. Wellbore Radius Uncertainty Analysis

Theoretically a greater wellbore radius indicates a bigger radius through which the fluid can flow. Thus, as the results for the productivity index in figure 4.20 it is seen that for model 4 which contains

the highest wellbore radius it also gives the greatest productivity index, contrary as the wellbore radius decreases the productivity index decrease. These wellbore effects also influence the necessary bottomhole pressure (Fig 21.) required to meet the gas rate constraint.

The effects of the wellbore radius in the oil bank extension are also perceived. Figure 4.22 displays the oil saturation extension for the different cases, it is appreciated that bigger values of r_w will generate a smaller oil bank extension due to a higher radius for the oil to flow. Therefore, one can conclude by an extension of the wellbore radius, through any method, will help to temporarily overcome the condensate bank "blockage" effects.

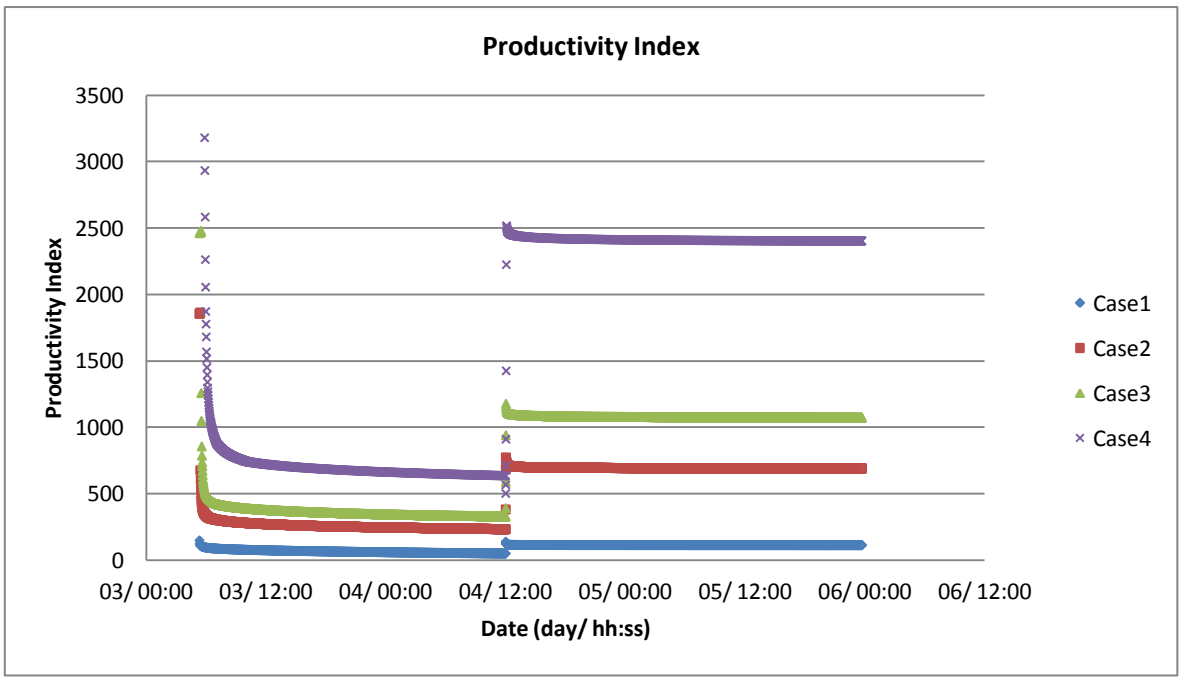

Figure 4.20. Productivity Index- Wellbore Radius Analysis

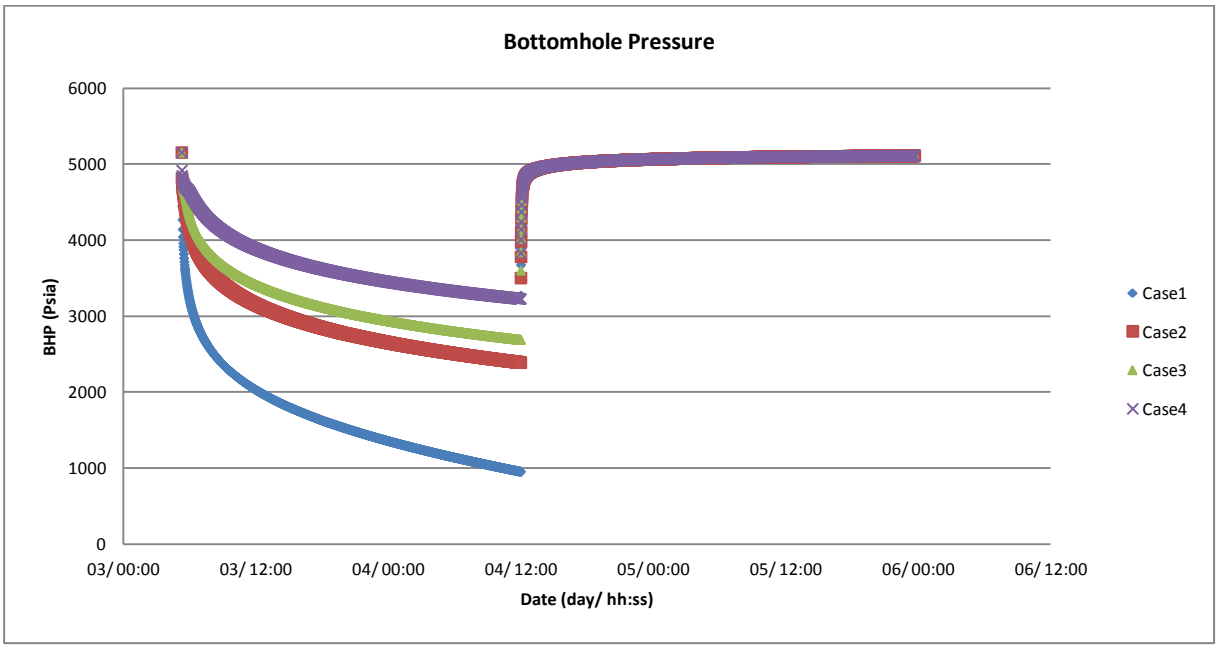

Figure 4.21. Bottomhole Pressure - Wellbore Radius Analysis

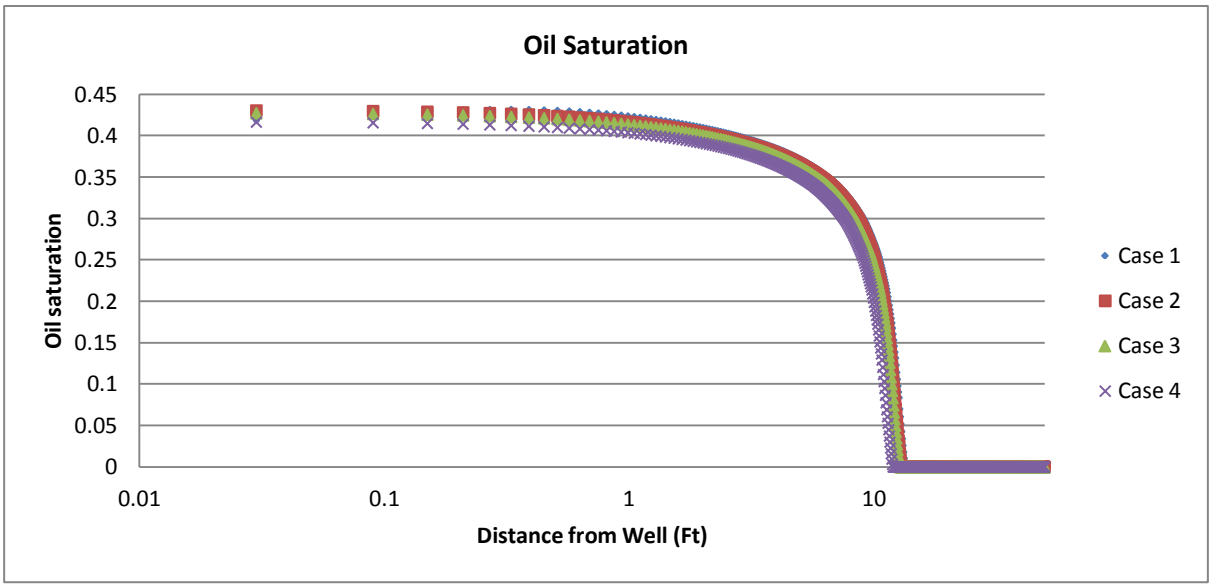

Figure 4.22 Oil Saturation - Wellbore Radius Analysis

4.4. Effects of Velocity Dependent Relative Permeabilities Curves.

The Sensitivity study of velocity dependent relative permeability (VDRP) is performed based on the Heriot-Watt model (Described in the theory section). Two main groups are divided by the VDRP model, firstly for the gas phase (VDRPG) and secondly the VDRP model for the oil phase (VDRPO); this was done in order to understand the individual influence of the VDRP model in each phase.

The required parameters for the VDRP model in the numerical simulation (E300) are the following:

- $M_{phase.}$ Controls the variability of the critical phase saturation with normalized capillary pressure.
- $N_{1phase.}$ It is the weighting value between miscibility and immiscibility of the relative permeability curves. (Along with N_{2phase})
- $N_{2phase.}$ It is the weighting value between miscibility and immiscibility of the relative permeability curves. (Along with N_{1phase})
- $N_{cbp.}$ Base Capillary number.

All of these parameters are normally suggested to be calculated experimentally, however as no special core analysis (SCAL) data was given for the time of this study, it was necessary to use as base data the default values given by ECLIPSE. Moreover, the capillary number (N_{cp}) defines the effects on the relative permeability curves, if the capillary forces tend to zero than the mixture behaves as miscible, therefore as the CN used in the simulator is the normalized capillary number, which is equal to:

$$N_{cnp} = \frac{N_{cbp}}{Ncp}$$

Hence, one can say that the base capillary number (N_{cbp}), represents the lower threshold value below for which the CN has no effect on the relative permeability curves (Ref 10). Therefore, it is concluded for the purpose of this study that the N_{cbp} will be the Sensitivity parameter in the study of VDRP, thus the rest of parameters required are kept constant through the different sensibilities.

As for the calculation of N_{cbp} it is suggested that this value is determined experimentally, however as mentioned previously no data was available. Consequently, it was necessary to calculate this value using the method presented in ECLIPSE Technical Description (2014):

Using the results of a Constant Volume Depletion (CVD) experiment it is possible to calculate the gas-oil surface tension and the gas viscosity at abandonment pressure. Also, it is suggested that the fluid velocities at distances far away from the wells will be approximately 10 ft/day. Thus, implementing the following equation one can determine for a starting point the base capillary number:

$$N_{cbp} = \frac{V_p * \mu_p}{\sigma}$$

Where:

Vp = Phase velocity (m/day)

μ_p= Phase Viscosity (kg/(m*day))

σ= Gas-Oil Surface tension. ((kg*meter)/(day^2*meter))

The capillary base number calculated was used as the base case. The sensitivity cases are presented in table X.

Group 1-VDRPG	N_{cbp}
Case 1 (base case)	2.31 X 10^{-8}
Case 2	1 X 10^{-2}
Case 3	1 X 10^{-6}
Case 4	No VDRP
Group 2-VDRPO	N_{cbp}
Case 4 (base case)	3.54 X 10^{-8}
Case 5	1 X 10^{-2}
Case 6	1 X 10^{-6}

Table 4.7. VDRP Sensitivity Cases

Velocity Dependent Relative permeability for gas phase (VDRPG).

In order to realize a proper analysis of the effects of VDRP in the model one must treat the matter with the order of complexity that merits. Thus, it is not only necessary to interpret the well performance variables but also one must attempt to understand the causes of the effects.

A first conclusion can be done by analyzing figures 4.23 and 4.24 (PI and BHP). Case 2 which represents the case with the highest capillary number shows the same results as case 4, meaning that for high base capillary numbers the effect of the VDRP model in the relative permeability curve are insignificant.

For cases 1 and 3 the capillary number effects are clearly reflected in the production index (Fig 4.24) and bottomhole pressure results (Fig 4.23). Higher capillary number results in a higher productivity index and less pressure drawdown in order to meet the required gas constraint. These capillary number effects its own by a system that behaves more miscible, meaning that the surface tension for cases 1 and 3 should be lower; this can be confirmed by comparing the surface tension of the all the cases (Figure 4.25). These results demonstrate how the change in relative permeabilities with capillary number can lead to a significant improvement in the well productivity.

Furthermore, the effects of VDRP are also visualized in its influence on the gas velocity in the near wellbore region during the drawdown period. In order to understand the development of the effects of VDRP on gas velocity, three plots during three different times are compared. Figure 4.26 presents the velocity profile for cases 1, 2 and 3, at the beginning of the drawdown period (27 minutes), at this time three velocity regions (please notice that the regions described here are Velocity regions and they are different than the regions identified in the derivative pressure analysis) can be identified, region 1 shows no gas velocity thus this region represents the single phase gas region which does not see (at this time) any effects of the well production. Region 2, it is still a single phase gas region; however, the gas starts to flow towards the well and thus the gas velocity starts to increase. Region 3 starts to present an increase in the condensate liquid drop out, though no significant change in the gas velocity by the influence of the condensate is perceived. Finally, at this point in time no remarkable gas velocity change is seen between the three cases, hence it can be assumed that the VDRPG model does not have any effects yet.

Figure 4.27 presents the gas velocity profile after 12 hours of production. As before three regions are identified, the first region represents the single gas phase which is not flowing. The second region shows an increase in the velocity for all the cases, and it is due to the pressure drawdown of the well and where we are still in presence of a single gas phase. The third velocity region, two main observations can be mentioned, firstly the gas condensate buildup increases and starts to flow together with the gas, secondly one can notice that the velocity for the three cases is different particularly for cases 1 and 3 the velocity is higher and the oil saturation is higher, which are the cases that have the lowest Base Capillary Number (BCN). Meaning that for low BCN the gas velocity will increase and it will also influence the mobility of the oil by increasing it.

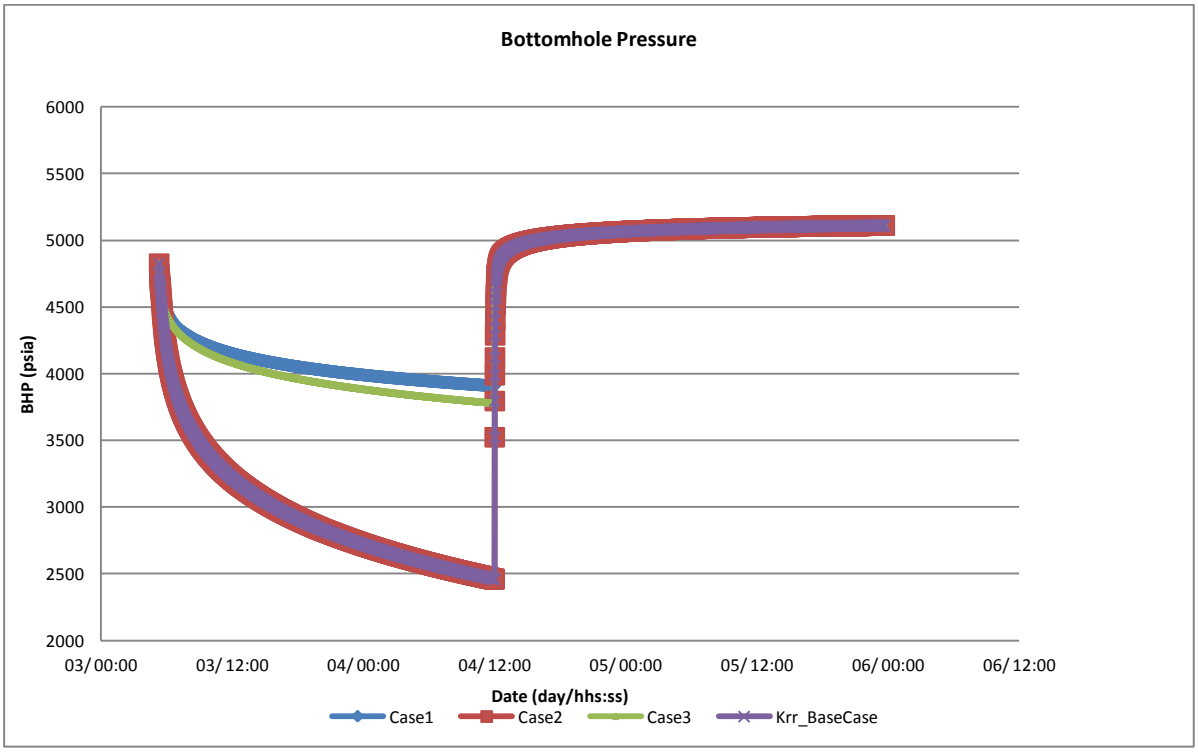

Figure 4.23 Bottomhole Pressure - VDRPG Analysis

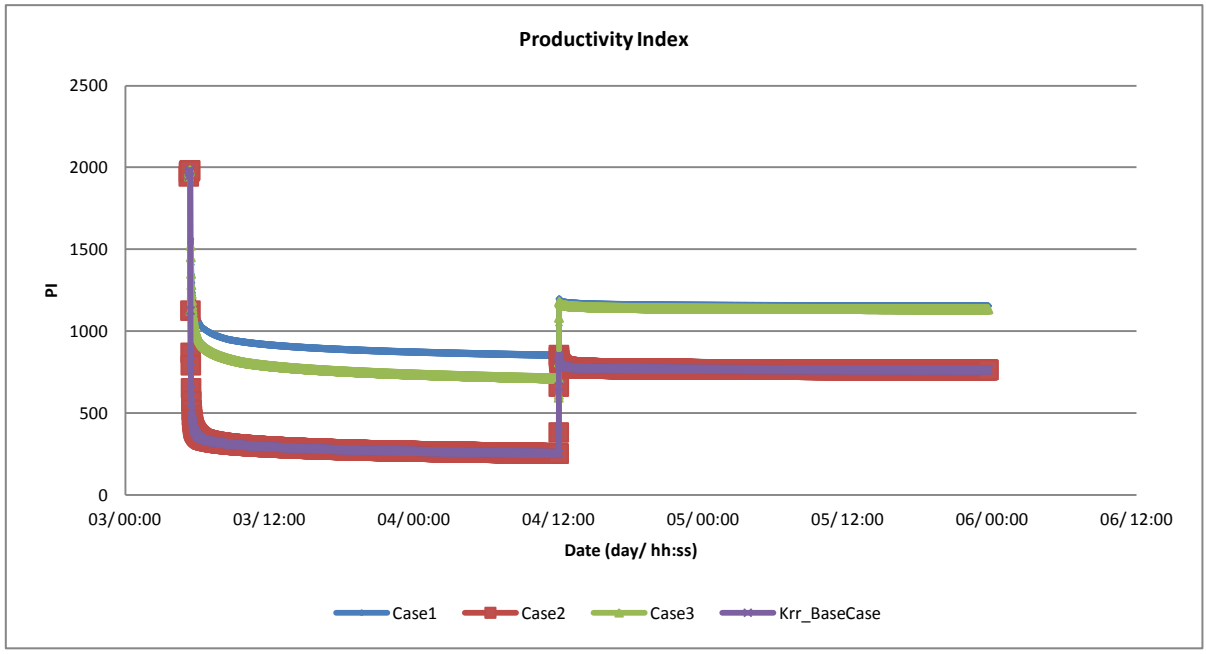

Figure 4.24 Productivity Index - VDRPG Analysis

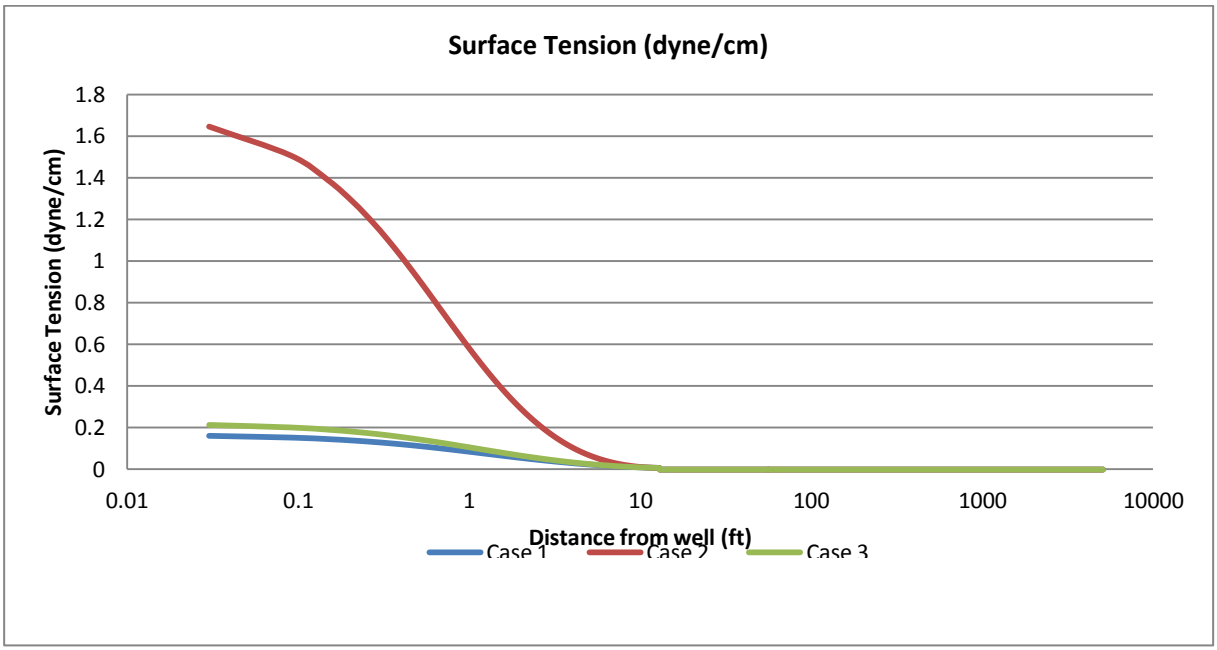

Figure 4.25 Surface Tension - VDRPG Analysis

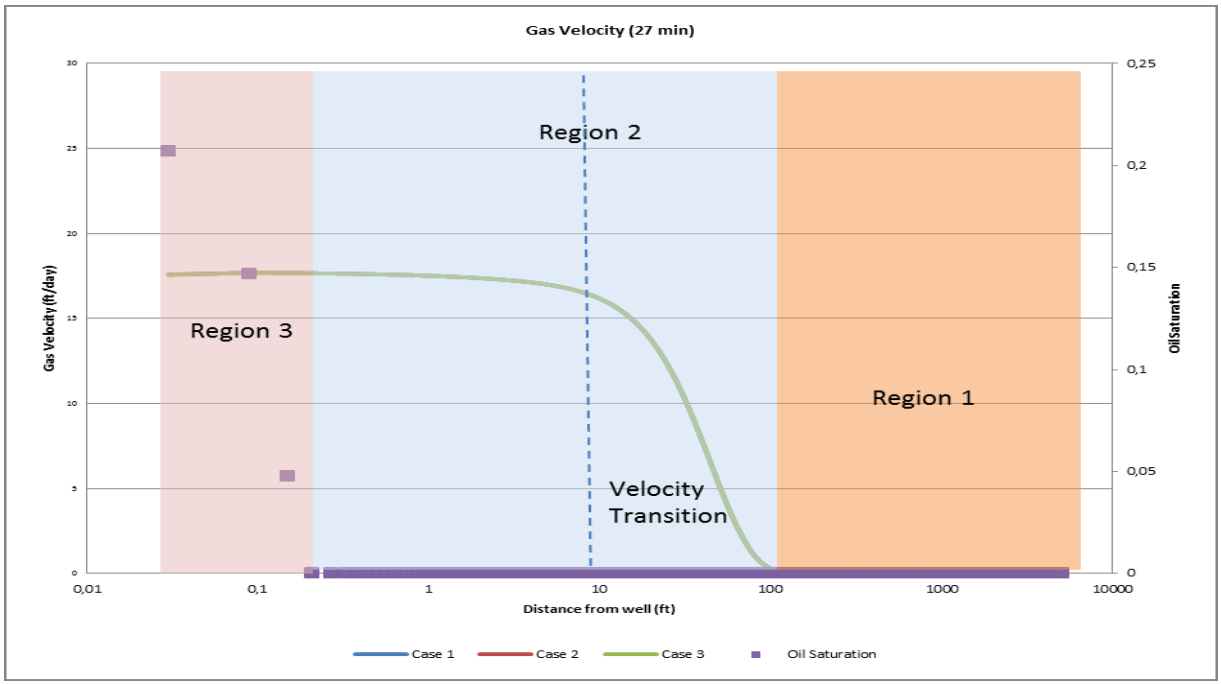

Figure 4.26 Gas Velocities (27min) - VDRPG Analysis. Notice that all the curves overlap.

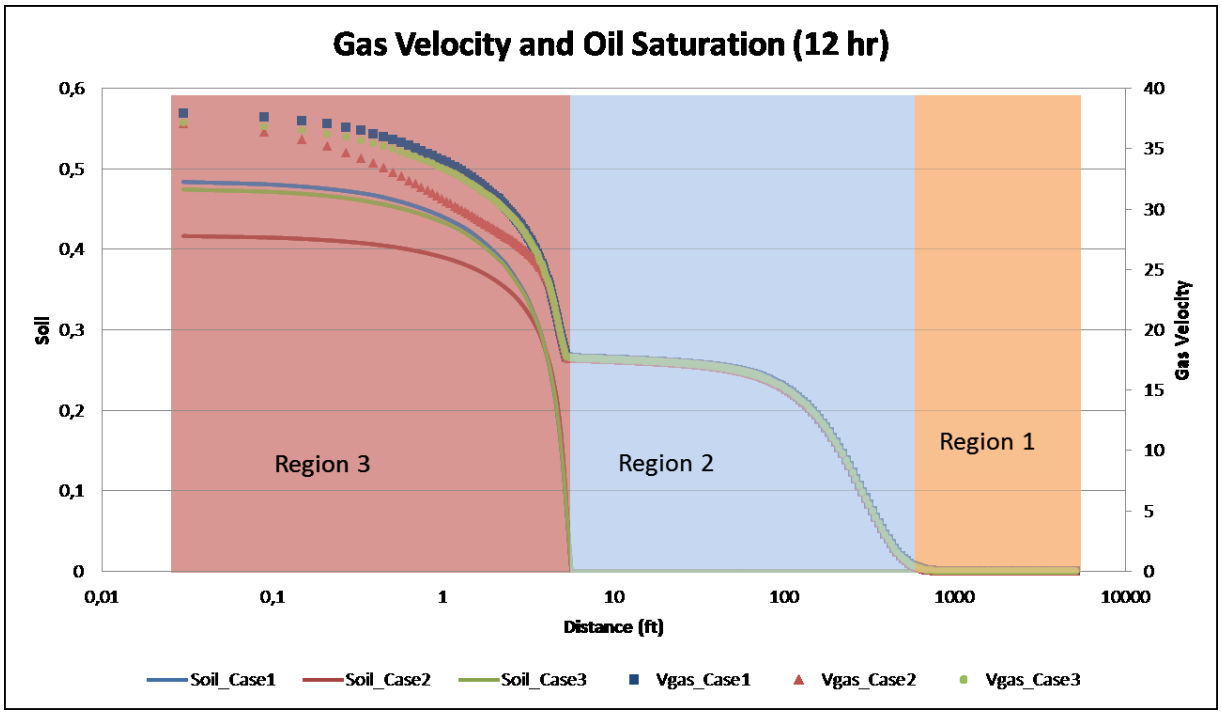

Figure 4.27 Gas Velocities and Oil Saturation after 12 hr - VDRPG Analysis.

Velocity Dependent Relative permeability for oil phase (VDRPO).

A similar analysis is performed for VDRPO, firstly the well productivity index and bottomhole pressure results are compered. Case 4 presents the highest productivity index, confirming the positive influence of a small base capillary number in well performance. Moreover, similarly to the results obtained for VDRPG, case 5 shows no influence of the capillary number effects in the results, thus it can be concluded that high base capillary numbers represents a flow which is mainly dominated by viscous forces.

The effects VDRPO in the relative permeability curves for cases 4 and 5 can be clearly visualized in figure 4.30, which presents the changes of maximum relative permeability of gas (Krgmax) and oil (Kromax) through the drawdown period at 0.24 ft. from the well. As it can be seen case 4 gives higher Krgmax through all the production period, which indeed is caused by the modification of the relative permeability curves to a more miscible system and thus an increase in the productivity. Likewise the Kromax for case 5 is higher than case 4.

Base capillary number was the sensitivity parameter of this study, therefore as all the parameters required by ECLIPSE for the VDRP models were constant, the influence of BCN was exclusively analyzed. Consequently, the results of the sensitivity study show that for high base capillary numbers the effects of VDRP are irrelevant, whereas for small BCN the effects of VDRP model is evidently detected.

Three interrelated effects of VDRP are seen, changes in the gas velocity in the near wellbore region, increase in the relative permeabilities and a decrease in the interfacial tension. All of these effects lead to a more miscible system, which causes an increase in the wells productivity and thus affects the analysis of the results.

Owing the significant influence which the velocity dependent relative permeability model can have in the simulation results, and thus the final forecast of the well productivity it is concluded that capillary number effects, if present, must be carefully determined and included in respective calculations.

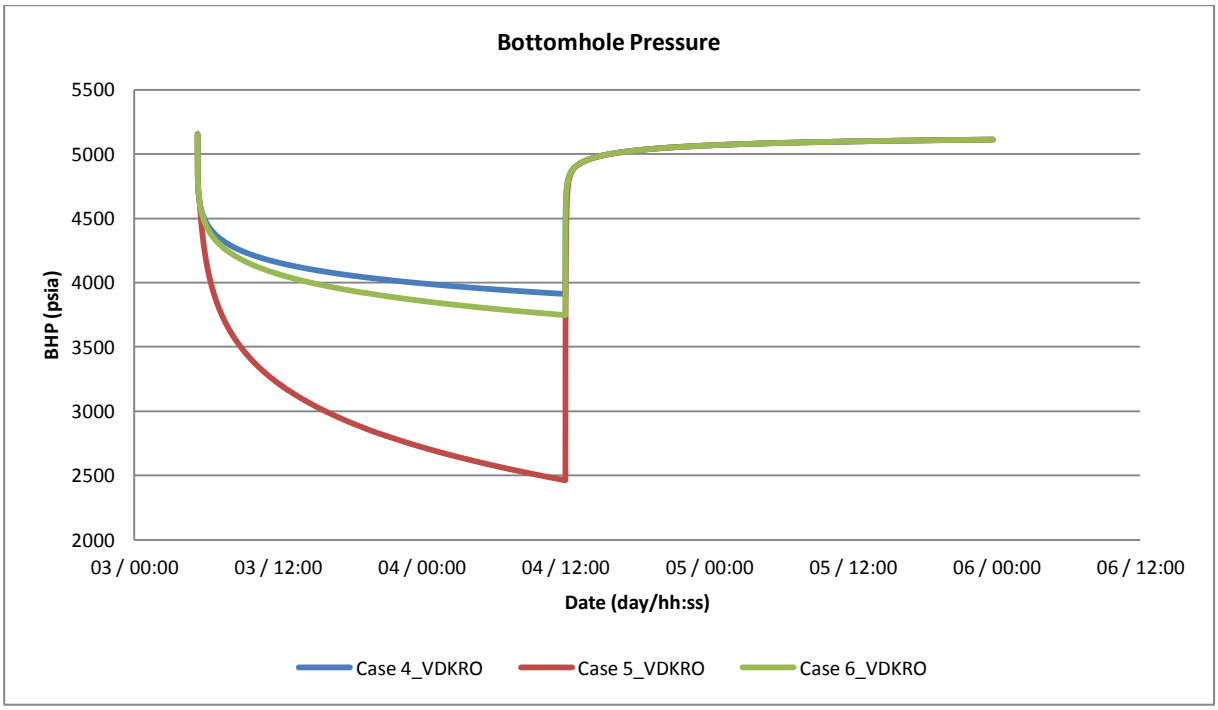

Figure 4.28. Bottomhole Pressure- VDRPO Analysis.

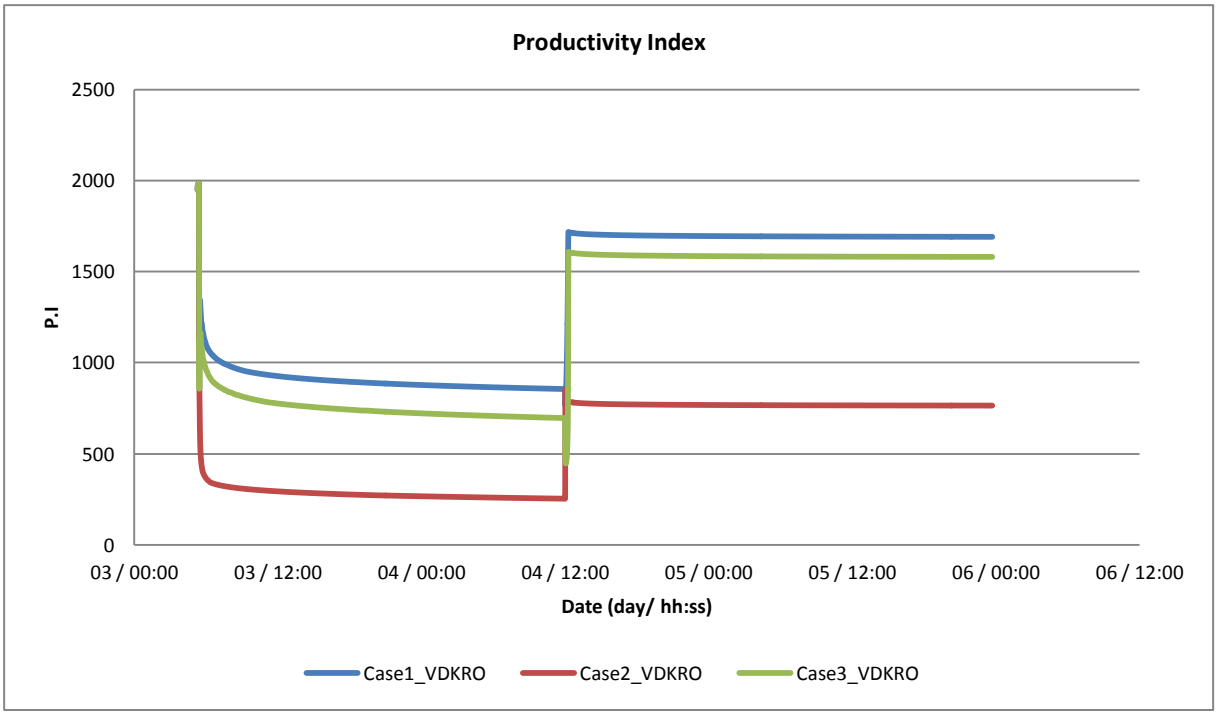

Figure 4.29. Bottomhole Pressure- VDRPO Analysis.

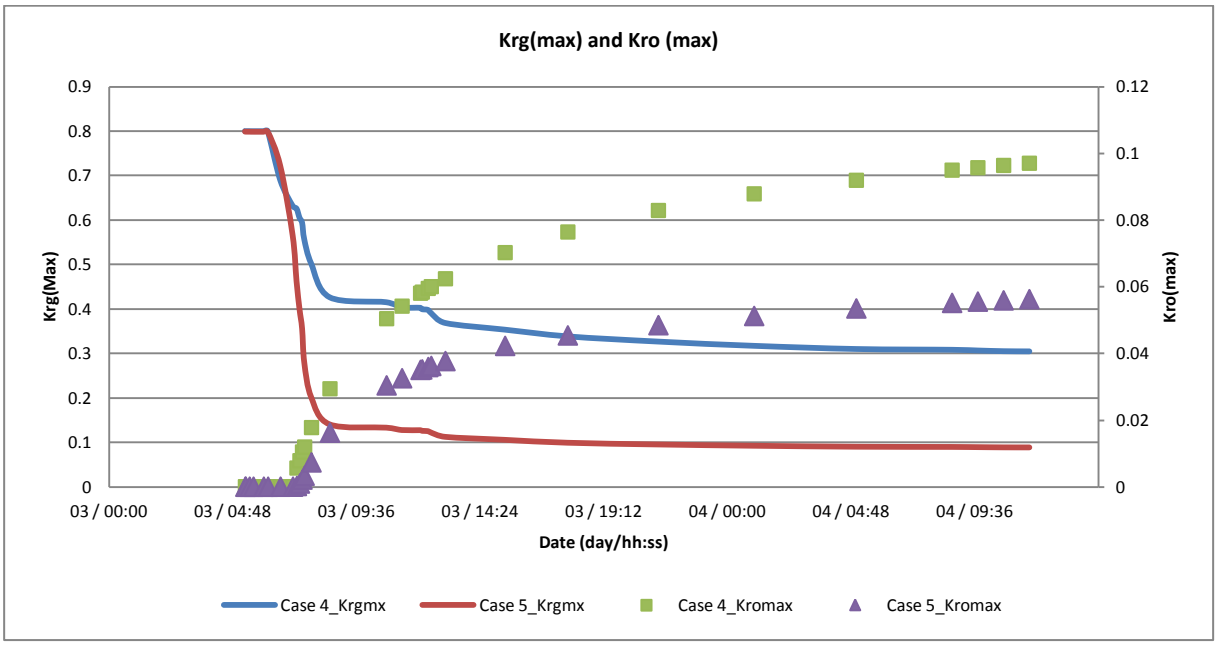

Figure 4.30. Maximum relative Permeability to the gas - VDRPO Analysis.

4.5 Grid Size study.

The study of well test analysis using numerical simulation in a gas condensate wells must be done with particular care. The drastic changes in pressure in the near wellbore region during the start of the well test implies the need of a detailed model, thus by implementing a radial model with small grid sizes, the pressure effects can be better captured. However, as it is normally required, the whole reservoir size must be simulated, hence having a small grid size in all the model is not a valid option due to computational requirements. Therefore, implementing small timesteps combined with small

grid sizes near the wellbore region and incrementing the size towards the boundary is a common solution. This methodology must be taken with caution, essentially due to the large changes in the grid size which perhaps will generate convergence problems, and thus numerical instabilities in the results.

Usually the solution is the implementation of radial grid using a logarithmic size distribution; however this can still lead to instabilities. In consequence, with the intention of validating the grid model, it was proposed to compare the radial-irregular size distribution grid with a radial-regular distribution grid size grid, which consists of 30000 cells and a constant grid size of 0.1 feet.

The results of the grid study are presented in figures 4.32 and 4.32. They show that, the grid sizes can be tuned in order to reduce the fluctuations of the results, thus as the difference in the results between the regular and irregular gird are nearly identical (Fig 4.31 and 4.32), it is possible to use the irregular grid for the simulation study. The details of the irregular grid are presented in the subsection 3.2.1.

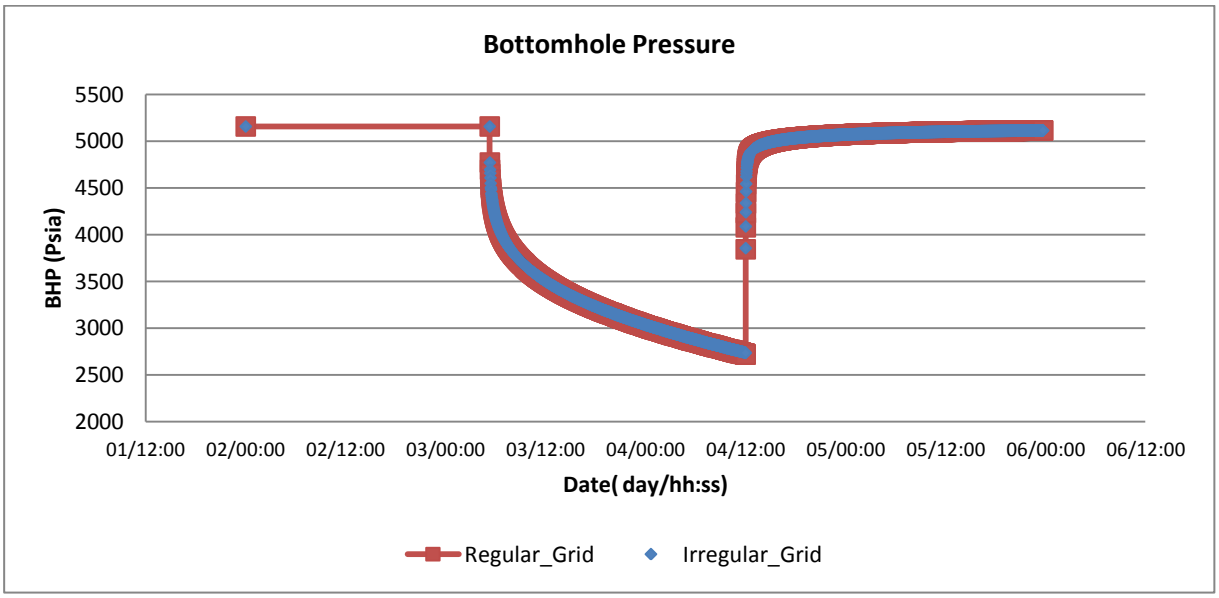

Figure 4.31. Bottomhole Pressure- Grid Analysis.

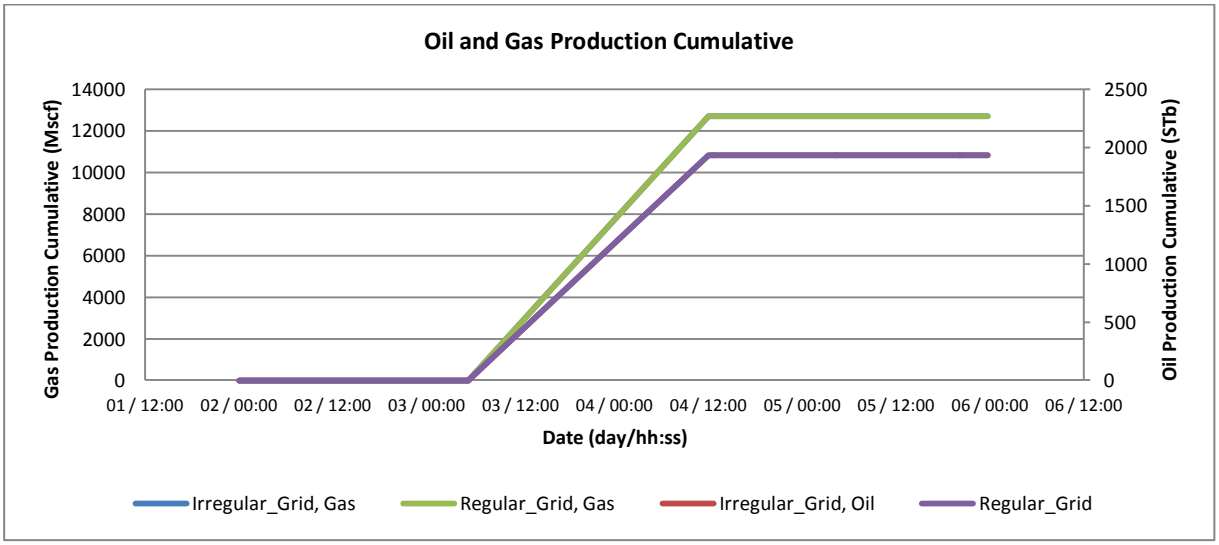

Figure 4.32. Oil and Gas Production cumulative- Grid Analysis, the curves of both cases overlap.

Chapter 5

History Matching of Well Test Data

Introduction

One of the aims of this study was to investigate the condensate banking effects and its development through time, these with the purpose of accurately predict the condensate bank extension and additionally to determine the consequences in production impairment and development of the condensate gas ratio. In order to accomplish this objective the retrograde gas condensate well “M1” was studied using a reservoir simulation radial model which attempted to match the results of previous well test data (Section 3).

As history matching of the well test data is complex process; first, the sensitivity analysis (Section 4) was performed which was convenient in order to determine the most uncertain and influential variables. Subsequently the intention was to first match the production data (Gas Constraint) and with this match the Bottomhole Pressure (BHP) of the well test data during the first drawdown and buildup period. After this first match had been accomplished, then the simulation results were compared with those of the Bourdet pressure derivate (Section 4.1), which showed a clear example of condensate bank build up. However, the matching of the pressure derivative was more complicated than the matching of the production and BHP, the main reasons are the following:

- Drawdown data can be affected by phase redistribution in the wellbore, and is sometimes not interpretable.
- Though the BHP and production data can be successfully match with several models, the pressure derivate will show if the corresponding mobilities zones are correctly modeled.
- PVT properties play a major role in the correct modeling of the pressure derivate. Thus, accurate and representative sample are crucial.

Therefore, in order to account and overcome the previous remarks it was necessary to perform the pressure derivative history match in conjunction with the production and BHP match.

Moreover, as it will be presented in this section, the history matching process consisted of two phases. The first phase resulted in match of the BHP and production data (gas rate), however, the pressure derivative could not be represented. Accordingly, a second phase was introduced, which consisted of changing the Condensate Gas Relationship (CGR). This phase was crucial for the correct history match of both production and pressure derivative data. The arguments and explanations of this new CGR will be described in detail in this chapter.

After a successful history matched model was achieved, the next stage was forecasting and comparison with field data.

5.1 History Match, Stage 1.

5.1.1. BHP and Production Match

During the beginning of the drawdown period, the values does not match very well, this difference is believed to be due to perturbations in the drawdown test, for instance due to phase redistribution. Hence the focus in the BHP match was the pressure at the end of the drawdown period, thus it is assumed that by having an accurate match of this pressure point one could achieve a successful match. Furthermore, regarding the buildup period, as a first impression, it is concluded that a good match is achieved during the beginning of the test. However, as the pressure starts to stabilize (orange dashed circle, Fig 5.1) the result slop of the simulation starts to deviate from the history date, nevertheless approximately after time 05/00:00 both curves star to match until the end of the test where the history is represented by the simulation model. Finally it is concluded that the BHP and gas constraint match is acceptable.

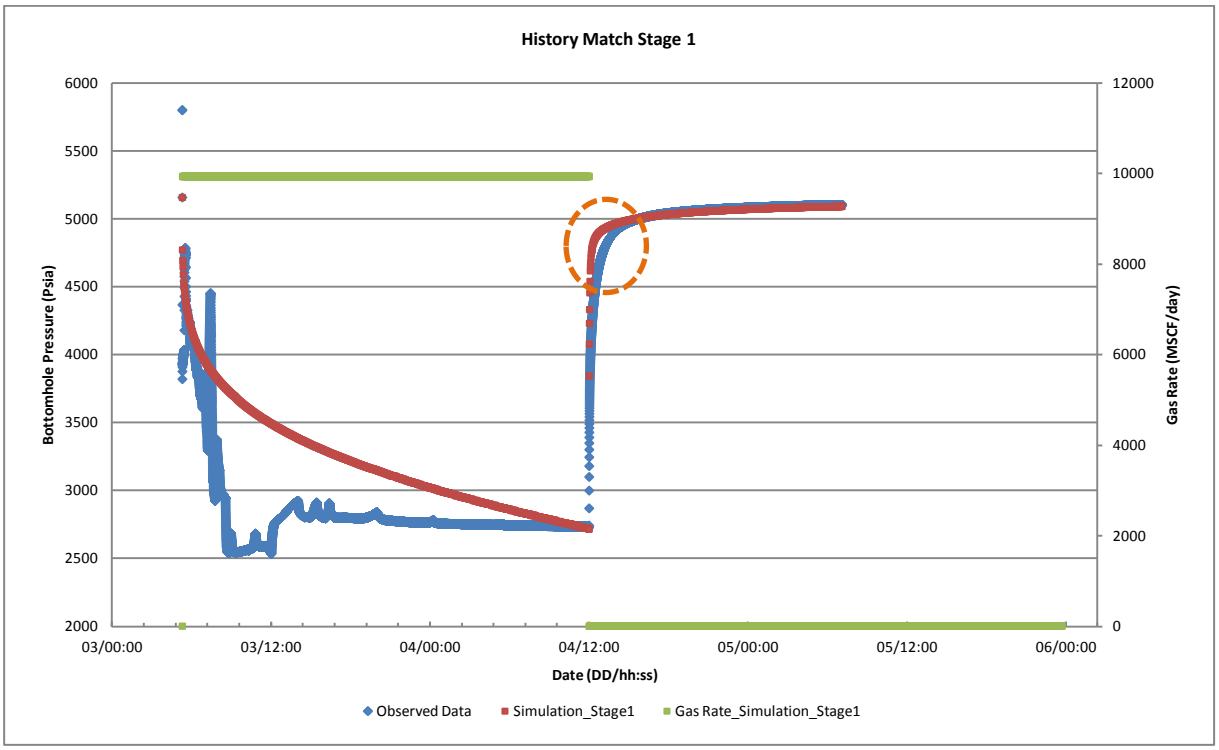

Figure 5.1. History Match Stage 1, BHP and Gas production simulation results and BHP history data

The necessary input data for this match was obtained after several sensitivities of the uncertainty parameters. The input data is described below:

5.1.2. Bourdet Pressure Derivative Match.

Figure 5.2 presents the results of the Bourdet pressure derivative for both history and simulation data. The procedure of the calculation of the derivative was the same as in section 3. As it can be seen, the match is not satisfactory for all the test, at early times both simulation and history data are close, which indicates that the near wellbore region (Region 1) is being well represented, however, as time advances, the simulation starts to differ from history data. This effect occurs through the entire second region, which represents the change in mobility due to condensate bank accumulation.

Further on, towards the end of the test, the match improves. This zone represents the radial flow area. Thus, it can be concluded that the effects of the near wellbore region and the radial region are been represented correctly, however, Region 2 is not representing the history correctly.

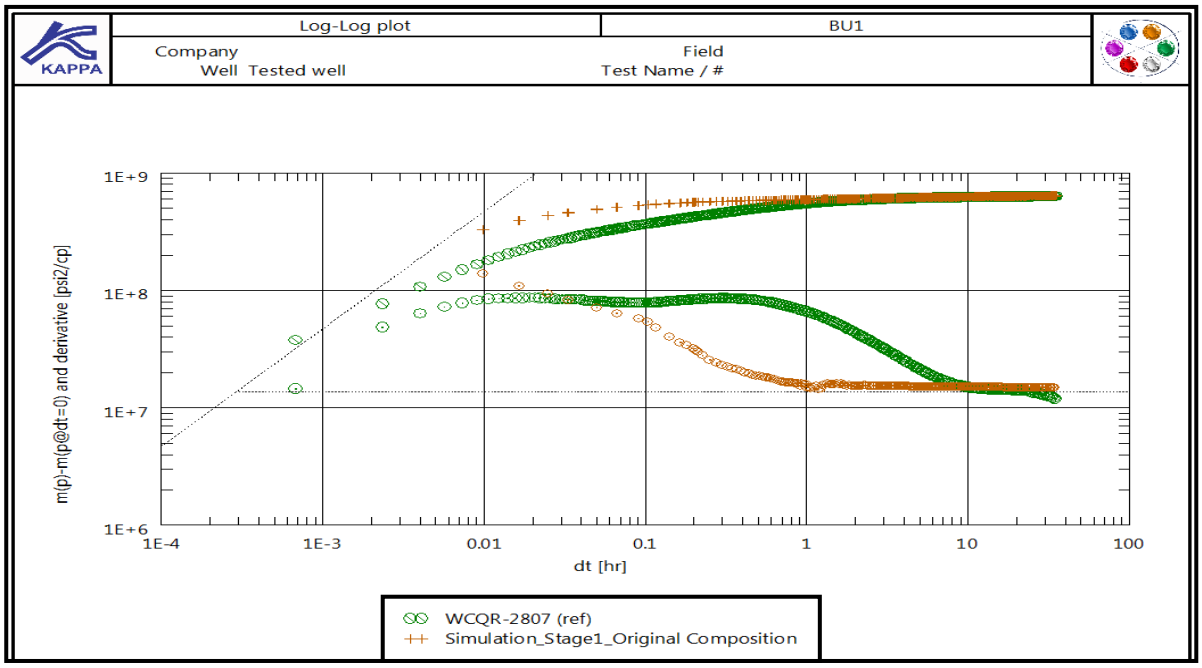

Figure 5.2. M1- Log-Log plot and Pressure derivative for BU1

The mismatch during region 2 occurs approximately between delta(t) equal to 0.1 to 8. Compering the derivative time period with the real time period (BHP Plot), it can be noticed that the mismatch occurs at the same time as that the mismatch of the BHP plot occurs (FIG. 5.1, “Dashed circle”). The reason for the mismatch was investigated, the conclusion was driven by the fact that the mismatch occurs during the 2nd Region, which represents the condensate bank extension, and is an indication that there is insufficient liquid dropout in the simulation model than in reality, hence a smaller condensate bank extension is build. Therefore, as the liquid dropout is controlled by the PVT properties, specifically by variables such as saturation pressure and Condensate Gas Relationship (CGR) it is believed that the combination of field measurement errors and the complexity of the fluid properties resulted in an incorrect CGR value. Whitson et al. (1999b) describes several causes of incorrect or non-representative in-situ samples, for instance due to two phase flow effects near the wellbore, which occurs when the BHP is below the saturation pressure.

Taking into account possibility of having an unrepresentative sample of the insitu reservoir fluid, which generates incorrect PVT properties calculations one could think that then the EOS characterization model will be also incorrect. Nevertheless, one should keep in mind that “any fluid sample that produces from a reservoir is automatically representative of that reservoir. After all the sample is produced from the reservoir” (Whitson et al. 1999b). Thus, the final EOS model characterization should match all the “accurate!” PVT properties, whether the sample is representative or not (Whitson et al. 1999b). Therefore, as the EOS characterization represents the fluids behavior correctly, one can assume that even by having a different fluid composition the EOS model should still represent the original fluid behavior.

Consequently, in order to confirm the idea of “insufficient liquid dropout” this study implements an approach of calculating a new gas composition using the EOS model generated using the sample fluid of the well. This method will increase the CGR, that in consequence will generate a higher liquid drop

out in order to achieve a better history match. This approach is presented in Stage 2 of the history match.

5.1.3. Uncertainty Parameters

As previously presented, the four uncertain variables were identified; these are the relative permeability curves, wellbore radius, velocity dependent relative permeability variables (VDRPO and VDRPG) and the absolute permeability. These parameters are modeled to achieve the match of the BHP and pressure derivative.

Relative Permeability Curves

The relative permeability curves used are based on three phase system (gas, oil, water), using Corey immiscible relative permeability correlation.

The final relative permeability curves are presented in Figure 5.3 and 5.4. Moreover, the Corey values are presented in table 5.1.

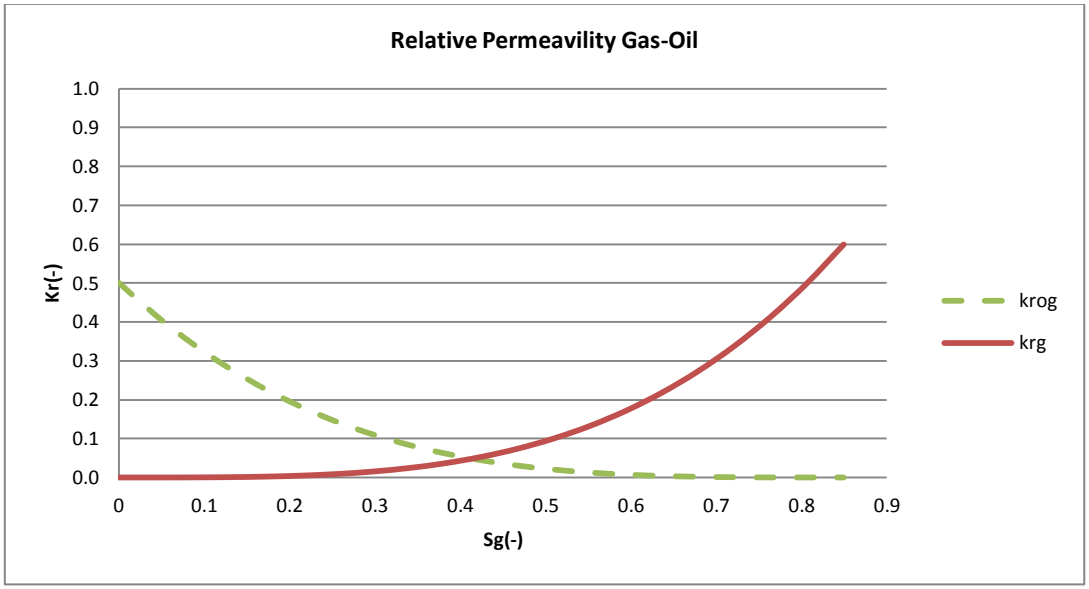

Figure 5.3. Relative Permeability Gas-Oil System

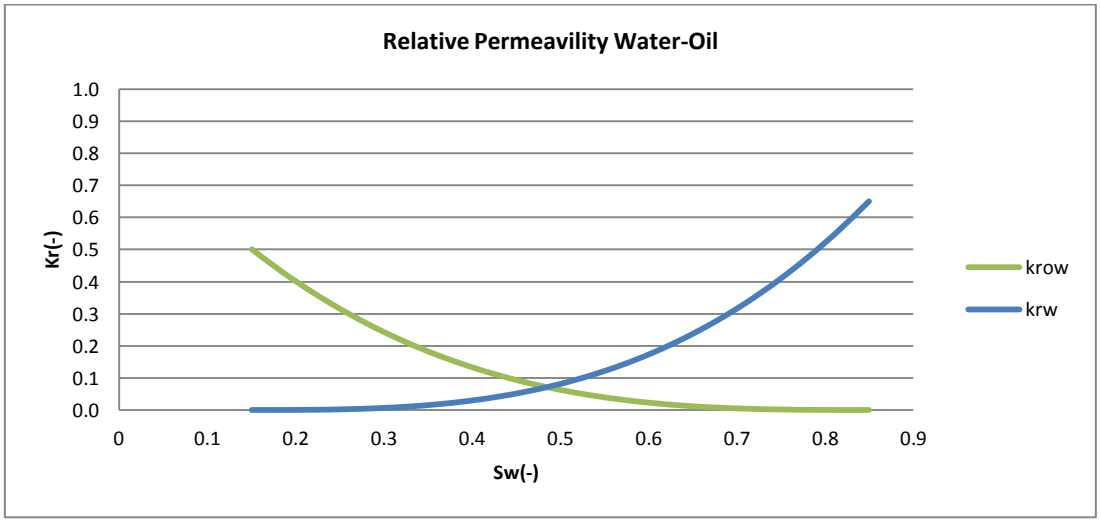

Figure 5.4. Relative Permeability Water-Oil System

Corey Immiscible relative permeability	
Gas-Oil System	
Sorg	0,15
Sgc	0
ng	3,5
no	3,5
krg(Sorg)	0,6
krog(Sgc)	0,5
Water-oil System	
Swc	0,15
Sorw	0,15
nw	3
no	2
kro(Swc)	0,5
krw(Sorw)	0,65

Table 5.1. Relative Permeability Corey Parameters

Wellbore radius.

The range of the wellbore radius was considered to be between 0.1 ft. and 2ft. The final match was achieved with a value of 0.5 ft. Therefore, it is assumed that the perforation depth is bigger than the wellbore radius reported by the Schlumberger CIT Report (2011), which was 0.165 ft.

Velocity dependent relative permeability (VDRP)

In order to model the stripping effects, the velocity dependent relative permeability option (VDRP keyword) was included. E300 provides two models, Heriot-Watt model and Fevang-Whitson Model. In each model, the calculation of the Capillary Number is required. Thus three Capillary Number (CN) models are available in the simulator. The best match was achieved using the Heriot-Watt model [1]. Moreover, the best match was achieved by including the VDRP option for both oil (VDRPO keyword) and gas (VDRPG keyword) phases, the parameters required for both VDRPO and VDRPG are presented in Table 5.2.

Several sensitivity runs showed slight effects of the Mg and Mo parameter. However, the N1,N2 and Ncb values had great influence in the results, therefore these parameters where the ones considered as the uncertainty parameters.

VDRPG			
Mg	$N1_g$	$N2_g$	Ncb
0	4	-1.0	1.0E-01
VDRPO			
Mo	$N1_o$	$N2_o$	Ncb
0	3	-1.5	4.0E-06

Table 5.2. VDRPG and VDRPO Parameters

Absolute Permeability (Kabs)

The well test analysis results showed different values of absolute permeability, 2.06md (2003) and 1.398 (2011). Therefore, the range of uncertainty of the absolute permeability was considered from 1.2md to 3.4md. The final match was obtained with a Kabs= 3.2 md.

5.1.4. Conclusion.

The following conclusions are obtained for the history match Stage 1:

- The target of matching the BHP and production data is achieved. However, the Bourdet pressure derivative could not be completely matched.

- The mismatch of the pressure derivate occurs in the 2nd region, which indicates that the simulation is not modelling correctly the condensate bank extension.

- It is believed that due incorrect or "non-representative" samples, the CGR is too low, which hence generates insufficient liquid dropout and thus a smaller condensate bank extension.

- The results presented above are a good indication of the importance of the Bourdet derivate analysis in gas condensate reservoirs. Without the pressure analysis one could believe that the BHP is correctly matched, and that the fluid behavior is been properly represented, however the Bourdet analysis gives us a clear indication that the simulation model is incorrect. This leaded to reevaluation of the entire problem.

5.2 History Match, Stage 2.

Due to the results of the history match "Stage 1", the necessity of restudy the input parameters was seen. As the Pressure Derivative could not be matched correctly, it was concluded that the simulation results exhibit insufficient amount of liquid drop out during the drawdown period. Thus, the idea was to calculate a new fluid composition, which in consequence will generate a higher liquid drop out. This section presents the methodology and results of implemented composition calculation process. Also it describes the results and discussion of the new history match results and its uncertainty parameters.

5.2.1 New Composition (CGR Match)

The calculation of a new composition was performed with the help of a thermodynamic fluid characterization software package, called PVTP from the company Petroleum Experts. This software provides two methods for calculating a new fluid composition, the first method is "Use separator Fluid" and the second method is called "Use fluid from Past". Both methods are based in the same main concept, which is to determine a base gas and oil composition derived from the system and afterwards recombine (Mixing Process) them until reaching a target Condensate Gas Relationship (CGR) using a known EOS model. The difference between both methods lies on the source of the "Base" gas and liquid to be mixed. The method implemented in this study was "Use Separator Fluid", and it consists of determining the base compositions once the fluid has passed through the separator train. The methodology for calculating the new composition is graphically presented in figure 5.5.

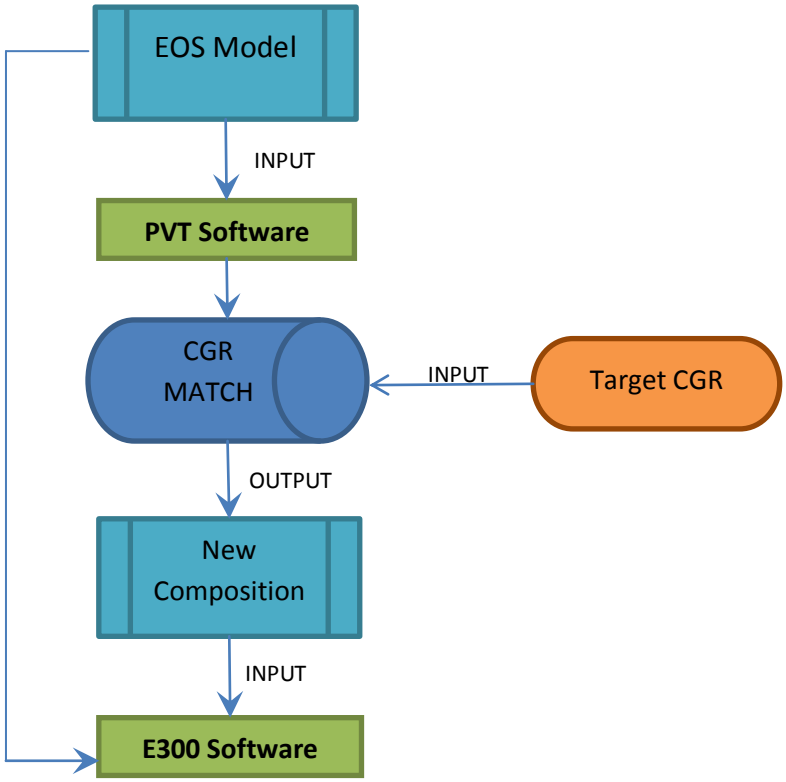

Figure 5.5. Workflow for New Composition Calculation.

One of the major concerns of using the above method was regarding the correct representation of the EOS by the PVTP software package. Therefore, in order to confirm the validity of the results, a cross validation of the PVT results was performed. Firstly, the EOS model was introduced to the PVTP software, secondly a Constant Composition Experiment (CCE) and a Constant Volume Depletion (CVD) experiment was performed using the PVTP software. Afterwards, the results of these experiments were compared with the results of the original PVT and the EOS matching results.

Figures 5.6 and 5.7 present a summary of these results, it can be seen that the PVTP software provide satisfactory results for most of the parameters, thus, it can be concluded that PVTP software is representing correctly the behavior of the fluid and thus honoring the EOS model.

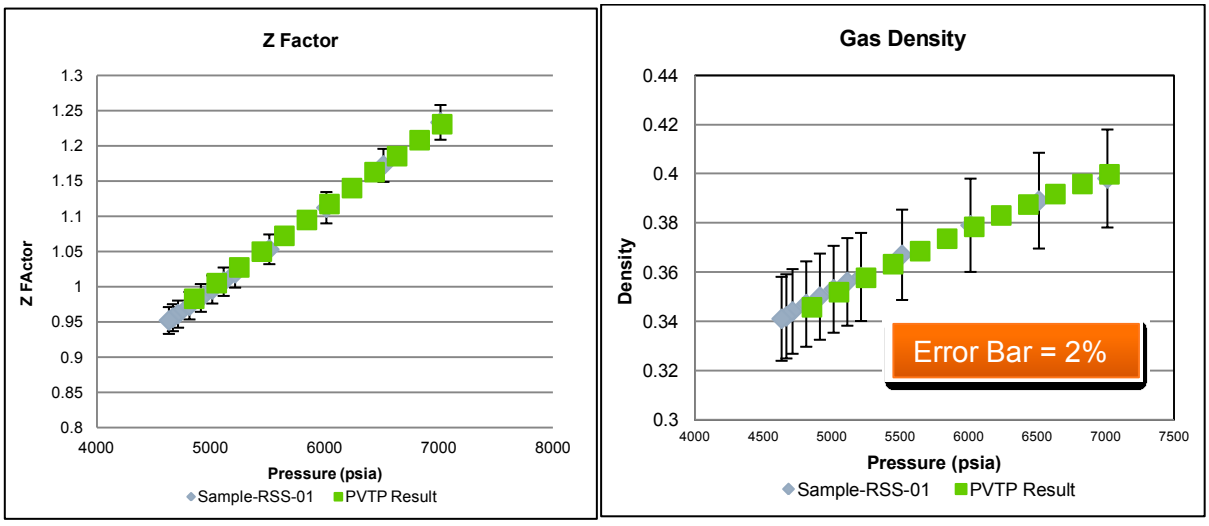

Figure 5.6. CCE Experiment. PVTP Results Comparison

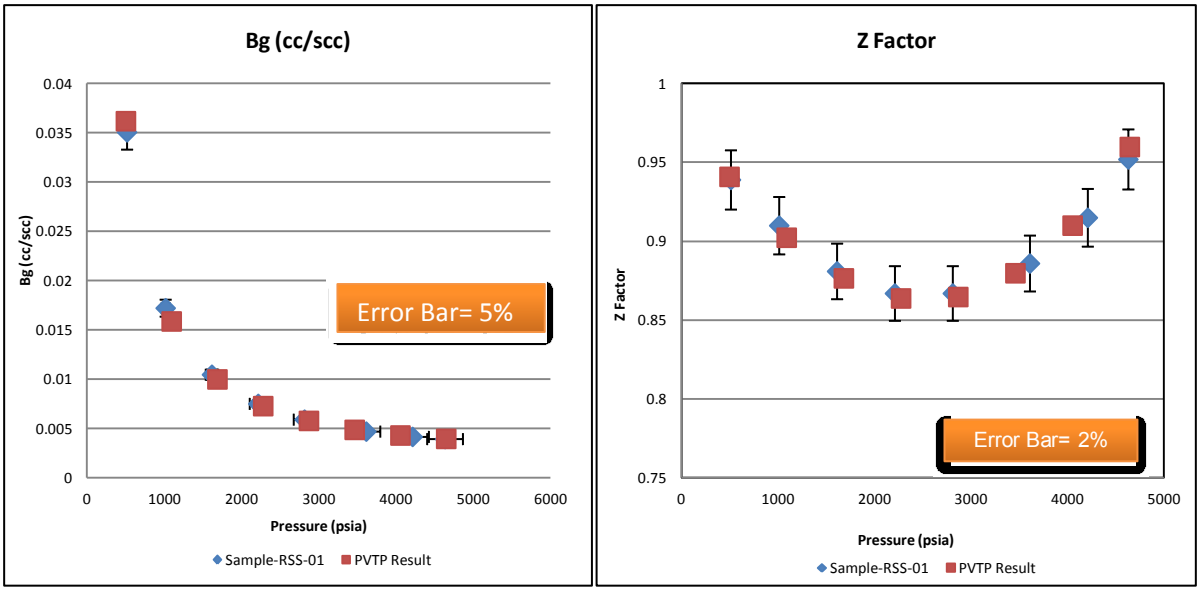

Figure 5.7. CVD Experiment. PVTP Results Comparison

As it can be seen in the previous workflow (Fig 5.5), two inputs are required, the EOS model which will be constant and the "target" CGR value. Thus, this parameter is now included as an uncertainty factor. Thus, several sensitivities were performed, having a range of uncertainty between 110 STB/MMSCF to 180 STB/MMSCF, it must be mentioned that this range was selected due to observed production values. Table 5.3 presents the results for 3 studied cases.

CGR	150 bbl/MMscf	140 bbl/MMscf	130 bbl/MMscf	115 (bbl/MMscf) Original
Components	Mole %	Mole %	Mole %	Mole %
C1N2	73,9764	74.4686	74.9673	76.0646
C2C3CO2	9,66766	9.72881	9.79077	9.92709
C4C6	5,88876	5.87514	5.86134	5.83099
C7C8	3,96094	3.80026	3.63742	3.2792
C9C10	2,6529	2.50564	2.3564	2.0281
C11C14	2,33499	2.19496	2.05306	1.7409
C15C35	1,51422	1.42272	1.32999	1.126
C36+	4,16887E-05	3,91694E-05	3,66164E-05	3,1E-05

Table 5.3. Target CGR values and New Compositions.

After obtaining several sets of different compositions for different CGR values, a new history match process was performed. The new composition was added to the E300 data file while using the same EOS model. Numerous sensitivities were performed in order to obtain the best history match, which was obtained with the values for the uncertainty parameters presented in the history match-stage 1 section. The final composition and results for the new history match are given below

5.2.2. BHP and Production Match

Figure 5.8 represents the best match for the BHP during the first drawdown and buildup period. These results were obtained using a new CGR equal to 150 Bbl/MMSCF, the composition is presented in Table 5.3,

Compering the previous BHP history match results (Original Composition with the new history match (New Composition), one can observe similar behavior during the drawdown period. At the beginning of the test no match of the BHP can be obtained, due to factors such as phase redistribution, further on the match improves until reaching the end of the drawdown period, where the BHP is matched properly. On the other hand, for the buildup period a better match is obtained with the new composition, particularly the improvement of the results between the time periods inside the dashed circle (Fig 5.8), where the original composition simulation fails.

Moreover, one can compare the condensate bank extension for both compositions, this in order to evaluate the difference of the liquid drop out. As it can be seen in figure 5.9, the new composition gives a higher condensate bank extension, approximately 49 ft. (14.96 m.) away from the wellbore, compared to 12.71 ft. (3.87 m) from the original composition. These results are encouraging for the pressure derivative match.

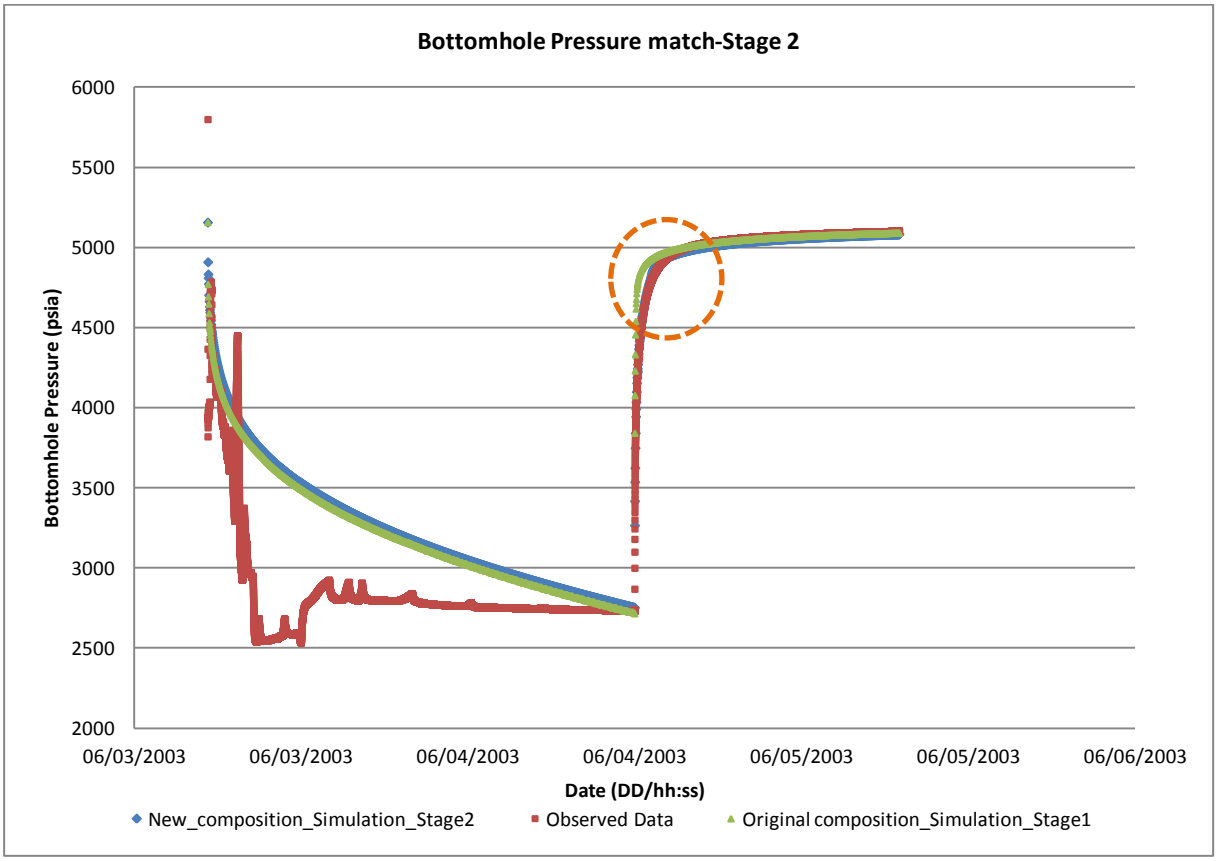

Figure 5.8. BHP Match-Stage 2.

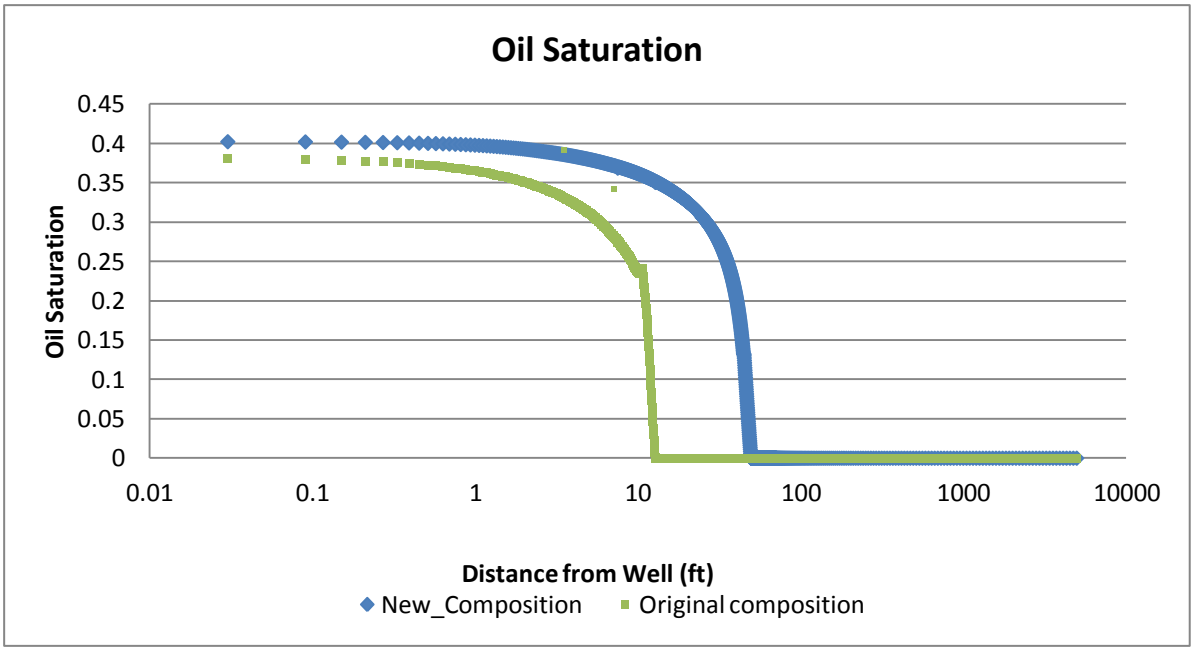

Figure 5.9. Oil Saturation-History Match-Stage2

5.2.3. Bourdet Pressure Derivative Match.

Results for the pressure derivative match are presented in figure 5.10. A clear improvement of the pressure derivative match is obtained with the new composition, it can be seen that the second region extends further than with the simulation results obtained with the original composition. These results indicate the influence of a higher extension of the condensate bank region. Moreover, an improvement of the first region is also seen, this may be due to influence of a higher oil saturation region in the velocity dependent relative permeability curves. Regarding the 3rd region, the Kh match can be considered as acceptable, however a perfect match could not be achieved in the derivative match.

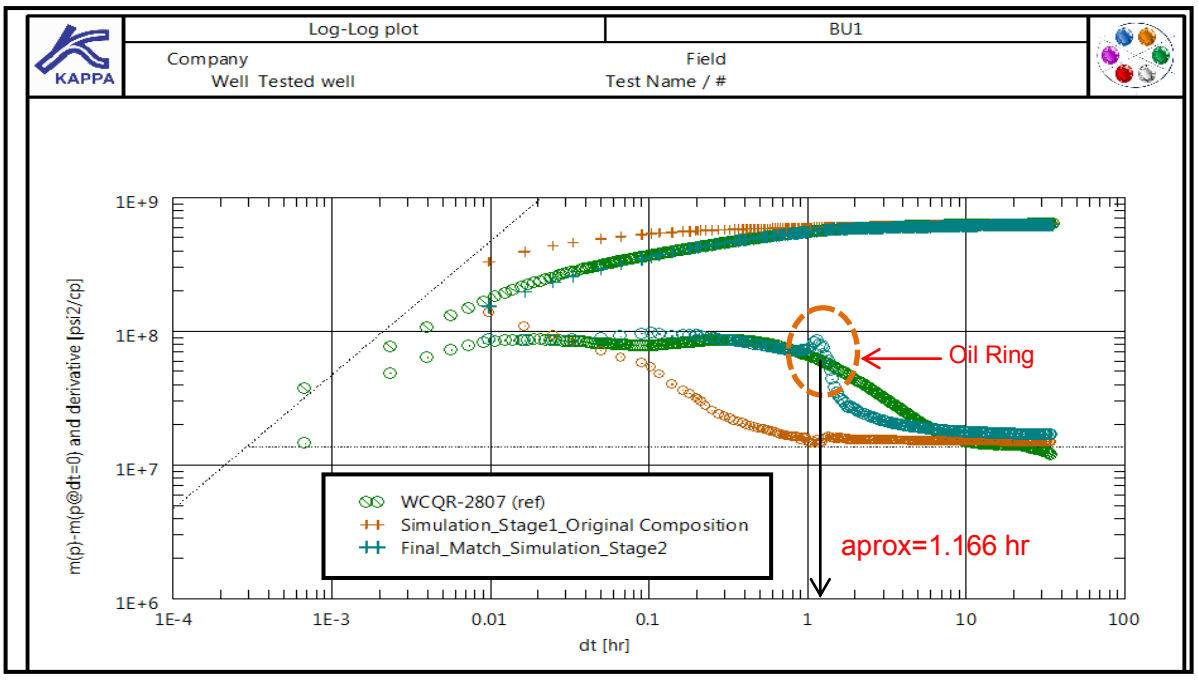

Figure 5.10. Bourdet Pressure Derivative Match-Stage2

One peculiarity can be observed in the pressure derivative curve (New Composition) approximately at delta(t)=1.166 hr. A “peak” rises which disturbs the continuity of the pressure derivative, the causes for this disturbance are analyzed.

Observing the behavior of the oil saturation during the buildup period at different times, as presented in figure 5.11, one can notice how the condensate bank saturation starts to increase towards the well and to reduce its extension (distance from the well), this behavior is due to compositional variations which occur during drawdown and buildup period, this phenomena will be analyzed in detail in the following subsection. Moreover, during the buildup period an irregularity in the distribution of the oil saturation is seen at 1.666 hr., an “oil ring” of maximum oil saturation forms in the outer boundary of the condensate bank extension, this “oil ring” is perhaps causing the distortion in the pressure derivative curve. Furthermore, the “Oil Ring” is just a transient effect and it disappears after the next time-step, as it can be seen in figure 5.11 (time= 1.2493 hr.).

The “Oil Ring” saturation forms at the same time as the pressure disturbance in the pressure derivative curve (“peak”) occur. Consequently, it is believed that this incorrect calculation of vapor /liquid equilibrium (“Oil Ring”) generates a disturbance in the continuity of the pressure derivate curve, as the curve bumps when it encounters a strong mobility change (oil saturation). The causes of this irregularity are discussed in the following paragraph.

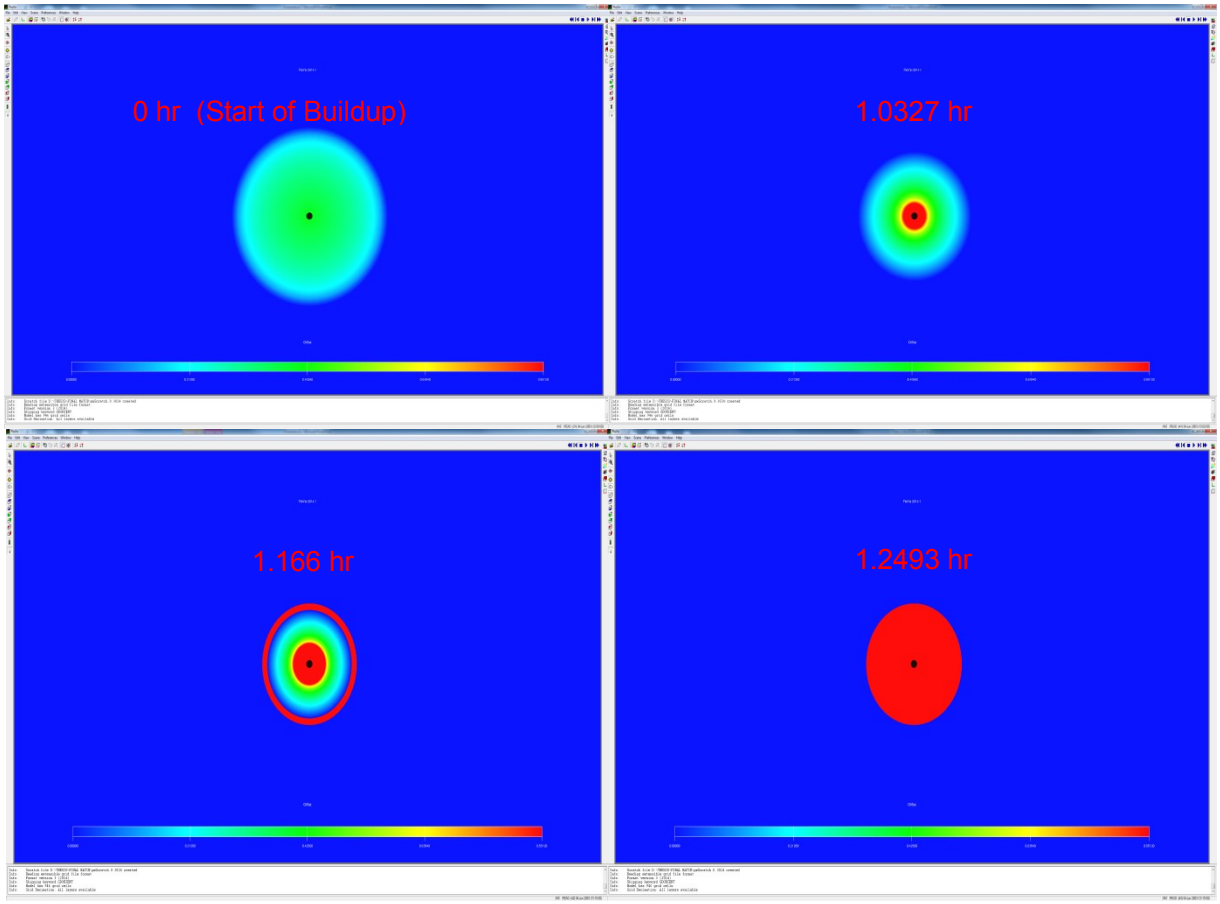

Figure 5.11. Oil Saturation profile during Buildup period

During each time-step the compositional simulator (E300) assumes complete phase equilibrium, which means that the following constraints must be fulfilled:

$$L + V = 1 \quad \text{(Eq. 5.1)}$$

$$L * Xi + V * Yi = 1 \quad \text{(Eq. 5.2)}$$

$$\sum_{i=1}^{N} Xi = \sum_{i=1}^{N} Yi = \sum_{i=1}^{N} Zi = 1 \quad \text{(Eq. 5.3)}$$

$$\sum_{i=1}^{N} \frac{Zi(Ki-1)}{1+V(Ki-1)} = 0 \quad \text{(Eq. 5.4)}$$

Where:
L= Liquid Phase
V=Vapor Phase
Xi= Moles of Liquid Composition
Yi= Moles of Vapor Composition
Zi= Moles of Fluid Composition
Ki= Yi/Xi = Vapor–liquid equilibrium, the ratio of vapor concentration to liquid concentration at equilibrium

This constrains forces that at each time-step the simulator within each cell must be at complete thermodynamic equilibrium, thus depending in the fluid composition it must decide if the fluid is classified as a gas or liquid phase. This condition may generate convergence issues during flash calculations are performed, mainly when solving the Rachford-Rice equation (Eq. 5.4) near to the critical points (Critical Temperature, Critical Pressure) at which the gas and the liquid phase become very similar-i.e., the phases become indistinguishable. The ECLIPSE 300 technical reference manual (2014) mentions the difficulty of solving the stability check constraint when the fluid composition is near the critical conditions.

Similar conclusions have been reported in Pattachini et al. (2014), which describes the issue of assuming complete phase equilibrium during each time-step in near-miscible gas flooding conditions. They mentioned that when phase equilibrium is assumed during gas flooding, the oil production is frequently overestimated.

In order to reduce distortion in the derivative curve, the smoothing option given by the SAPHIR software called. This option uses a "3 point central" derivative obtained from the weighted sum of the slopes between the given point and a point before and a point after. For the first and last data points, a "3 points right" and a "3 points left" derivative is used to reduce end effects. The "Smoothing" option opens a time window (X-L, X+R) around the point (X) and the derivative is calculated with respect to the points just before and just after this window (Houzé et al. 2015). The advantage of this option is that the data points which are out of the curve trend are now recalculated in order to construct a “smoother” curve, such as the “peak” in the pressure derivative results.

The final pressure derivative curve, after applying a smoothing window of 1, is presented in figure 5.12. One can notice that the simulation results after smoothing give a much better match of the pressure derivative, hence with these results it is concluded that the Bourdet pressure derivative has

been correctly match, and thus the constructed reservoir simulation model gives an acceptable representation of the well test analysis history.

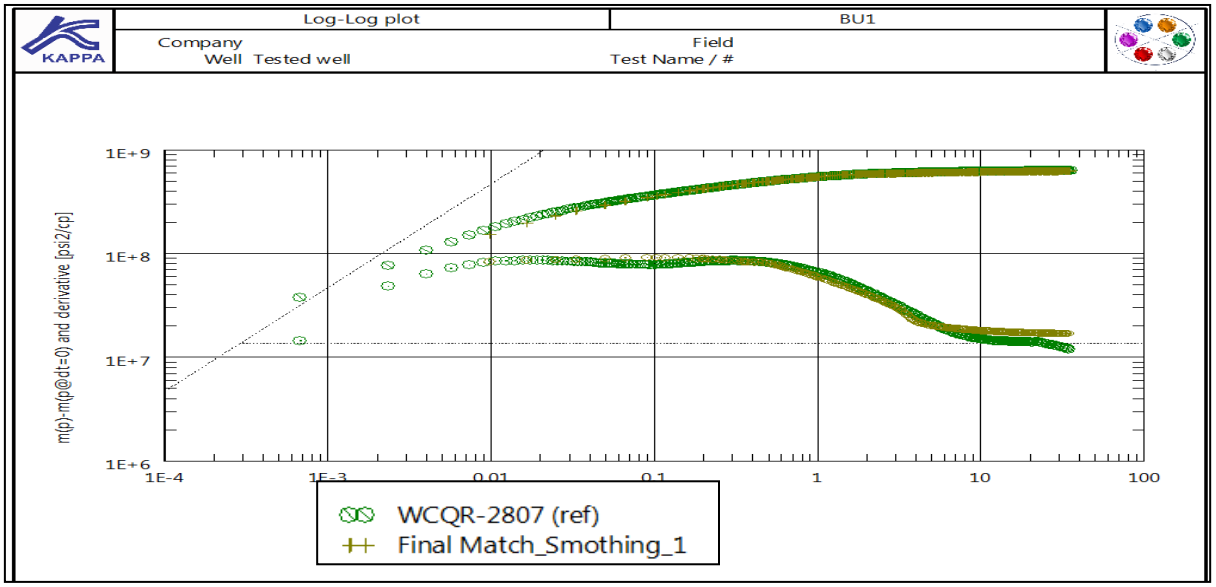

Figure 5.12. Bourdet Pressure Derivative Match - After Smoothing -Stage2

5.2.4. Uncertainty Parameters

As in the history match stage, the uncertainty parameters are defined in this section. The relative permeability curves are the same as in the history match stage 1, however the wellbore radius and the velocity dependent relative permeability parameters changed as follow:

Wellbore radius.

The range of the wellbore radius was considered to be between 0.1 ft. to 2ft. The final match was achieved with a value of 2 ft. Therefore, it is assumed that the perforation depth is bigger than the wellbore radius reported by the Schlumberger CIT Report (2011), which was 0.165 ft.

Velocity dependent relative permeability (VDRP)

The final parameters for the velocity the velocity dependent relative permeability model is presented in table 5.4.

VDRPG			
Mg	$N1_g$	$N2_g$	Ncb
0	4	-1.0	1.0E-03
VDRPO			
Mo	$N1_o$	$N2_o$	Ncb
0	3	-1.5	4.0E-06

Table 5.4 VDRPG and VDRPO Parameters

5.2.5 Further Analysis.

This Section will discuss some of the matters encountered during the process of the achievement of the study aims. The issue elaborates on the effect of compositional changes during depletion and pressure buildup.

5.2.5.1 Compositional Changes during well test analysis.

In order to confirm the theory of compositional changes mentioned in the theoretical section, a detailed analysis of phase envelope variation with time was performed. The analysis investigates the cell (1, 1, 1), which represents the cell connected to the well, and thus being the cell where the biggest pressure changes occurs during both drawdown and buildup.

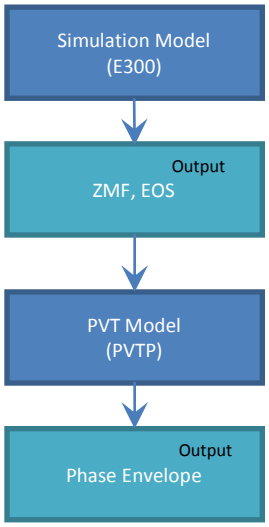

Figure 5.13. Workflow of Phase Envelope Calculation

Furthermore, the phase envelope was calculated using PVTP software where the EOS used both in PVTP and E300 was modeled and validated. The input composition was obtained from the overall composition (ZMF) values delivered by E300. The workflow is presented in Figure 5.13.

Drawdown

During DD1, three times are evaluated. At the beginning of the test (Initial composition), after 15 hours and at the end of the test (30 hours). The results are presented in figure 5.14.

The phase envelope diagram shows a clear indication of the composition change during depletion, below the dew point pressure, gas condensate dropout starts, where the heavier components start to accumulate in the liquid phase and the lighter components are produced faster due to its higher mobility. Consequently, as it is seen in the phase envelope diagram, not only the shape of the envelope changes, but most importantly the critical point, which indicates that the fluid system is changing its classification from gas condensate to volatile or black oil fluid. Moreover, compositional changes effects is mostly seen in the near wellbore region, since it is where the biggest pressures draws occurs.

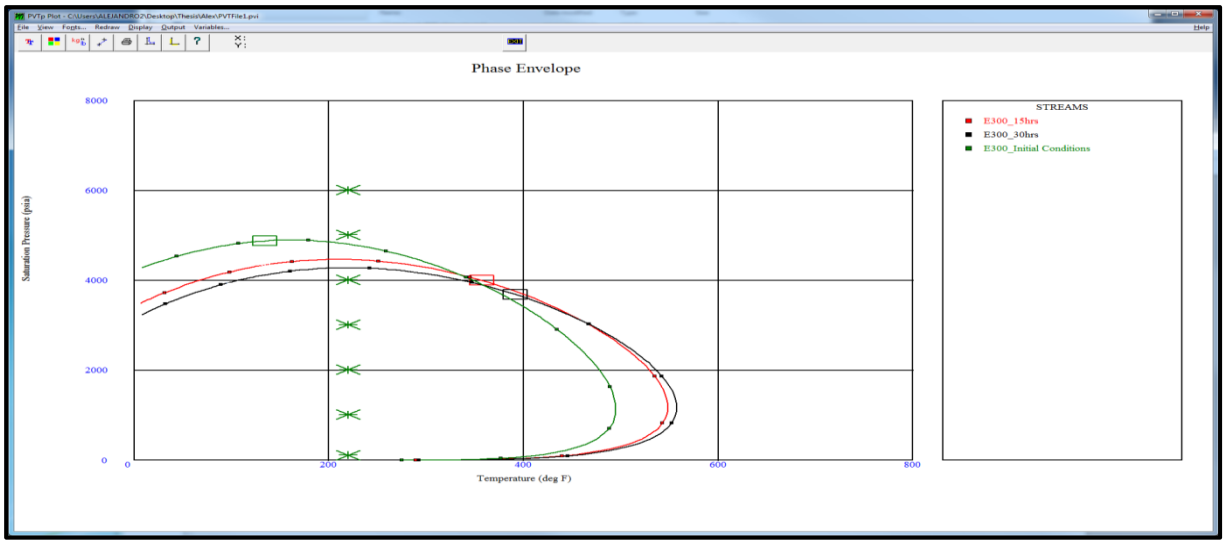

Figure 5.14 Phase envelope changes (Cell "1,1,1"), Drawdown.

Buildup

Similar to the DD1 analysis three periods of time were studied during the BU1, however the second time evaluation was done only 22 minutes after the buildup start, since the changes in composition are very small during the buildup period. The results are shown in figure 5.15.

The results shows little or almost no variation of the phase envelope shape and its critical values, this due to no production of the reservoir fluids, thus after a period of time the molecules within both phase reach equilibrium.

Additionally, it is seen that for the cell (1,1,1), the fluid changes its condition towards a more volatile oil, thus as the pressure increases the gas will condense until all the system becomes liquid. This phase change (gas to liquid) occurs in the near wellbore region (Condensate bank) where the fluid system changed its properties due to the accumulation of the heavy components and production of the lighter ones. On the contrary, in the outer region of the condensate bank where the oil saturation is less at the end of the drawdown (Fig 16.), the fluid still behaves as a retrograde gas since the compositional change effect was not as strong as in the near wellbore region. The phase envelope for the outer region cell is visualized in Figure 5.17.

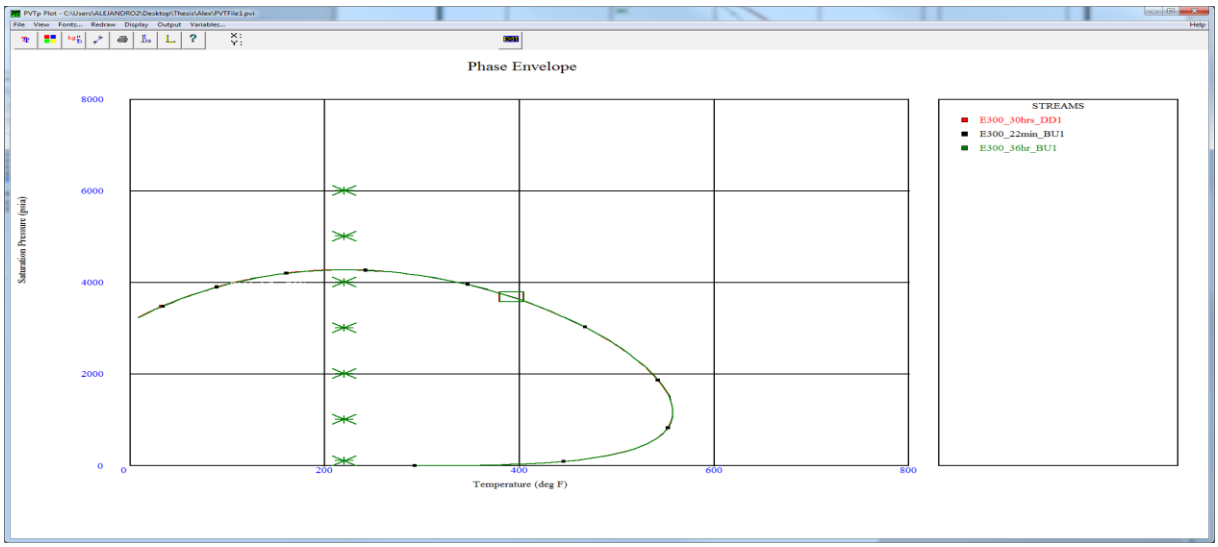

Figure 5.15. Phase envelope changes (Cell [1,1,1]), Buildup

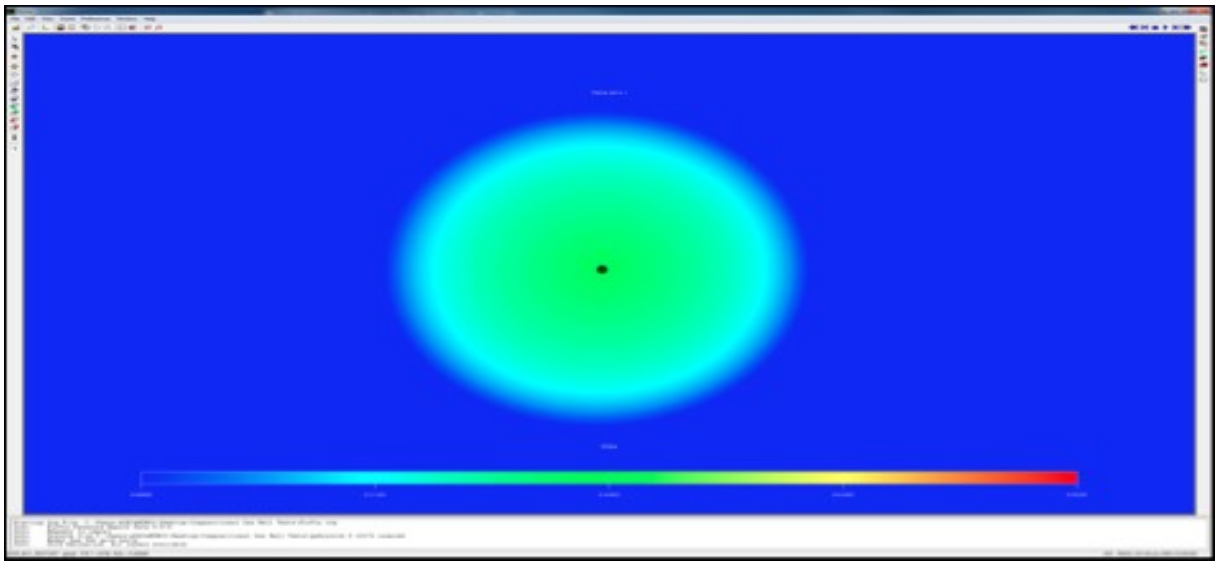

Figure 5.16. Oil Saturation at the end of DD1

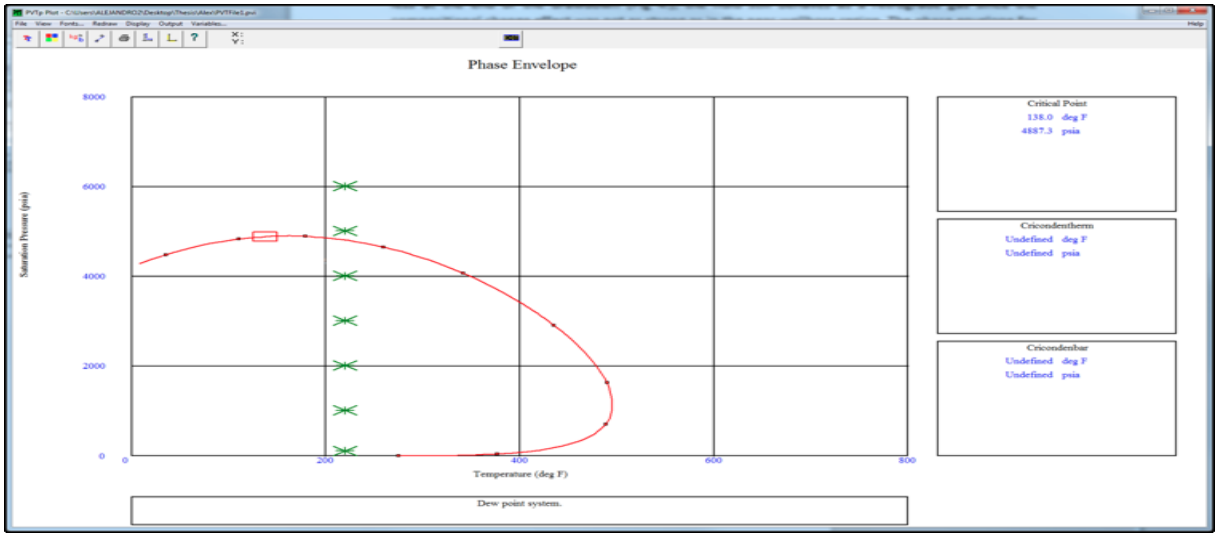

Figure 5.17. Phase Envelope for the Outer Cell of the Condensate bank at end of DD1

5.3. Conclusion.

It is concluded that an acceptable match of the well tests analysis has been accomplished. This match was achieved after introducing a new fluid composition which represented a higher CGR (150 STB/MMscf) than the original (115 STB/MMscf). Moreover, throughout the simulation and analysis of the new composition model, an incorrect fluid saturation profile during the buildup period was perceived; the causes of this have been generally analyzed, however, no direct solution within the simulation software was found. Furthermore, it was seen that the fluid saturation miscalculation generated an irregularity of the Bourdet pressure derivative curve; this issue was solved by applying a smoothing method which was available in the well test analysis software.

The achievement of history match while applying the new fluid composition model, demonstrates the importance of the correct measurement of the fluid properties. Also, it remarks the significance of performing a well test analysis in gas condensate reservoirs, especially the analysis of the Bourdet pressure derivative curve, which as in this study, can be used as a tool for confirming the validity of the simulation model and thus the used PVT model.

Chapter 6

Forecast.

This study performs a forecast analysis in order to evaluate the influence of the condensate bank in well performance. The impact of the new composition model (CGR=150 STB/MMscf) is compared with the original composition model, moreover the influence of the stripping effects are also evaluated.

The forecast analysis setup is the following; the analysis is done with a gas rate target of 6000 Mscf/day, this value is determined as an average of the latest reported production rates of the well. Furthermore, a bottomhole pressure lower limit of 1450.38psia (100 bar) is assumed. The total production time is 20 years.

For the sake of simplicity of the following analysis, we will refer the "old composition" model as Case 1, "New Composition" model as Case 2, the "New Composition" model without stripping effects as Model 3 and the "Old Composition" without stripping effects as Case 4.

Cases	Name
Case 1	Old composition
Case 2	New Composition
Case 3	New Composition model without stripping effects
Case 4	Old Composition without stripping effects

Table 6.1 Studied Cases

6.1 Analysis.

A first analysis is done by comparing the difference of the gas production rates for cases 1 and 2. As presented in figure 6.1 one can notice a remarkable difference between the duration of both plateaus, for case 1 the gas plateau extends until 1775 Days (4.9 Years) after the beginning of production, in contrast with case 2 which only extends until 204 Days (0.56 Years). Furthermore, as the gas production declines for both cases, a different behavior in the decline slope can be noticed. For Case 1 the decline is faster, this is caused by the effects of a longer and higher gas production which will cause a higher depletion of the gas in place and pressure. Thus, when comparing the reservoir pressure for both cases, the reservoir pressure for case 2 is higher (Fig. 6.2). The pronounced discrepancy between the gas rate plateaus are the most notable feature, reaching an overestimation in the gas plateau by a factor of 8.7, which may have significant effects in the correct field development plan of the reservoir.

Figure 6.4 compares the cumulative gas rate for the model with the Case 2 (CGR=150 STB/MMScf) and the Case 1 (CGR= 110 STB/MMScf), moreover table 6.2 presents the values final values for both cases after 20 years of production. The results of this plot demonstrate the negative influence of higher condensate bank in the gas productivity; the gas cumulative production is overestimated by 8.6%, and also the recovery factor is overestimated by 4%.

Regarding the condensate production rate (Fig 6.3), a substantial difference is seen only at the beginning of the production period. However as production continues both rates become more similar. Nevertheless, case 2 which represents the model with the highest CGR always gives higher condensate production. The difference between both cases can be better visualized when comparing the cumulative oil production (Fig. 6.5), which is being underestimated by 8.03 % and the oil recovery factor is being overestimated by 20.4% (Table 6.3). Moreover, the impact of the higher condensate gas ratio case (Case 2) can be seen in the condensate bank extension (Fig. 6.5), where case 2 leads to a higher oil saturation in the reservoir.

Moreover, with the intention of a better understanding of the effects of the condensate bank one can analyze figure 6.6, which represents the comparison of four variables (oil and gas flow rate at reservoir conditions, oil saturation and reservoir pressure) at the beginning of the production period (01/03/2016). As it can be seen, Case 1 (Red curve) starts producing gas at a high gas flow rate, and no condensate bank has forms since the pressure has not reached the dew point pressure, thus no oil is formed. On the other hand, the pressure for Case 2, has already reached the dew point pressure, which in consequence causes condensate to dropout and as the saturation is higher than the critical saturation it starts to flow. This condensate bank formation causes a decrease in the gas flow rate and thus lower relative permeability to the gas.

Until now we have only analyzed the influence of a new composition with higher CGR on the forecast. Thus, with the intention of evaluating the influence of the velocity stripping effects a further comparison is performed between case 1-4 and 2-3. First comparing the results in production cumulative for both gas and condensate, figures 6.7 and 6.8 respectively, no difference is found in the results, meaning that in this case the stripping effects are not perceived in the total well productivity. On the other hand, if one compares the BHP in figures 6.9 and 6.10, a different decline behavior for the cases without the stripping effects during first months of production is visible, however after the pressure continues to decrease the influence of the capillary number effects (For Cases 1 and 2) appear to be defeated by the effects caused by the decrease in BHP. The idea is the following, as the BHP decreases more liquid dropout (Fig 6.10) will start to accumulate in the near wellbore region (region where the capillary number effects are present), this liquid will be rich in heavy components due to compositional changes (Section 5.2.5.1), which in consequence will increase the surface tension (6.9) between liquid and gas, and increase the liquid viscosity. The combination of high surface tensions and high viscosity will cause the capillary number effect to be neglected.

6.2 Conclusion.

The importance of having a correct PVT model is highlighted in this section, in particular the impact of an incorrect measurement of the CGR over the predictions of gas cumulative production. Particularly, this section has presented the influence of a higher CGR in the prolongation of the gas production plateau, where an incorrect underestimated measurement of 23% in the CGR (Original CGR equal to 115 STb/MMscf) could lead to an overestimation of the gas plateau by a factor of 8.7, which will cause and incorrect field development plan and thus has severe economic consequences.

Furthermore, an analysis was carried in order to understand impact of stripping effects in well productivity. The results showed that the influence of the stripping effects for this case were negligible in terms of gas and oil production cumulative. Nonetheless, the impact of the stripping

effects was noticed only during the first months of production, especially in the BHP and the oil saturation profile. However, after certain pressure decline the stripping effects were not noticed.

Cases	Cumulative Gas Production	Recovery Factor
Case 1	47000 MMscf	60.63 %
Case 2	45330 MMscf	57.87 %
Difference	8.6 % (Overestimation)	4.7 % (Overestimation)

Table 6.2 Cumulative Gas Production

Cases	Cumulative Oil Production	Recovery Factor
Original Composition	988 MSTb	19 %
New Composition	1074 MSTb	15.75 %
Difference	8.03 % (Underestimation)	22 % (Overestimation)

Table 6.3 Cumulative Oil Production

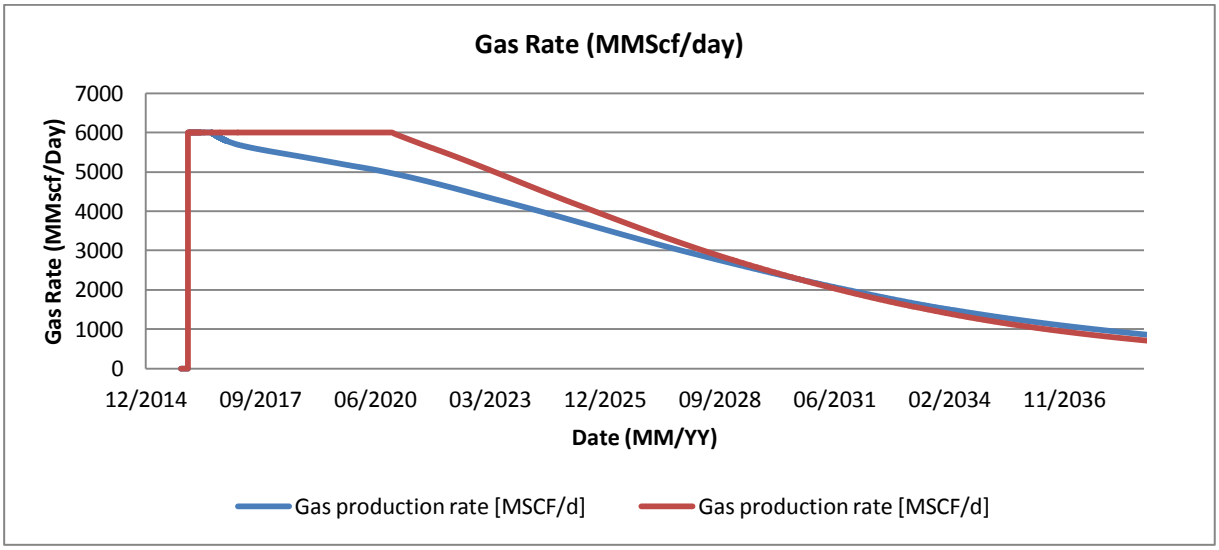

Figure 6.1 Gas Production Rates.

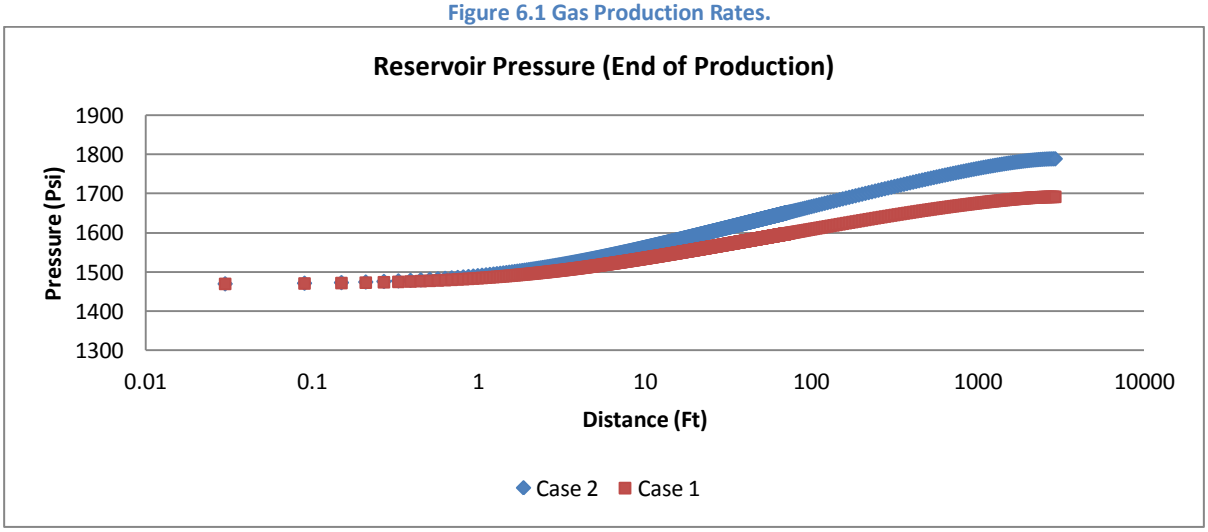

Figure 6.2 Reservoir Pressure at End of Forecast

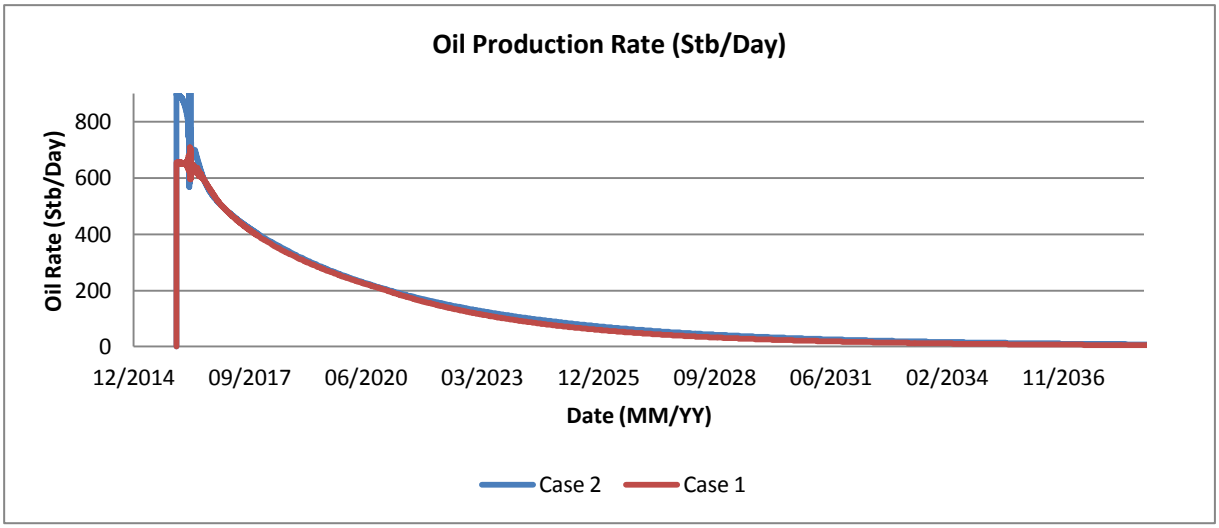

Figure 6.3 Oil Production Rates

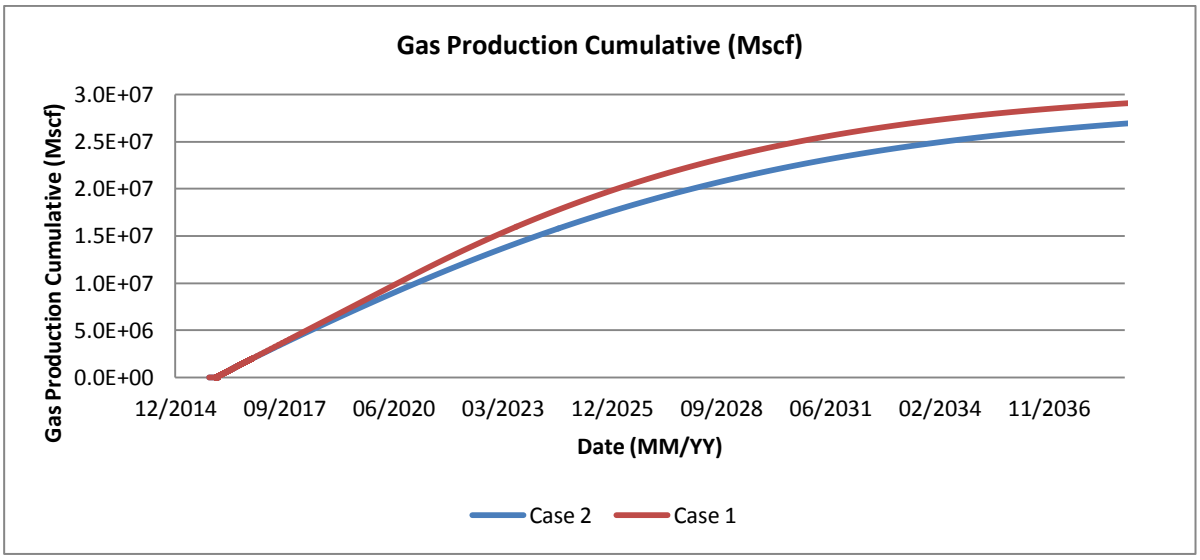

Figure 6.4 Gas Production Cumulative

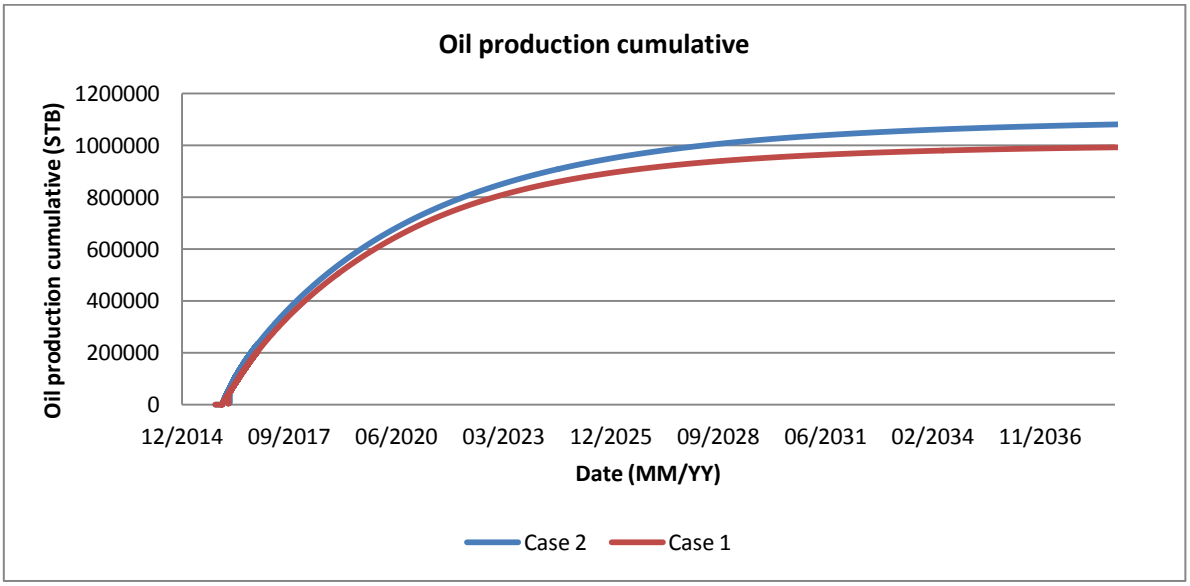

Figure 6.5 Oil Production Cumulative

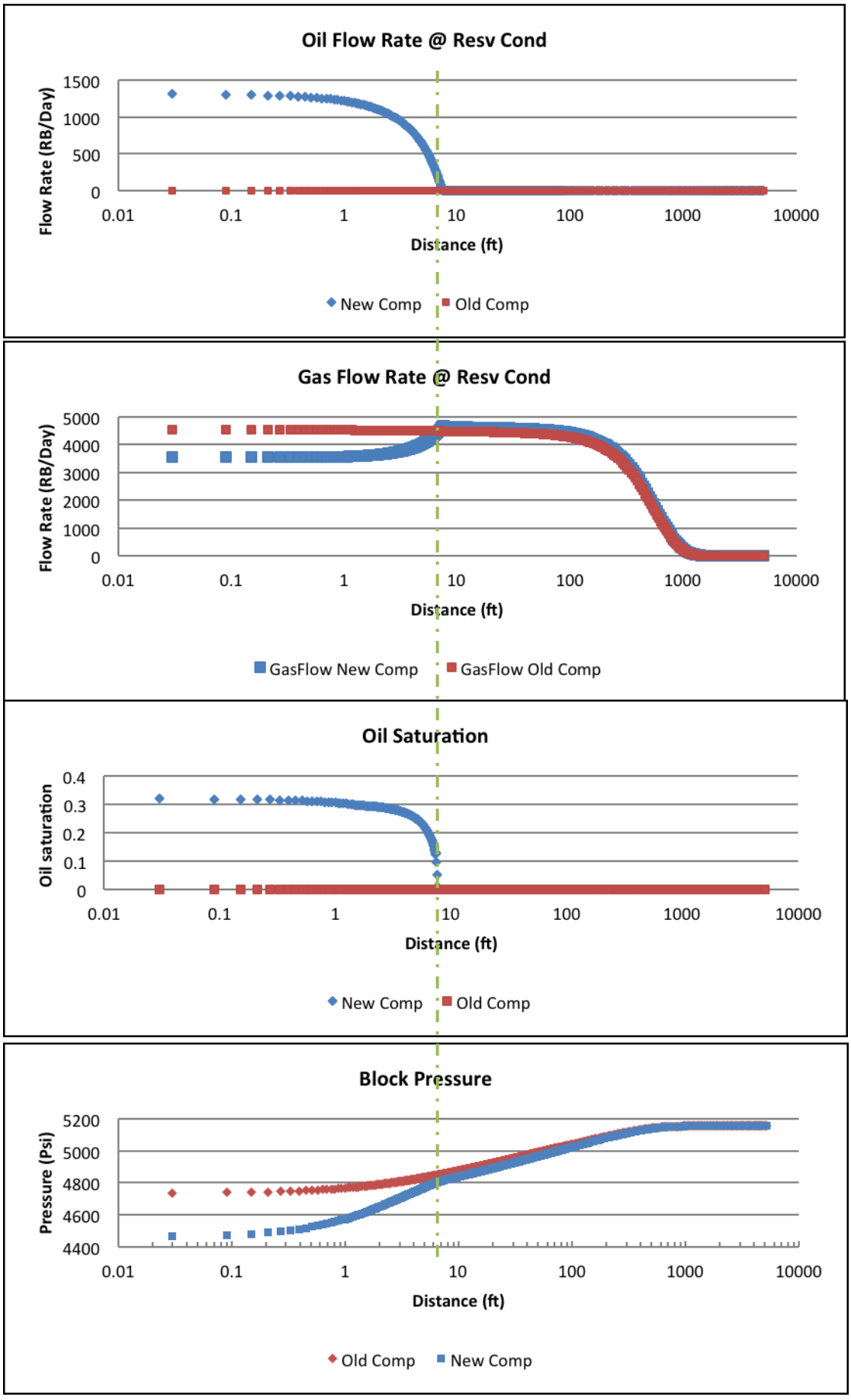

Figure 6.6 Oil saturation, Reservoir Pressure, Oil and Gas flow rate at Beginning of production period

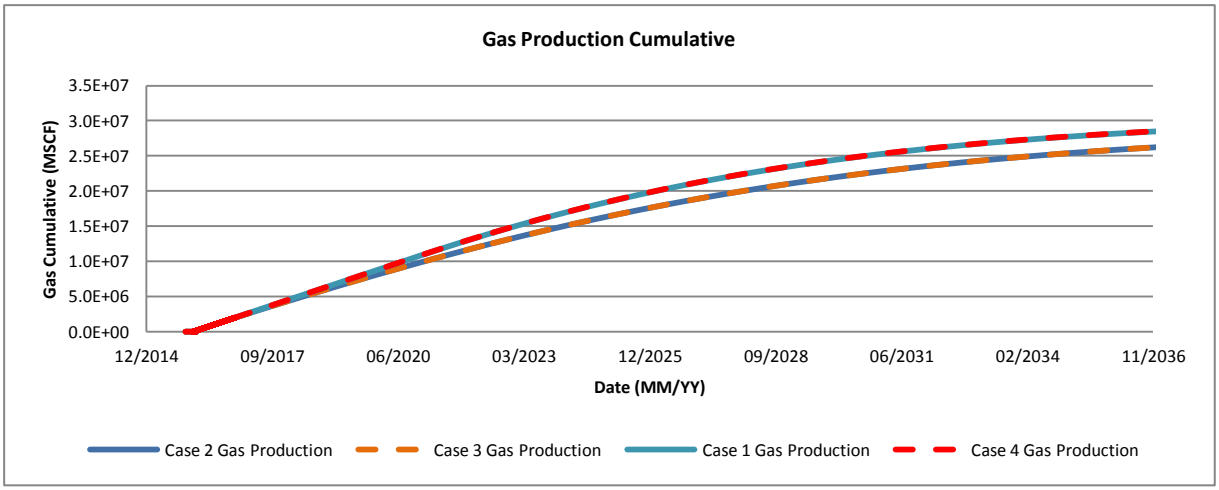

Figure 6.7 Gas Production Cumulative, the curves for cases 3-2 and 4-1 overlap

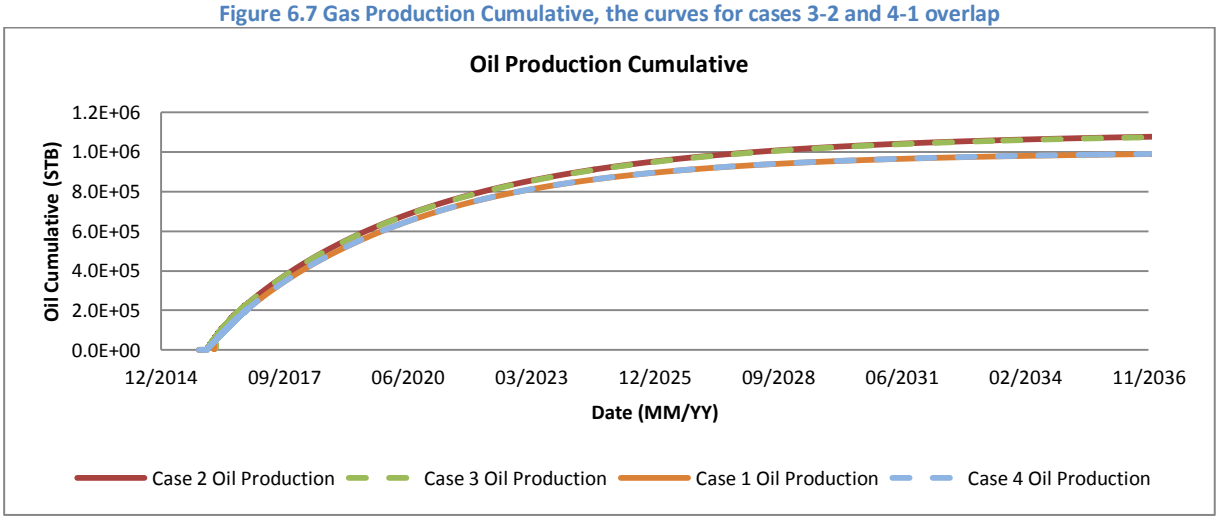

Figure 6.8 Oil Production Cumulative, the curves for cases 3-2 and 4-1 overlap

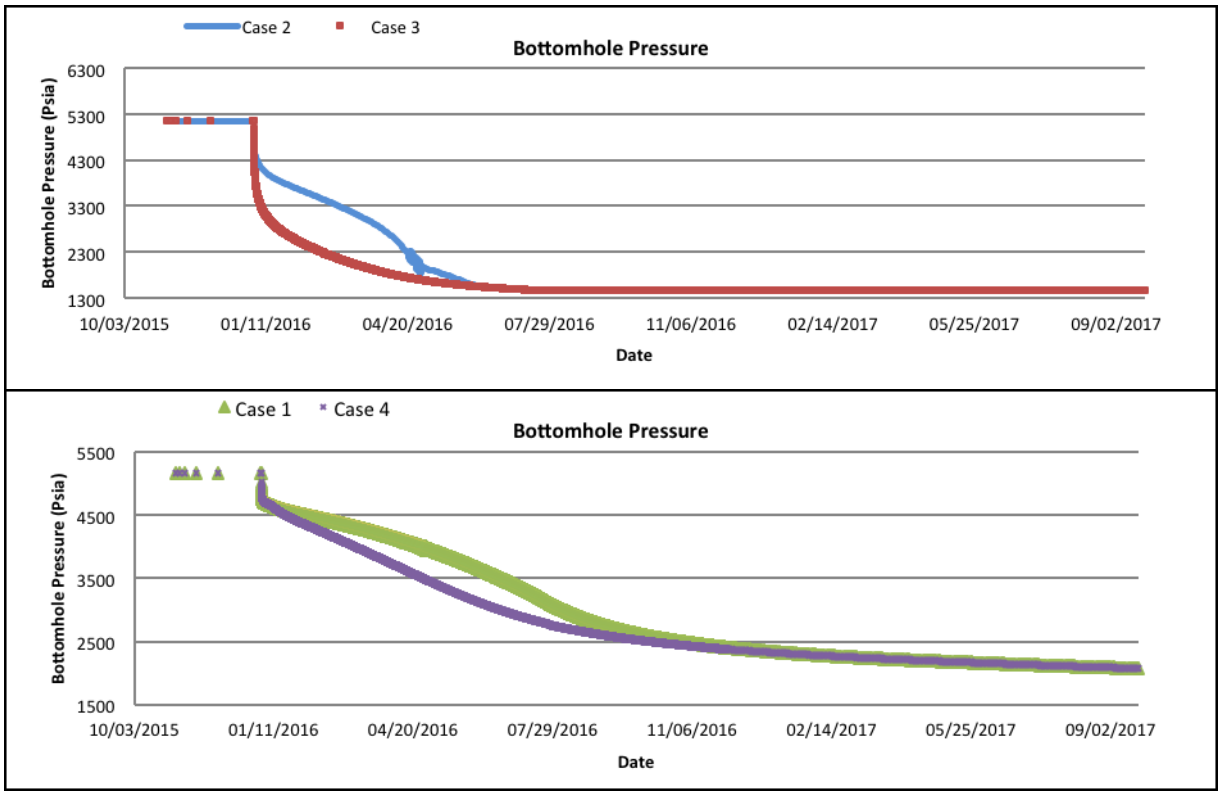

Figure 6.8 Oil Production Cumulative

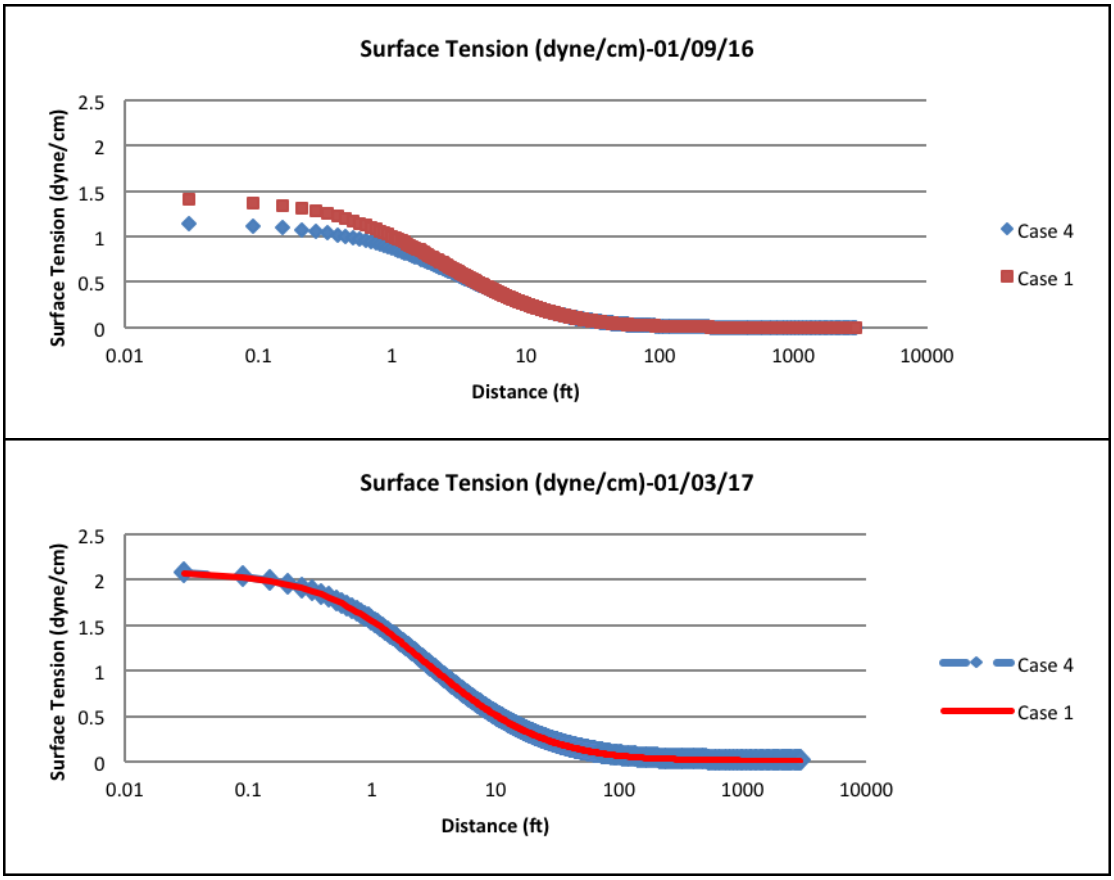

Figure 6.9 Surface Tension Changes

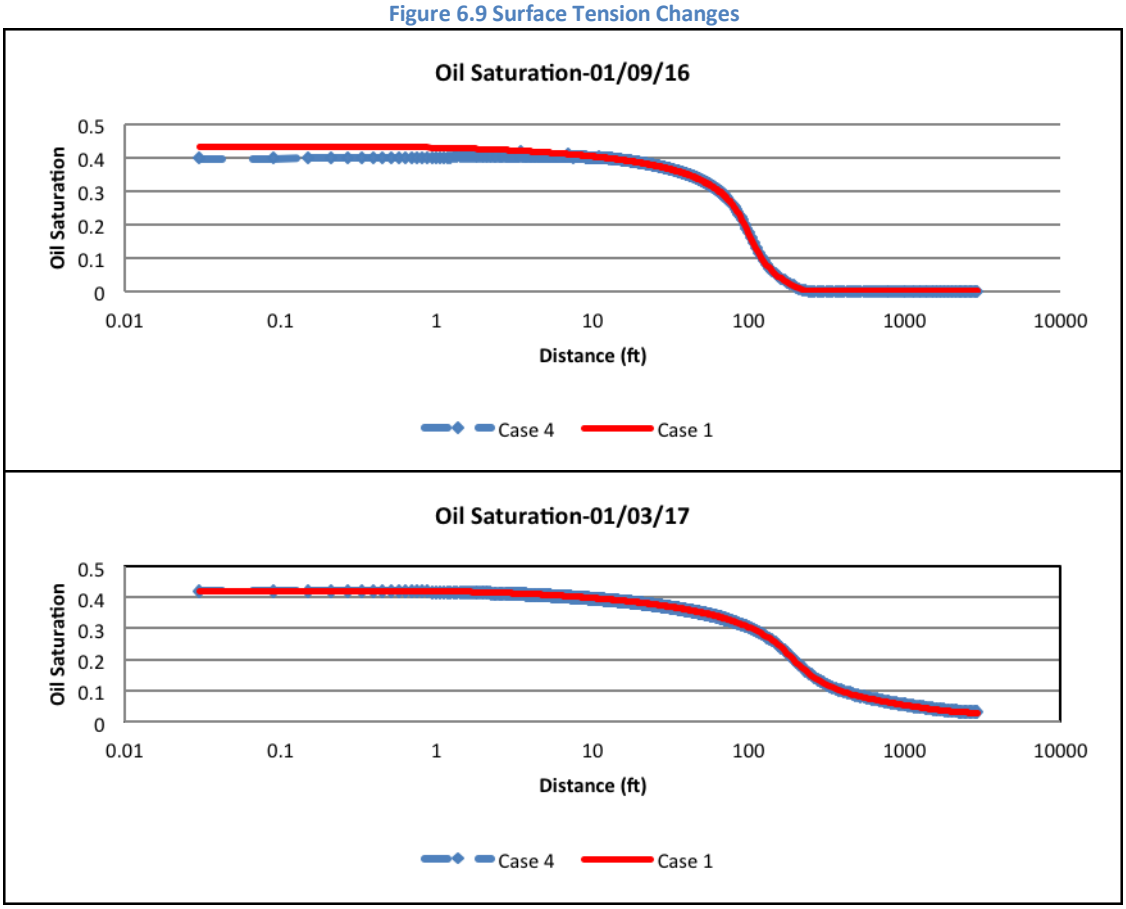

Figure 6.10 Oil Saturation Changes

Chapter 7

Conclusions

Sensitivity Analysis

A sensitivity analysis was performed in order to understand the impact of the most uncertain values in the simulation model. The most remarkable conclusions for this study are the following:

- The influence of the critical oil saturation on well productivity seems to be low. However, it was noticed that by having a bigger value of the Soc the condensate bank extension is higher, since higher Soc means that higher oil saturations must exist in order be mobile. Thus, with a higher Soc the longer the condensate bank extends into the reservoir.

- The influence of the Corey exponents in the relative permeability curves is transmitted as the curvature of the relative permeability curve. Values which approach to 1 will generate curves that approach the "X" shape, thus having higher values of relative permeability. The impact of different Corey exponent values in the simulation model was in agreement with the theory. For high values, the productivity index of the evaluated phases decreased, on the contrary for low values (towards 1) a higher productivity index was seen. Moreover, the influence of the Corey exponents on the condensate bank was also seen, its effects were mostly in the accumulation of the condensate in the near wellbore region and not in the extension of the condensate from the well.

- The influence of the relative permeability end points was also studied. The gas relative permeability at irreducible liquid saturation ($K_{rg(Sorg)}$) had a greatest impact in the well productivity and in the condensate bank extension, the overall conclusion is that a lower $K_{rg(Sorg)}$ causes a lower availability of the rock to transmit system fluids (Gas-Oil), meaning that each fluid component will travel with more difficulty and thus accumulating while increasing the fluids viscosity and decreasing the total mobility of the fluid towards the well, thus generating lower productivity and higher condensate bank extension.

- The wellbore radius had the greatest impact in well productivity, and not in the condensate bank extension and saturation. Moreover, it was seen that the extension of the wellbore radius, will help to temporarily overcome the condensate bank "blockage" effects.

- The study of the influence of the velocity dependent relative permeability curves showed that for high base capillary numbers (BCN) the effects of VDRP are irrelevant, whereas for small BCN the effects of VDRP model is evidently detected. Moreover, three interrelated effects of VDRP are seen, changes in the gas velocity in the near wellbore region, increase in the relative permeabilities and a decrease in the interfacial tension. All of these effects lead to a more miscible system, which causes an increase in the wells productivity and thus affects the analysis of the results. Finally, it is concluded, that owing to the significant influence which the velocity dependent relative permeability model can have in the simulation results, and thus is the final determination or forecast of the well productivity it is

concluded that capillary number effects, if present, must be carefully determined and included in respective calculations.

Well Test Match

The main objective of this study was to match the well test data (BHP and Production) and the well test interpretation Bourdet derivative curve. This goal was successfully accomplished; the most important conclusions are the following:

- A first match of the well test data (BHP and Production) was achieved. However, the Bourdet derivative match could not be accomplished, mainly in the second region (Condensate bank). The reasons for this mismatch were studied, the main conclusion was that the properties of the fluid (given by the PVT) showed insufficient liquid dropout, thus a low condensate bank extension in the simulation results.

- It was concluded that the insufficient liquid dropout could be due to incorrect field measurement, which lead to an incorrect condensate gas relationship (CGR) calculation. This is influencing the composition given by the EOS model.

- The Bourdet derivative curve was successfully matched after a new fluid composition with a CGR equal to 150 STb/MMscf was used. The calculation of the new composition was performed with the same EOS model, this in order to maintain the volumetric and phase behavior of the fluid.
- Compositional changes during the drawdown and buildup period were seen. The changes lead to substantial alteration of the fluid behavior. Hence, in the near wellbore region, the reservoir fluid behaved as a volatile oil instead of gas condensate. The biggest compositional changes occur in the near wellbore region.

- It is concluded that stripping effects exist, and impact the history match. Thus the stripping effect was included in the final history match model.

- The importance of the Bourdet derivative curve in gas condensate reservoirs is highlighted in this study. It was presented how the derivate can be used as a tool to confirming the validity of the simulation model, as it captures effects which are not seen in the conventional history matching process.

- Since phase behavior of gas condensate fluids is very complex and its correct PVT representation is subjected to different errors such as incorrect measurements. The methodology applied in this thesis can help validate the PVT model.

Forecast

Forecast was performed in order to evaluate the impact and difference between the proposed “new” comp and the “old” composition; the main conclusion is the following:

- An incorrect PVT model will generate a substantial effect in the simulation results, it was shown how an underestimation of the CGR of 23% percent will lead to an overestimation of the gas plateau of a factor of approximately 9. This difference in gas productivity is generated

by the impact of different liquid dropout in both models. Thus, it also confirms the negative influence which the condensate bank has in well productivity.

References

1. Ali, J. K., McGauley, P. L., and Wilson, C . J. 1997. Experimental Studies and Modelling of a Gas Condensate Flow Near Wellbore. Presented at LACPEC, Rio de Janeiro, Brazil 30 August. SPE 39053.
2. Al-Hussainy, R., and Ramey, H.J., Jr. 1966. Application of Real Gas Flow Theory to Well Testing and Deliverability Forecasting. Jour. Petroleum Technology 18 (05), May 1966. SPE 1243-B-PA.
3. Brooks, R. H. and Corey, A. T. 1966. Properties of porous media affecting fluid flow, J. Irrigation Drainage Division. Proc. of ASCE, 92(No. IR2), 61–88.
4. Bardon, C. and Longeron, D.G. 1980 Influence of Very Low Interfacial Tensions on Relative Permeability. SPE Journal 20 (05), October. SPE-7609-PA, 1980.
5. Bourdet D., Whittle T.M., Douglas A and Pirard Y. M. 1983. A New Set of Type Curves Simplifies Well Test Analysis. World Oil (May): 95.
6. Coats, K., & Smith, B. 1964. Dead-End Pore Volume and Dispersion in Porous Media. SPEJ 4 (01). SPE-647-PA
7. Danesh, A., Henderson, G.D., Tehrani,D.H., and Peden, J.M. 1994. Gas condensate recovery studies. Presented at the DTI Improved Oil Recovery and Research Dissemination Seminar, London, 22June.
8. Danesh, Ali. 1998. PVT and Phase Behavior of Petroleum Reservoir Fluids, Development is Petroleum Science, 47, Amsterdam; New York: Elsevier, 1998.
9. Economides, M.J., Dehghani, K., Ogbe, D.O., and Ostermann, R.D., 1987, Hysteresis Effects of Gas Condensate Wells Undergoing Buildup Tests below the Dew Point Pressure, Presentation at SPE Annual Technical Conference and Exhibition, Dallas, USA, SPE 16748
10. ECLIPSE 2014. Technical Description.
11. Favang. Whitson, C. H. 1996. Modelling gas Condensate Well Deliverability. Presented at SPE Reservoir Engineering 11 (04), November 1996. SPE 30714.
12. Feteke Association. 2012. Theory and Equations. (http://fekete.com/SAN/TheoryAndEquations/HarmonyTheoryEquations/Default.htm) (accessed 20 January 2016)
13. Fussell, D.D. 1973. Single- Well Performance Predictions for Gas Condensate Reservoirs. Presented at JPT 25 (07), July 1973. SPE 4072.
14. Henderson, G.D, Danesh, A., Tehrani, D.H. 1999. Effect of positive rate Sensitivity Inertia on Gas Condensate Relative Permeability at High Velocity. Presented at EAGE-10th , Brighton, UK, 18-20 August 1999.
15. Heimo Anton. “Reservoir Management-Understanding the Reservoir”. University of Leoben. 2015.
16. Houze O., Viturat D. and Fjaere O. 2013. Dynamic Data Analysis v4.30. KAPPA. (http://www.kappaeng.com/documents/flip/dda43001) (accessed 20 January 2016)

17. Manijeh Botorgzadeh, Alian C. Gringarten. 2006. Condensate-Bank Characterization from Well-Test Data and Fluid PVT Properties. SPE Reservoir Evaluation & Engineering 9 (05), October. SPE 89904.
18. Montazeri G.H., Dastkhan H. Z. Aliabadi. 2011. Effect of relative permeability on well testing behavior of Natural Fractured Lean Gas Condensate Reservoir. International Journal of Chemical, Molecular, Nuclear, Materials and Metallurgical Engineering 5 (6). 1156.
19. Manijeh Botorgzadeh, Alian C. Gringarten. 2007. Estimating Productivity-Controlling Parameters in Gas/Condensate Wells from Transient Pressure Data. SPE Reservoir Evaluation & Engineering 10 (02), April. SPE 94018-PA.
20. Novosad, Z., 1996. Composition and Phase Changes in Testing and Producing Retrograde Gas Wells. SPE Reservoir Engineering 11(04), November. SPE-35645-PA.
21. Patacchini L., Sebastien D., Bourgeois M., Moncorge A. and Pallotta Q. 2014. Simulation of Residual oil Saturation in Near-miscible gas Flooding Through Saturation-dependent Tuning of the Equilibrium Constants. Presented at the Abu Dhabi International Petroleum Exhibition and Conference held in Abu Dhabi, UAE, 10 –13 November 2014. SPE 171806-PA.
22. Whitson C. H., Øivind Fevang and Aud SÆvareid. 1999. Gas Condensate Relative Permeability for Well Calculations. Presented at SPE ATCE, 3-6 October, Houston, Texas. SPE 56476.
23. Whitson C. H., Øivind Fevang and Tao Yang. 1999. Gas Condensate PVT-What is really important and why?. Presented at the IBC Conference “Optimisation of Gas Condensate Fields”, London, Jan. 28-29.
24. Whitson C. H and Brule M. R. 2000. Phase Behavior. SPE Monograph Volume 20. Henry L. Doherty Series.

Appendix A

The following is the Original Composition EOS model for 8 components. For the new calculated composition, the only variable changed was the composition (Zi)

```
-- Unit system:
-- FIELD
-- ------------------------------------------------------------------------
-- E300 EOS PVT file generated by PSM/Tk
-- ------------------------------------------------------------------------
-- Confirm number of components
NCOMPS
8
/
-- Specify which equation of state is to be used
EOS
PR /
-- Request modified Peng-Robinson EoS
PRCORR
-- Specify standard conditions
STCOND
60   14.696
/
-- Specify Reservoir Temperature (F)
RTEMP
220  /
-- Component names
CNAMES
 C1N2
 C2C3CO2
 C4C6
 C7C8
 C9C10
 C11C14
 C15C35
 C36+
/
-- Molecular weights
MW
  16.552   36.360   68.894  101.523  126.608
 164.326  254.643  520.000
/
-- Critical Temperatures (R)
TCRIT
 337.320  573.460  825.530  997.860 1077.900
1174.430 1337.870 1605.700
/
-- Critical Pressures (PSIA)
PCRIT
 658.889  694.030  508.564  452.901  407.309
```

```
 350.520  266.815  173.939
/
-- Acentric factor
ACF
 0.01176  0.12298  0.22232  0.27743  0.33083   0.41340  0.58897  0.98273
/
-- Equation of state shift parameters
SSHIFT
-0.15064 -0.05702 -0.03581 -0.03391 -0.05483  -0.06316 -0.07053 -0.13444
/
-- Overrides default Omega A values
OMEGAA
 0.457236  0.457236  0.457236  0.457236  0.457236   0.457236  0.457236  0.457236
/
-- Overrides default Omega B values
OMEGAB
 0.0777961  0.0777961  0.0777961  0.0777961  0.0777961   0.0777961  0.0777961  0.0777961
/
-- Component boiling points (R)
TBOIL
 197.810  350.220  537.090  666.440  736.650  828.140  996.160 1293.640
/
-- Critical Z-factors
ZCRIT
 0.29000  0.29000  0.29000  0.29000  0.29000  0.29000  0.29000  0.29000
/
-- Critical Z-factors for viscosity calculations
ZCRITVIS
 0.28642  0.27764  0.27294  0.27586  0.28064  0.28545  0.29682  0.34063
/
-- Component parachors
PARACHOR
   70.49   118.05   213.92   278.66   338.86  429.38   646.14  1283.00
/
-- Binary interaction coefficients
BIC
-0.00097
0.00214    0.00017
0.03461    0.00009    0.00000
0.04331    0.00009    0.00000    0.00000
0.05513    0.00009    0.00000    0.00000    0.00000
0.07568    0.00009    0.00000    0.00000    0.00000    0.00000
0.16541    0.00009    0.00000    0.00000    0.00000    0.00000    0.00000
/
-- Sample Name: M-1
ZI
0.760647 0.099271 0.058310 0.032792 0.020281 0.017409 0.011260 0.000031
/
-- C1N2     C2C3CO2    C4C6     C7C8     C9C10     C11C14     C15C35    C36+
```